ERDC/CRREL TR-12-9

Cold Regions Research and Engineering Laboratory

US Army Corps of Engineers®
Engineer Research and Development Center

ER-1691

Dissolution Rate of Propellant Energetics from Nitrocellulose Matrices

Susan Taylor, Katerina Dontsova, Susan Bigl, Colleen Richardson, James Lever, Jonathan Pitt, John P. Bradley, Marianne Walsh, and Jiří Šimůnek

September 2012

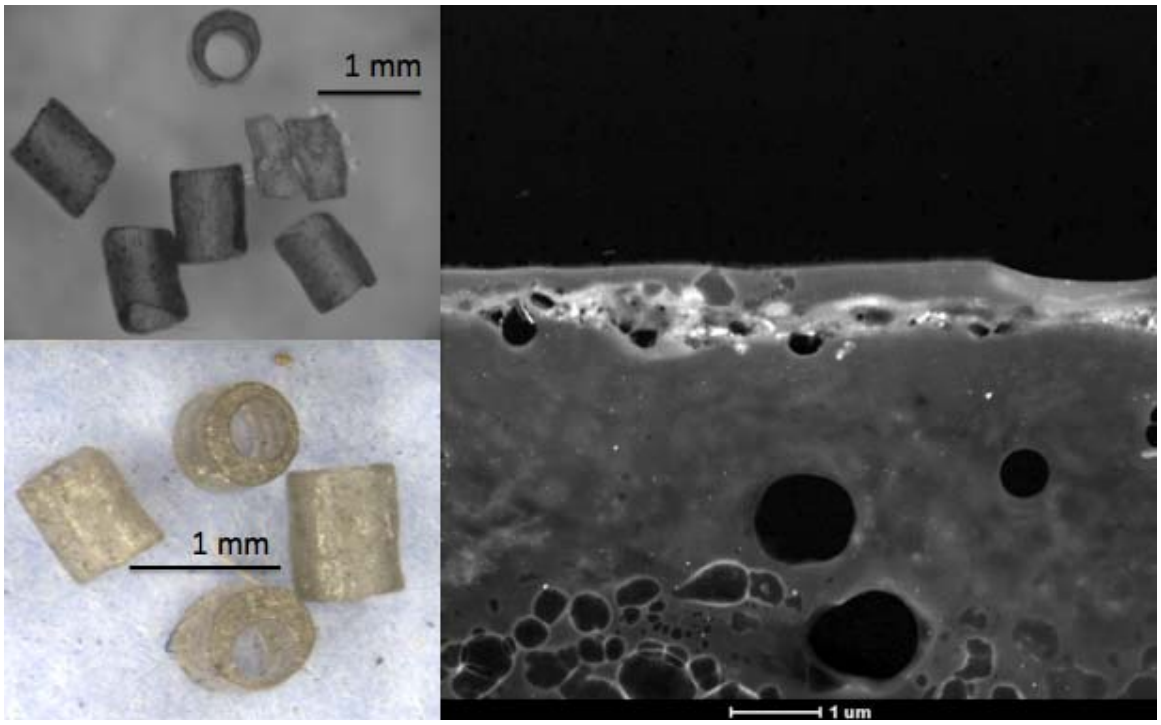

Approved for public release; distribution is unlimited.

Cover: Black and white and color optical images of fired M2 propellant grains and a transmission electron microscope image showing the heated edge of the propellant.

ER-1691

ERDC/CRREL TR-12-9
September 2012

Dissolution Rate of Propellant Energetics from Nitrocellulose Matrices

Susan Taylor, Susan Bigl, Colleen Richardson, James Lever, and Marianne Walsh

Cold regions Research and Engineering Laboratory
U.S. Army Engineer Research and Development Center
72 Lyme Road
Hanover, NH 03755

Katerina Dontsova

Biosphere 2 Earthscience,
University of Arizona
845 N. Park Avenue
Tucson, AZ 85721-0158

Jonathan Pitt

The Pennsylvania State University
PO Box 30, Mailstop 3320B
State College PA 16804

John P. Bradley

Institute of Geophysics and Planetary Physics
Lawrence Livermore National Laboratory
Livermore, CA 94551

Jiří Šimůnek

Department of Environmental Sciences
University of California Riverside
Riverside, CA 92521

Final report

Approved for public release; distribution is unlimited.

Prepared for The Strategic Environmental Research and Development Program

Under SERDP ER-1691

Abstract:

During firing, propellant residues are scattered onto the soil surface where their energetic compounds can be dissolved by precipitation. The residues, like the unfired propellants, are composed of nitrocellulose imbibed with either 2,4-DNT (single-base), nitroglycerin (NG) (double-base) or NG and nitroguanidine (NQ) (triple-base). Although nitrocellulose is insoluble, 2,4-DNT, NG, and NQ are soluble; and 2,4-DNT and NG are also toxic. Consequently, data on how quickly 2,4-DNT, NG, and NQ are dissolved from propellant residues are needed to determine the flux of these compounds to soil. Once in soil solution, the partition coefficient, K_d, and degradation rate, k values are needed to predict the transport of energetics through the vadose zone and to groundwater.

We measured the 2,4-DNT, NG, and NQ dissolution rates for different propellants using laboratory batch and drip tests where no soil was present and soil column studies, which used similar propellant and residues as source terms, to determine partition coefficients and degradation rates. Because the surfaces of propellants and residues may play an important role in dissolution of the energetic constituents, we studied these using both light and electron microscopy.

We found that 2,4-DNT is well bound to NC and dissolves out slowly, but that both NG and NQ have fast initial dissolution followed by slower mass loss. The amount of NG dissolved is a function of the NG/NC ratio in the propellant and both our mass loss data and our microscopy results suggest that NG exists as fine liquid droplets within an NC matrix rather than as dispersed molecules. NG droplets near the grain surface are quickly dissolved and once this layer of liquid NG is depleted, NG diffuses through the NC matrix slowly ($\sim 10^{-14}$ $cm^2 s^{-1}$). The NQ also dissolves rapidly initially but quickly mass loss for the NQ becomes smaller than that for NG, despite higher NQ concentrations in the studied triple-base propellants. NQ is added as a crystal during manufacturing, and was observed to remain solid in the propellant, so dissolution of the NQ crystal would have to precede its removal by water. Both 2,4-DNT and NG are added as liquids and cannot be distinguished from the NC matrix. Therefore, their distribution and movement within the nitrocellulose matrix is poorly understood, hampering our ability to derive a physically based dissolution model that can predict energetic losses from a variety of propellant types.

Different interactions between 2,4-DNT, NG, NQ, and the soils were seen in both the soil batch and column studies. The 2,4-DNT interacted strongly with soils and had the highest adsorption and transformation rates measured. As a result, no 2,-4-DNT was detected in column outflow. NG experienced both adsorption and transformation in the soils, resulting in retardation of the breakthrough curve and decreased concentrations in the outflow. The short half-life of NG in most soils suggests that it should rarely reach groundwater. NQ, on the other hand, does not readily adsorb to soil, and does not degrade or transform. We would expect that NQ dissolved from propellants would reach groundwater.

DISCLAIMER: The contents of this report are not to be used for advertising, publication, or promotional purposes. Citation of trade names does not constitute an official endorsement or approval of the use of such commercial products. All product names and trademarks cited are the property of their respective owners. The findings of this report are not to be construed as an official Department of the Army position unless so designated by other authorized documents.

DESTROY THIS REPORT WHEN NO LONGER NEEDED. DO NOT RETURN IT TO THE ORIGINATOR.

Table of Contents

Abstract: ii

List of Figures and Tables v

Preface ix

1 Background 1

2 Materials and Methods 5

2.1 Propellant samples 5
2.2 Microtome sections and microscopy 7
2.3 Dissolution tests 8
2.3.1 Drip tests 8
2.3.2 Batch tests 8
2.4 Propellant–soil interactions 9
2.4.1 Batch soil studies 9
2.4.2 Soil column tests 10
2.5 Analytical methods 11

3 Results and Discussion 13

3.1 Propellant characteristics 13
3.1.1 Optical Images 13
3.1.2 Thin sections 16
3.1.3 Scanning electron microscopy images 19
3.1.4 Scanning transmission electron imaging and spectroscopy 24
3.2 Laboratory drip and batch tests 26
3.2.1 Single-base propellants 26
3.2.2 Double-base propellants 28
3.2.3 Triple-base propellants 32
3.2.4 Mass balance 34
3.3 Diffusion modeling of NG from small arm propellants 36
3.4 Model and experiment comparison 41
3.5 Propellant–soil interactions 46
3.5.1 Batch soil studies 46
3.5.2 Soil column studies 51
3.6 HYDRUS modeling 65
3.6.1 1-D HYDRUS studies of propellant dissolution and transport in the soil columns 65
3.6.2 2-D HYDRUS simulations of energetic dissolution from M31 propellants 68
3.6.3 Axi-symmetrical 2-D HYDRUS simulations of propellant in soil column 69
3.7 HYDRUS model and experiment comparisons 70
3.7.1 Propellant dissolution and transport in the soil columns 70

3.7.2 2-D HYDRUS simulations of energetic dissolution from M31 propellants..... 73
3.7.3 Axi-symmetrical 2-D HYDRUS simulations of propellant in soil column 76

4 Conclusions and Implication for Future Research 77

5 Case Study: Sampling for NG at the Automatic Record Fire (ARF) Range, Florence, AZ 80

5.1 Introduction..... 80
5.2 Materials and methods 82
5.3 Results 85

6 References 88

Appendix A: Propellant and Soil Property Data..... 94

Appendix B: Soil Properties and Soil Column Test Data 98

Appendix C: Breakthrough Curves for Soil Column Tests 101

Appendix D: Raman Spectroscopy of Propellants 113

Appendix E:-List of Publication Resulting from This Work..... 117

Report Documentation Page

List of Figures and Tables

Figures

Figure 1. Conceptual model showing processes needed to transport energetic compounds to groundwater. 4

Figure 2. Laboratory set-up for drip tests measuring the dissolution of energetics from propellants. 8

Figure 3. Experimental setup used for the soil tests. 10

Figure 4. Side view and end view of M1 single-perforated propellant. 13

Figure 5. Seven-holed M1 propellant used to fire the 105-mm howitzer rounds and the resultant fiber residues 14

Figure 6. Unfired and fired M45 propellant used to fire a 120-mm mortar from a Stryker vehicle. 15

Figure 7. Unfired and fired M9 propellant used to fire 81-mm illumination mortars. 15

Figure 8. Unfired grains and fired residues used to fire a 0.50-caliber machine gun 15

Figure 9. M9 unfired propellants used in drip tests 16

Figure 10. Thin section of M10 propellant viewed in reflected light 16

Figure 11. Images of thin sections of an unfired 9-mm propellant placed in water. 17

Figure 12. Triple-base propellants studied 18

Figure 13. Thin section of M31 triple-base propellant viewed in reflected light. 18

Figure 14. Reflected, dark field and transmitted light of thin section of an M31 not exposed to water and thin section of an M31 used in drip test. 19

Figure 15. Appearance of M31 thin section exposed to water: 19

Figure 16. Images of a series of 9-mm propellant grains showing how the grains change with increased heating 20

Figure 17. High magnification images of surfaces showing the initiation of pits and the bright metal particles that are concentrated on the residue surface. 20

Figure 18. SEM image of WPR289 propellant used to fire 9-mm pistol 21

Figure 19. Images of the M1 propellant 21

Figure 20. Images of unfired 0.50-cal. propellants 22

Figure 21. Images of unfired M9 propellants 23

Figure 22. Images of unfired M31 propellants 23

Figure 23. Energy loss image of sectioned unfired WPR289 propellant immersed in water and not wetted 24

Figure 24. Energy loss maps made of the surface and interior regions of a sectioned M2 propellant. 25

Figure 25. Figure showing an energy loss map for carbon (left), an EELS spectrum and a map of the sample at 6eV showing very bright regions 25

Figure 26. Percentage of 2,4-DNT and 2,6-DNT dissolved into water from unfired seven perforation M1 propellant grains and from fired residues 27

Figure 27. Percentage of NG dissolved for a variety of double-based propellants. We show the single-base M1 for comparison. 28

Figure 28. Plot showing the % NG dissolved normalized by the NG/NC ratio versus time. 29

Figure 29. Percent NG dissolved versus time for unfired and fired (F) small arms propellants. 31

Figure 30. Drip test results showing the percent NG and NQ dissolved versus time for unfired M31 single-perforation propellants. 33

Figure 31. Batch tests results showing the percent NG and NQ dissolved versus time for unfired M31, M31A1 and M31A2 triple-base propellants. 33

Figure 32. Laboratory data from batch tests and drip tests compared with model predictions of solid-phase diffusion of NG from spherical NC grains 37

Figure 33. Analytical model for spherical grains and constant diffusivity compared with data from batch tests using single, unfired grains. 41

Figure 34. Analytical model for spherical grains and constant diffusivity compared with data from drip tests using multiple, unfired grains. 43

Figure 35. FEM predictions compared with data for 5.56 mm unfired grains in batch test (constant wetting). 44

Figure 36. FEM predictions for constant and variable diffusivity with 5-wet/2-dry cyclic wetting (red curves) compared with data for 5.56 mm unfired grains in drip test and FEM predictions for variable diffusivity and continuous wetting 7-wet/0-dry and cyclic 1-wet/6-dry. 45

Figure 37. Concentrations of 2,4-DNT, NG, and NQ found in suspensions of Sassafras, Plymouth, and Catlin soils as a function of time. 47

Figure 38. The natural logarithm of 2,4-DNT, NG, and NQ in suspensions of Sassafras, Plymouth, and Catlin soils concentrations plotted as a function of time. 48

Figure 39. Adsoprtion coefficints plotted as a function of carbon content for: the soils we studied and (iterature values 50

Figure 40. Photographs of unfired propellants and residues used in the column study: 52

Figure 41. Breakthrough curves for continuous water flow onto unfired and fired 0.50-cal. (WC 860) propellants. 54

Figure 42. Breakthrough curves for interrupted water flow onto unfired and fired 0.50-cal. (WC 860) propellants. T 55

Figure 43. Breakthrough curves for interrupted water flow onto unfired M31 propellant. T 56

Figure 44. Breakthrough curves for continuous (CF) and interrupted (IF) water flow at 0.02 mL min^{-1} rate onto unfired M31 propellant in Sassafras and Plymouth soils. 57

Figure 45. Breakthrough curves for interrupted (IF) water flow onto unfired M31 propellant in Sassafras soil at two different flow rates, 0.01 and 0.02 mL min^{-1}. 61

Figure 46. A schematic of the HYDRUS-2D axi-symmetrical domain showing modeled processes for dissolution of energetic from propellant particles and their transport in soil. 69

Figure 47. Observed and HYDRUS-1-D generated breakthrough curves for NG and NQ 71

Figure 48. Observed and HYDRUS-1-D generated cumulative dissolution curves for NG from M31 propellant particle in drip studies without soil. 74

Figure 49. Automatic Record Fire range at the AZ National Guard Florence Military Reservation. 80

Figure 50. National Cooperative Soil Survey, Web Soil Survey map of the Florence Military Reservation area that includes the Automatic Record Fire range. 81

Figure 51. Rainfall record for Florence Military reservation. 81

Figure 52. A Google Earth image showing the Automatic Record Fire (ARF) range at National Guard Florence Military Reservation, AZ. 83

Figure 53. Firing position 7. 83

Figure 54. Sampling a soil pit and view of pit showing a low permeability white caliche layer. 84

Figure 55. Depth and NG concentration of pit samples collected at the Automatic Record Fire range. 87

Tables

Table 1. Propellants tested and types of studies performed on each propellant. 6

Table 2. Solubility and molecular formulae for energetic compounds studied. 26

Table 3. Mass balance calculations for single-based propellants used in the drip and batch experiments. 27

Table 4. Mass balance calculations for double-based propellants used in the drip and batch experiments. 29

Table 5. Mass balance calculations for triple-based propellants used in the drip and batch experiments. 35

Table 6. Parameters used in analytical model, eq 7 derived for spherical grains with constant diffusivity, using radius for grain of equivalent mass (r = 1.6 g/cm^3) 42

Table 7. Fate and transport parameters for propellant constituents in soils determined in batch adsorption studies. 49

Table 8. Soil column experiments. 52

Table 9. Composition of propellants used in column experiments 53

Table 10. NG loss from unfired and fired WC860 propellant tested in column experiments at 0.01 and 0.02 mL min^{-1}. 58

Table 11. NG and NQ loss from unfired M31 propellant in column experiments conducted at 0.01 and 0.02 mL min^{-1} flow. 59

Table 12. Enrgetic compounds recovered in leachate, extracted from the soil and extracted from propellants at end of column experiments 63

Table 13. Solute transport parameters obtained by HYDRUS-1-D for column saturated flow experiments involving Br^{-1} and WC 860 and M31 propellants in Plymouth and Sassafras soils. 72

Table 14. HYDRUS 2-D-determined parameters for dissolution of NG and NQ from M31 particles in drip studies in the absence of soil: 75

Table 15. Summary of important characteristics determined for single-, double- and triple-based propellants. 79

Table 16. Record of ammunition fired on the Automatic Record Fire (ARF) range between 1 October 2010 and 9 Augus, 2011. 82

Table 17. Concentration of NG in multi-increment surface samples collected at the Automatic Record Fire range. 85

Table 18. Concentration of NG, mg kg^{-1} soil, from the 0–1 cm layer in the soil pits at the Automatic Record Fire range. 86

Preface

This study was conducted for the Strategic Environmental Research and Development Program, SERDP ER-1691.

The work was performed by Dr. Susan Taylor, Susan Bigl, Colleen Richardson, and Marianne Walsh (Biogeochemical Sciences Branch, Dr. Terrence M. Sobecki, Chief), Dr. James Lever (Force Projection and Sustainment Branch, Dr. Edel Cortez, Chief), U.S. Army Engineer Research and Development Center–Cold Regions Research and Engineering Laboratory (ERDC-CRREL); Dr. Katerina Dontsova (University of Arizona); Dr. Jonathan Pitt (The Pennsylvania State University); Dr. John P. Bradley(Lawrence Livermore National Laboratory); and Dr. Jiří Šimůnek (University of California Riverside). At the time of publication, Dr. Justin Berman was Chief of the Research and Engineering Division. The Deputy Director of ERDC-CRREL was Dr. Lance Hansen and the Director was Dr. Robert Davis.

The authors thank Nancy Perron for her many and varied contributions and Julie Richardson, Claire Hornig, Catherine Ledna, and Edward Hunt for laboratory support. Michael Walsh is thanked for arranging most of the propellant firing tests from which samples were obtained. Dr. Charles Daghlian and the WISP students from Dartmouth College who worked on this project made the SEM analyses possible. Steven Ritchie from ATK provided much needed information. The authors also thank Gavin Fielding, Cleanup/ Remediation Manager, and SGT Gregory Gamboa, of the Florence Military Reservation, for permission and help sampling the range. The Strategic Environmental Research and Development Program, SERDP ER-1691 sponsored this work, and Dr. Andrea Leeson, Dr. Anne Andrews, and Dr. Jeffrey Maqusee are thanked for their support.

COL Kevin J. Wilson was the Commander and Executive Director of ERDC, and Dr. Jeffery P. Holland was the Director.

List of Acronyms and Definitions

2,4-DNT	2,4- dinitrotoluene
DoD	Department of Defense
DPA	diphenylamine
EC	ethyl centralite
ERDC	Engineer Research and Development Center
ER	Environmental Restoration
$K_{d,}$	partitioning coefficient
k	the reaction rate constant
MC	munitions constituents
NC	nitrocellulose
NG	nitroglycerin
NQ	nitroguanidine
PV	pore volume
SEM	scanning electron microscope
SERDP	Strategic Environmental Research and Development Program
SON	statement of need

Single-base propellant= NC+ 2,4-DNT

Double-base propellant= NC+NG

Triple-base propellant= NC+NG+NQ

1 Background

Propellants are chemical mixtures formulated to burn at a controlled rate, to contain the oxygen needed to burn and to evolve gas. It is the expanding gas that propels the bullet or the round. Modern propellants are generally composed of a polymer, a plasticizer, and a stabilizer. These three components provide the structure, contribute the oxygen and fuel, and slow the deterioration of the propellant, respectively. Most common are the nitrocellulose-based propellants. About 12 million kg (26 million lb) of nitrocellulose is manufactured each year in the U.S. (Richie 2012; a partial listing is given in Table A1). This wood-like compound is used as the structure of the propellant. Propellants are nitrocellulose (NC) impregnated with either 2,4-dinitrotoluene (2,4-DNT single-base), nitroglycerin (NG double-base), or NG and nitroguanidine (triple-base). Although nitrocellulose does not dissolve, 2,4-DNT, NG, and NQ are soluble in water (Rosenblatt et al. 1991; Windholz 1976). Furthermore, screening levels for 2,4-DNT and NG are low in residential water (2,4 DNT = 0.2 $\mu g\ L^{-1}$; NG = 1.5 $\mu g\ L^{-1}$; NQ = 1.6×103 $\mu g\ L^{-1}$; U.S. EPA 2012) and 2,4-DNT is classified as carcinogen (Human Health Screening Values 2012) making their fate and transport of interest. Limited toxicological data for NQ suggests it is far less toxic (Nipper et al. 2009).

We know that the processes controlling the dissolution of propellant compounds are quite different from those controlling explosive dissolution (Lever et al. 2005; Taylor et al. 2009a, b). Unlike TNT and RDX, nitrocellulose (the main constituent of most propellants) does not dissolve in water. While solid pieces of high explosives decrease in size as they dissolve, many nitrocellulose-based propellants do not change shape as the energetics leach from their NC matrix. Furthermore, propellants do not break apart and, because propellant grains are made to specification, they have a narrower size distribution than explosives.

How much 2,4-DNT, NG, or NQ reaches groundwater depends on four main factors. First, how much energetic is deposited on the soil surface after firing a given weapon (deposition). Second, the number of rounds expended for each weapon during a training session and the number of training sessions per year (accumulation). Third, the rate at which 2,4-DNT, NG, and NQ dissolve from the residues when wetted by precipita-

tion. Fourth, the fraction of the dissolved energetics that is chemically or biologically degraded in the soils during their transit to groundwater.

Previous work focused on quantifying factors 1, 2, and 4. These studies found that propellant residues are scattered onto the soil surface at firing points and that the residues consist of grains or fibers of nitrocellulose that contain energetic compounds (Walsh, M.E. et al. 2007). Jenkins et al. (2008) quantified the concentrations of 2,4-DNT, NG, and NQ in soils at firing points and Walsh, M.R. et al. (2007) published robust estimates of the amount of the energetic compounds deposited on clean snow from single firings of different weapon systems. In all of these studies, the samples were chemically extracted to measure the concentration of energetics. Although this ensures that all of the energetic contained within the nitrocellulose matrix is analyzed, it does not provide information on how quickly or how much of the energetic is dissolved from the nitrocellulose matrix by rainfall.

Once in solution, 2,4-DNT, NG, and NQ can be carried by infiltrating precipitation to the groundwater. During transit through the vadose zone, the energetics can interact with soil in a variety of ways: they can be reversibly bound to the soil, irreversibly bound, or transformed altogether. K_d, the adsorption or partition coefficient, characterizes the affinity of the energetics to sorb onto soil organic matter or mineral surfaces. When the relationship between the concentration on the soil and in water phases is linear with respect to total concentration, the partition coefficient can be described as

$$s = K_d\, c \tag{1}$$

where

s = soil concentration in mg kg^{-1}
K_d = adsorption or partition coefficient (L kg^{-1} or cm^3 g^{-1})
c = water concentration (mg L^{-1})

As the values of K_d increase, the chemical resides mostly on the solid phase and little is transported downward in the moving pore water.

The energetics can also be broken down chemically or biologically while in solution. The rate at which the energetic is mineralized or transformed is related to its concentration in solution by k, the reaction rate constant. In

this case the concentration of the constituent in the soil water and the rate of loss from the aqueous phase can be described as

$$dc/dt = -k\,c \tag{2}$$

where

c = concentration of the specific chemical in solution
t = time
k = reaction rate constant.

Thus, if the partition coefficient (K_d) and the rate constant k are known, the fate of the chemical in the soil system can be modeled. As both K_d and k vary for different soils, laboratory batch and soil column experiments are run to estimate these parameters.

Different types of laboratory experiments provide estimates for these parameters. To estimate K_d, batch experiments shake the energetic in a soil suspension until the solution concentration remains constant (Pennington et al. 1999, 2001; Brannon et al. 2002; Speitel et al. 2002; Yamamoto et al. 2004; Mirecki et al. 2006) (see Tables A2 and A3). Similar experiments are run to estimate k, but the concentrations are measured as a function of time (Miyares and Jenkins 2000; Jenkins et al. 2003; Mulherin et al. 2005). In soil column tests, energetics in the outflow are measured. Some researchers have dripped clean water on columns containing contaminated soils (Hewitt and Bigl 2005), while others use clean soils onto which solutions of energetics are dripped or propellant grains or residues are leached with clean water (Dontsova et al. 2009). The K_d values measured for NG on a variety of soils range from near 0 to about 4 $cm^3\ g^{-1}$. These low values suggest that NG should not be retarded moving through most soils. However, estimates of the half-life of NG in various soils ($t^{1/2} = 0.693/k$) vary from much less than an hour to about 0.49 days indicating fast degradation (Jenkins et al. 2003). Figure 1 summarizes the processes we think need to occur if propellant energetics are to reach groundwater.

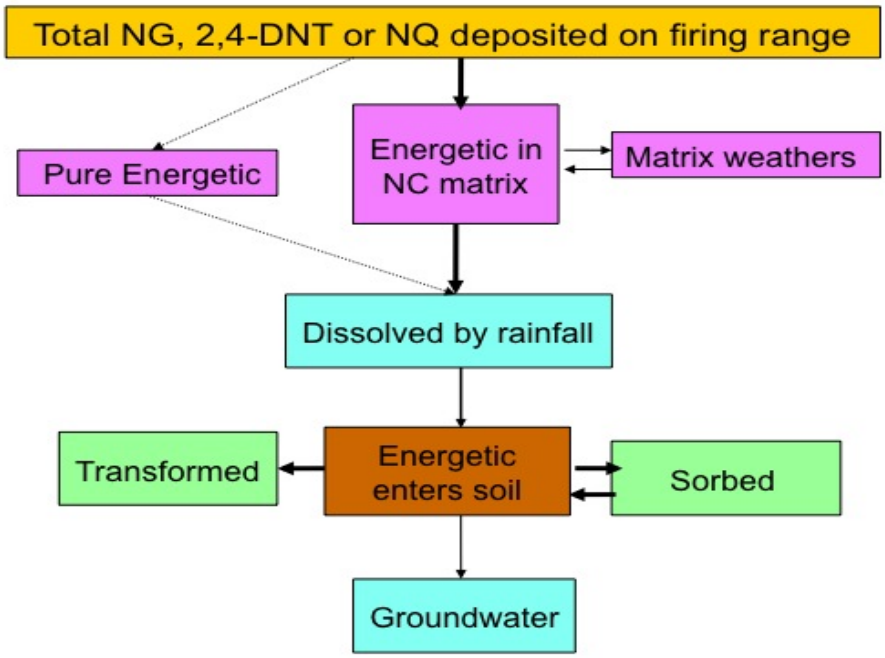

Figure 1. Conceptual model showing processes needed to transport energetic compounds to groundwater.

The NG, 2,4-DNT and NQ are always found in NC, indicating they are not deposited as pure product and must dissolve, diffuse, or desorb from their NC matrices. To model this process, we need information on how these compounds are bound in and released from the nitrocellulose. For example, does the NC form a solid through which the energetics have to diffuse or do the NC fibers sorb the energetics and release them when in contact with water? The latter process implies two or more distinct phases. We used microscopic techniques to help distinguish between these processes.

2 Materials and Methods

We used field collected propellant residues and unfired propellant grains for laboratory drip and batch tests (involving no soil) and for soil column studies. Together, these data allow us to better understand the dissolution rate of propellant-derived 2,4-DNT, NG, and NQ given the rainfall rate and provided insight into how well vadose transport models predict dissolution rates for these energetic compounds.

2.1 Propellant samples

Table 1 lists all the propellants tested during this study. A list of nitrocellulose-based propellants used by the U.S. military is given in Table A1. We examined three single-base propellants, eight double-base propellants and three triple-base propellants. Many of these, M1, M2, M9, M10, M45, WC844, WC846, WC860, WPR289, and AT-4 propellants were collected from live fire exercises using aluminum trays set near the gun muzzle or by melting and filtering snow that contained residues. A live-fire test, where triple-base propellants were used, produced little residue in the particle traps (Walsh, M.R. et al. 2011).

For the M1 single-base propellants, we collected both residues and unfired grains from single- and seven-perforation M1 propellants. The fired single-perforation propellant deposited sand-sized, clear, potassium sulfate grains that contained no 2,4-DNT (Walsh, M.E. et al. 2007) and consequently the residues were not included in our dissolution tests. The seven-perforation propellant, on the other hand, left slivers of NC with 2,4-DNT concentrations similar to those of the unfired propellant (Walsh, M.R. et al. 2007). We have tested the unfired single perforation M1 propellant and both the unfired seven-perforation propellant and its residues. We also have unfired and fired M10 propellant, also single-base, but as it only contains NC, which is insoluble, this propellant was not included in our dissolution tests.

Table 1. Propellants tested and types of studies performed on each propellant. All samples were photographed optically.

Propellant	Weapon System	Energetic	%	Mass (mg) per grain	Drip		B	S	T
M10- grain	60-, 81-mm Mortar	NC	100					x	x
M1-1 hole	155-mm Howitzer	NC & DNTs	10	10 ± 0.4			U	x	x
M1- 7 hole	105-mm Howitzer	NC & DNTs	10	~100	U	F	U		
M9-1 hole	81-mm Ill. Mortar	NC & NG	40	1.23 ± 0.1	U		U	x	x
AT-4- sheet	Rocket	NC & NG	36.5	NA		F			
M2-1 hole	40-mm grenade	NC & NG	19.5	0.32±0.06		F	F	x	x
WPR289-grain	9-mm pistol	NC & NG	12-18	0.05±0.02	U	F	U	x	x
M45-1 hole	120-mm mortar	NC & NG	10	4.0±0.4	U	F	U	x	
WC844-grain	M-16 Rifle	NC & NG	9-11	0.16±0.06	U	F	U	x	
WC846-grain	7.62-mm mach. gun	NC & NG	8-11	0.18±0.06	U	F	U	x	
WC860-grain	0.50-cal mach. gun	NC & NG	8-11	0.45±0.10	U	F	U	x	x
M31-1 hole	Heavy artillery	NC & NG & NQ	20&55	47 ± 1.2	U		U	x	x
M31A1-7 hole	Heavy artillery	NC & NG & NQ	20&55	1405 ± 13			U		
M31A2-7 hole	Heavy artillery	NC & NG & NQ	20&55	874 ± 7	U		U	x	

U=Unfired, F= Fired, B= Batch, S=SEM, T=TEM

For the double-based propellants, we collected unfired grains and fired residues for most of the formulations (Table 1). We were not able to collect grains of unfired M2 propellant or a sheet of unfired propellant used to fire AT-4 rocket as the unfired propellant could not be safely separated from either munition. We collected unfired M9 propellant grains (used to fire the 81-mm illumination rounds) but no residues.

For the triple-base propellants we have only unfired grains. Although we sampled from a live fire test that used M30 to fire a self propelled Howitzer, the test yielded no residues we could measure (Walsh, M.R. et al. 2011). We, therefore, obtained three triple-based unfired propellants from Radford ammunition plant and tested these in drip and batch tests.

For all of the field tests, we collected unfired propellants from bullets or bags, whenever possible, and included them in our dissolution tests. Although unfired propellants are not intentionally dumped on the ground, excess, unfired propellant bags are often burned in the field a process that scatters propellant grains (Walsh, M.R. et al. 2009). Furthermore, comparisons of the dissolution behavior of unfired and fired grains provide insight on how firing changes their composition and dissolution rate.

2.2 Microtome sections and microscopy

We used a Leica Ultracut UCT to produce thin (2.5–15 μm) slices of the propellants for optical microscopy and TEM analyses. The goal was to map the different components in single- (NC with or without 2,4-DNT), double- (NC and NG) and triple- (NC, NG, and NQ) base propellants.

We took both optical and scanning electron microscope (SEM) images of the propellants and their residues. The color of the propellants can be seen in the optical microscopy images, whereas the SEM images show fine details that can only be seen at high magnification. The optical images were taken at CRREL using a Leica DMLM microscope equipped with a digital camera. We used an FEI XL-30 field SEM at Dartmouth College to obtain high magnification images of the propellant surfaces. The SEM had both secondary and backscatter electron detectors and an X-ray microanalysis light element Si(Li) detector for analyses of all elements heavier than carbon.

To quantify the carbon, nitrogen, and oxygen and map their distributions in the propellant grains, we used the scanning transmission electron microscope (SuperSTEM) capable of ultra high-resolution imaging (0.1 nm) located at Lawrence Livermore National Laboratory. The instrument images a specimen using a high angle annular dark field (HAADF) and can analyze sub-Angstrom spots with an electron energy loss spectroscope (EELS). The specimens are generally ultra-microtomed into thin sections. The SuperSTEM is an 80–300 keV FEI TITAN equipped with a monochromator, dual spherical aberration (C_s) correctors, a EDAX Genesis 4000 Si(Li) solid state energy dispersive x-ray (EDX) spectrometer, and a high-resolution electron energy-loss spectrometer (Tridiem Gatan Imaging Filter). TEM brightfield/darkfield images and STEM high-angle annular dark field (HAADF) images were acquired at magnifications of 10,000 to 100,000×. Compositions were measured using EDX and electron energy-loss spectroscopy (EELS) at accelerating voltages of 80, 200, and 300 keV. Energy-filtered imaging or “EFTEM” was used to map the distribution of C, N, and O.

2.3 Dissolution tests

2.3.1 Drip tests

Before beginning the drip tests, we weighed ~50 mg of each type of unfired propellant and residue on a Mettler A230 balance (0.1 ± 0.1 mg) and extracted and analyzed these to determine how much of the energetic compound was present as a function of their mass. Once we determined the concentration of energetics in our starting materials, we placed a collection of either unfired propellants or fired residues into separate, 1-cm-diameter Buchner funnels fitted with glass frits (Fig. 2). A syringe pump was used to drip Milli-Q water (pH = 6) at 0.5 or 1.0 mL hr^{-1} onto the propellants. The water flowed through the frits into 20-mL scintillation vials. We replaced the vials every weekday, measured the water volume, and determined the concentration of the propellant constituents using high-performance liquid chromatography (HPLC). At the end of each test, we again weighed the unfired propellants or the residues and extracted them in acetonitrile to determine the energetic mass remaining in the NC matrix and estimate a mass balance for the test.

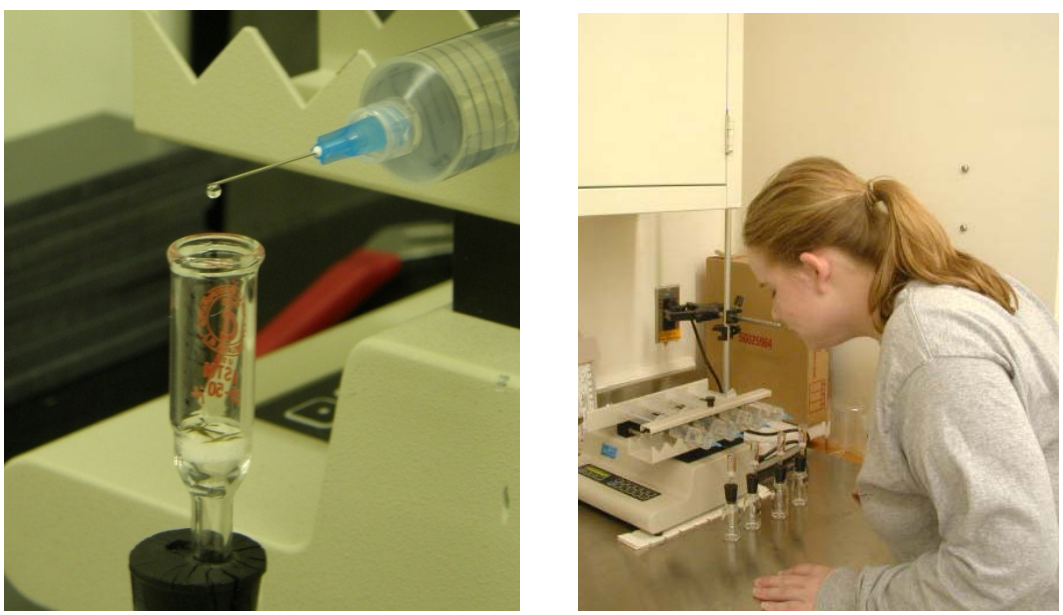

Figure 2. Laboratory set-up for drip tests measuring the dissolution of energetics from propellants.

2.3.2 Batch tests

A single-propellant grain was massed using a Mettler Toledo MX5 microbalance (1 ± 1μg) and imaged using an optical microscope before beginning the test. Each sample was then placed in its own 20-mL glass scintil-

lation vial and deionized water (3 or 6 mL depending on the grain size) was added by volumetric pipette. The vials were capped and placed on a Lab-Line Instruments Junior Orbit Shaker, set to 100 rpm.

At intervals throughout the experiments, the water in the vials was removed and replaced with new deionized water. The removed water (sample) was then massed by weighing the vial it was decanted into before and after addition of the water. The energetic compounds present in the water were detected and measured using HPLC. The tests were stopped when the concentration of the energetic in the water samples neared the detection limit. The propellant samples were then allowed to air dry, and were re-imaged using the same optical microscope.

2.4 Propellant–soil interactions

2.4.1 Batch soil studies

To determine how 2,4-DNT, NG, and NQ interact with soils, we measured the changing concentrations of aqueous solutions of 2,4-DNT, NG, and NQ in contact with clean soils. For these sorption studies, 0.5 mL of a 10,000 mg L^{-1} stock solutions of 2,4-DNT, NG, and NQ were added to 250 mL of a 0.05M $CaCl_2$ solution to create a 2 mg L^{-1} input solutions. Triplicate tests were conducted using 4:1 solution/soil mixture of the three propellant constituents and three soil types. Each propellant constituent was studied separately. The three soils selected for the study were Catlin silt loam (fine-silty, mixed, mesic, superactive Oxyaquic Argiudolls), Plymouth sandy loam (mesic, coated Typic Quartzipsamments), and Sassafras loam (fine-loamy, siliceous, mesic Typic Hapudults) (Appendix B). Two of these soils, Plymouth sandy loam and Sassafras loam, were collected on military installations, Massachusetts Military Reservation and Aberdeen Proving Ground, respectively. We also used these soils in the column studies.

Samples were placed on a reciprocating shaker and equilibrated for 1, 2, 6, 12, 24, 48, 72, 96, and 120 h and then centrifuged for 30 min. The supernatant solution was analyzed for target compounds by HPLC using U.S. EPA Method 8330b for 2,4-DNT and NG, and the Walsh, M.E. (1989) method for NQ. Linear distribution coefficients (K_d) and degradation/transformation constants (k) were calculated (eq 1 and 2).

2.4.2 Soil column tests

To determine how 2,4-DNT, NG, and NQ dissolving from fired propellants interact with soils, we conducted saturated flow column experiments using propellant residues collected at the same time as those used in drip studies. Our flux-controlled flow-through columns consisted of Supelco (Bellefonte, PA) glass tubes (7-cm high with 1.18-cm internal diameter) with PTFE caps (Fig. 3). Silanized glass wool was used on top and bottom to prevent migration of the particles. A Cole-Parmer (Vernon Hills, IL) Master Flex peristaltic pump was attached to the top of each column to supply solution at a given flux. Outflow samples were collected continuously into 4-mL HPLC vials using a Teledyne ISCO (Lincoln, NE) Foxy 200 Fraction collector with a 200-vial capacity. This experimental setup allowed us to run up to 10 columns at the same time.

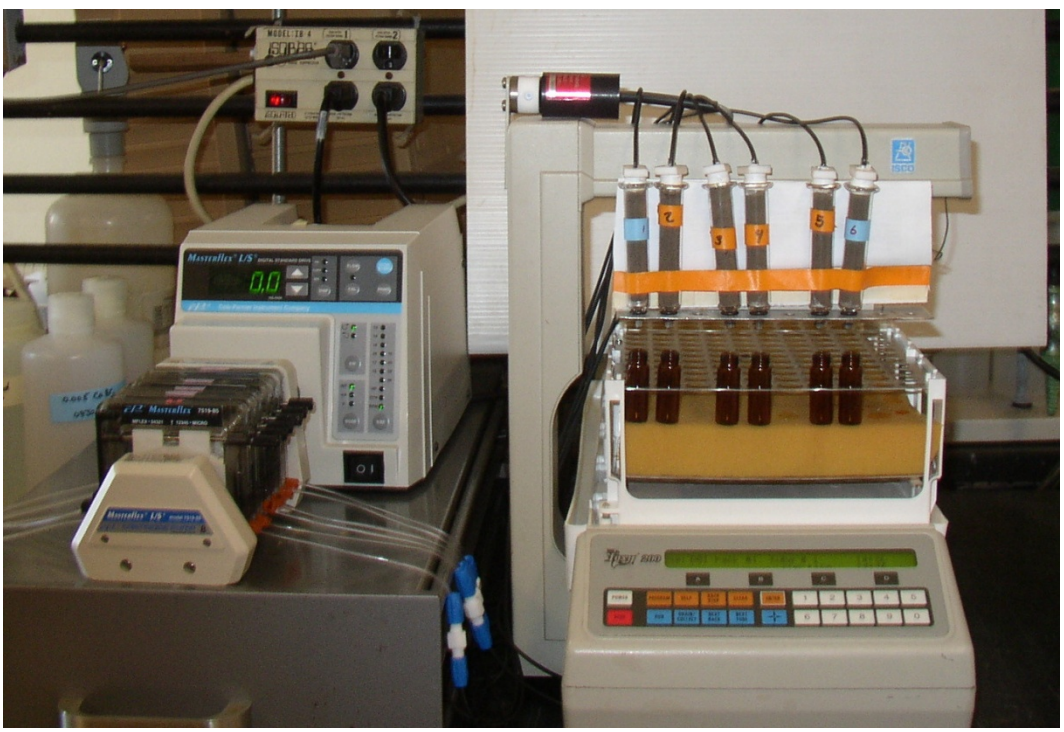

Figure 3. Experimental setup used for the soil tests.

Columns were packed with soil and saturated from the bottom up with a 0.005-M $CaBr_2$ solution, to avoid air entrapment. Pore volume (PV) was determined during saturation as the volume of solution necessary to fill the packed column. Propellants were then placed on the soil surface, the tops of the columns were connected to the pump and the flow was started. Two flow rates were used: 0.01 mL min^{-1} (0.55 cm h^{-1} flux) and 0.02 mL min^{-1} (1.1 cm h^{-1} flux). These were similar to fluxes used in the drip stud-

ies. We tested: M1, fired (0.005 g per column) and unfired (one particle or 0.115 ± 0.003 g per column); WC 860, fired (0.0166 g per column) and unfired (0.1 g per column); and M31 unfired (two particles or 0.091 ± 0.002 g per column). After about 35 to 60 PV, the propellants were removed and the flow continued for another 20–30 PV to evaluate desorption of the energetics from the soil. We used a conservative tracer (Br^-) analyzed using ion chromatography (Dionex ICS 5000 with electrical conductivity detector) to distinguish between physical and chemical non-equilibrium processes and to determine dispersion and diffusion in the columns. Outflow from the columns was analyzed using HPLC as described below.

To determine how much 2,4-DNT, NG, and NQ remained in the soil at the end of the tests, we extracted the soil samples for 18 h in acetonitrile at 1:2 soil/acetonitrile ratio. Extracts were diluted with water to achieve 1:3 acetonitrile to water ratio, filtered through 0.45-µm PTFE filter, and analyzed using HPLC, as described below. For sets IV and V, we performed soil extractions in three layers: for top, middle, and bottom of the soil column.

2.5 Analytical methods

We quantified 2,4-DNT and NG in the propellants and water samples using SW-846 Method 8330B (EPA 2006) and NQ using a separate method (Walsh, M.E. 1989). For method 8330B, 3 mL of the water sample are added to the 1 mL acetonitrile, extracted, and filtered through a 0.45-µm Millipore cartridge. High Performance Liquid Chromatography separates the NG, 2,4-DNT, and their co-contaminants using a Water NovaPak C8 column eluted at 1.4 mL min^{-1} (28°C) with 85:15 water: isopropanol mix and detected by UV at 254 or 210 nm. For NQ the water sample is injected straight onto a mixed-mode PR18/cation column. This column is eluted with 1.5 mL min^{-1} water and NQ detected by UV at 263 nm. The certified reporting limit for water was 5.0 µg L^{-1} (Walsh, M.E. 1989).

Commercially available standards (Restek), specifically developed for Method 8330, are used for calibration. We prepared 1 and 10 ppm 8095A standards. Sample concentrations of around 1 ppm are expected, but if their concentrations are outside of the linear range for the calibration, ~20 ppm, we diluted and reanalyzed the samples. The 1-ppm standard was used to recalibrate the instrument after every tenth samples. Blanks were run before each standard run to minimize the possibility of carryover, which would produce a poor calibration. The 10-ppm standards were in-

terspersed with the samples as unknowns, and a blank was run after each to minimize carry over. The concentrations of energetics in all the water samples were lower than solubilities for the energetic compounds.

3 Results and Discussion

3.1 Propellant characteristics

3.1.1 Optical images

We found that the shape of the original propellant grain and the presence or absence of holes (perforations made to increase the burn rate) dictated the appearance of the residue (Fig. 4–8). For example, propellants without perforations tended to leave residues that were smaller versions of the original propellant. Propellant grains with a single perforation left rings or crescent shaped residues (Fig. 6), while multiple perforations left slivers.

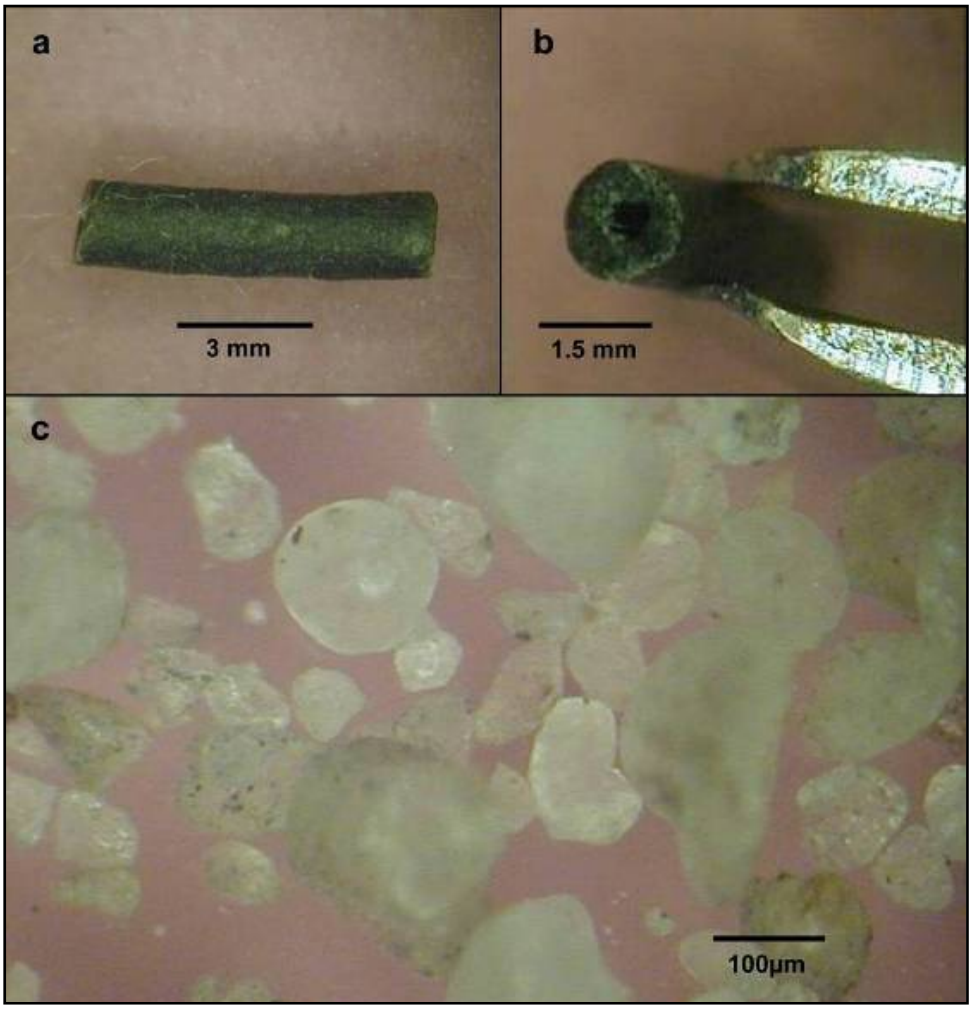

Figure 4. Side view (a) and end view (b) of M1 single-perforated propellant. Clear grains deposited from firing this propellant (c) contain potassium and sulfur, but no 2,4-DNT.

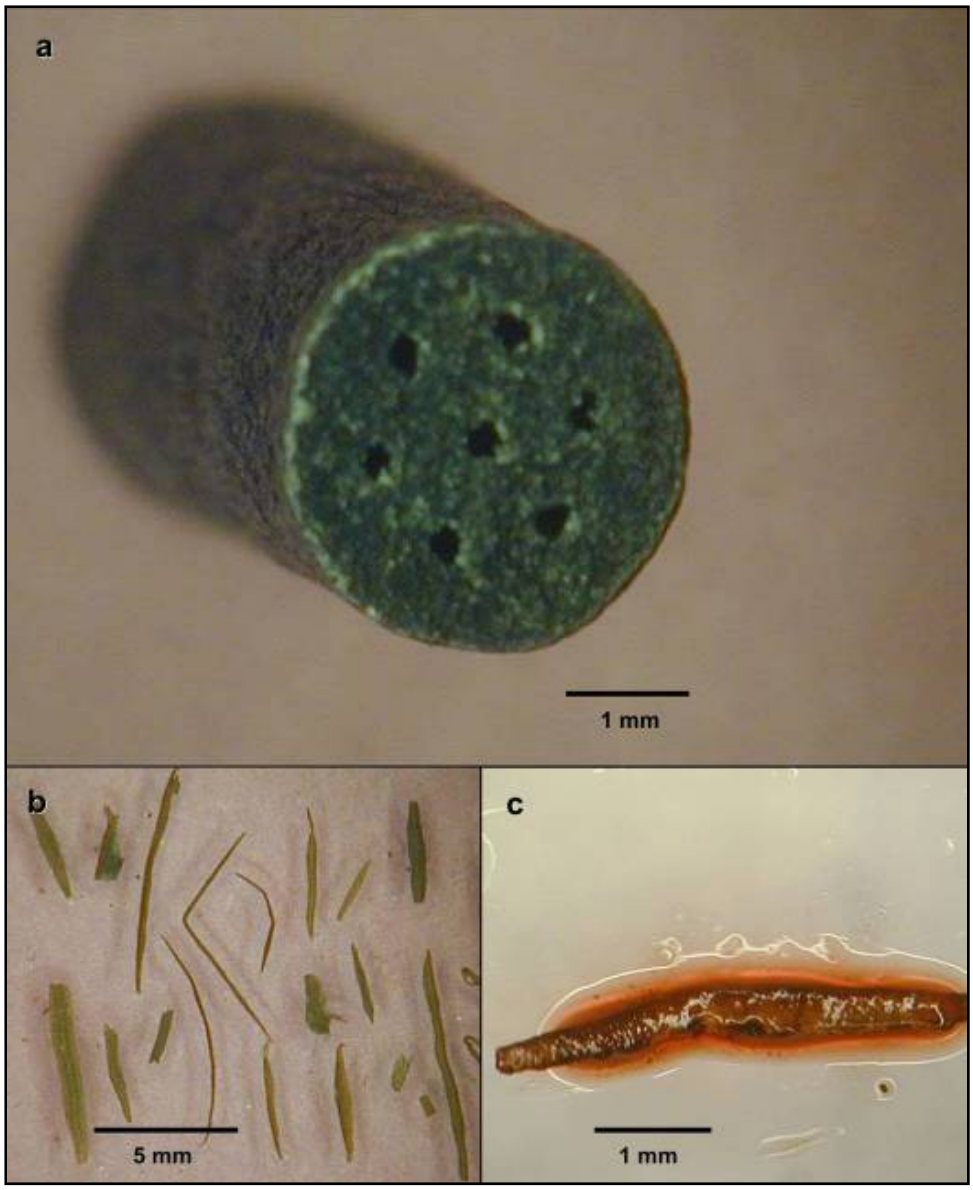

Figure 5. Seven-holed M1 propellant used to fire the 105-mm howitzer rounds (a) and the resultant fiber residues (b). Tetra butyl ammonium hydroxide placed on a fiber (c) shows that it contains 2,4-DNT.

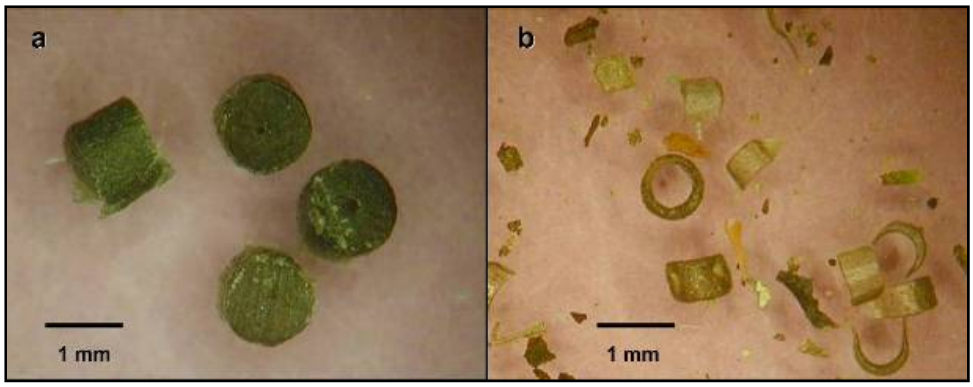

Figure 6. Unfired (a) and fired (b) M45 propellant used to fire a 120-mm mortar from a Stryker vehicle.

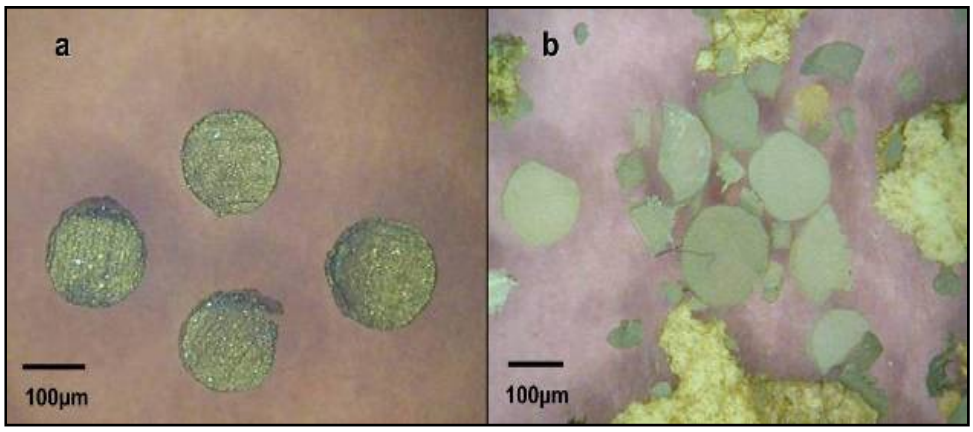

Figure 7. Unfired (a) and fired (b) M9 propellant used to fire 81-mm illumination mortars.

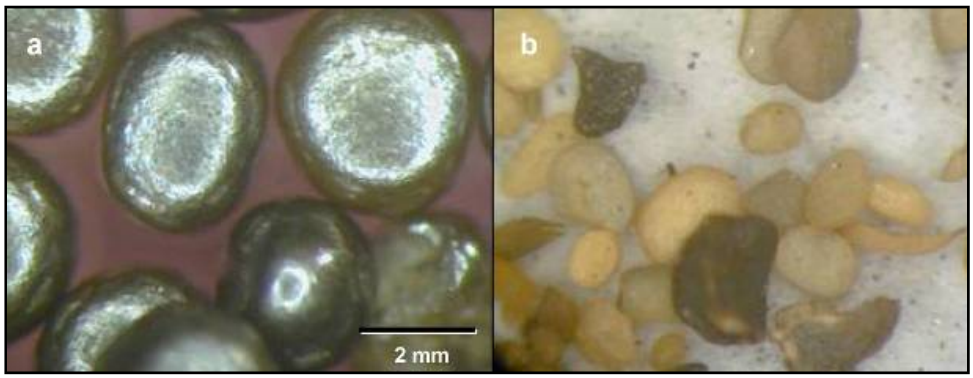

Figure 8. Unfired grains (a) and fired residues (b) used to fire a 0.50-cal. machine gun (photographed at the same scale).

For propellants composed mainly of nitrocellulose (>85%), wetting or submersion did not change the shape of the grain. This finding is reasonable given the fact that nitrocellulose is hydrophobic and those samples measured have extremely small pores (10–30 nm radii) making it difficult for water to penetrate the NC (Ksiazczak et al. 2003). For the M9 propel-

lant that contained <60% nitrocellulose, however, we saw a collapse of some of the grains. After being dripped on for 40 days, the M9 propellants developed a "skirt" where the propellants touched the glass frit (Fig. 9). This "skirt" was all that remained of two of the eight M9 grains tested. We think that, as the NG was removed from the propellant, the remaining NC was not strong enough to retain its shape and it collapsed into a disk with a diameter slightly larger than that of the original propellant grain.

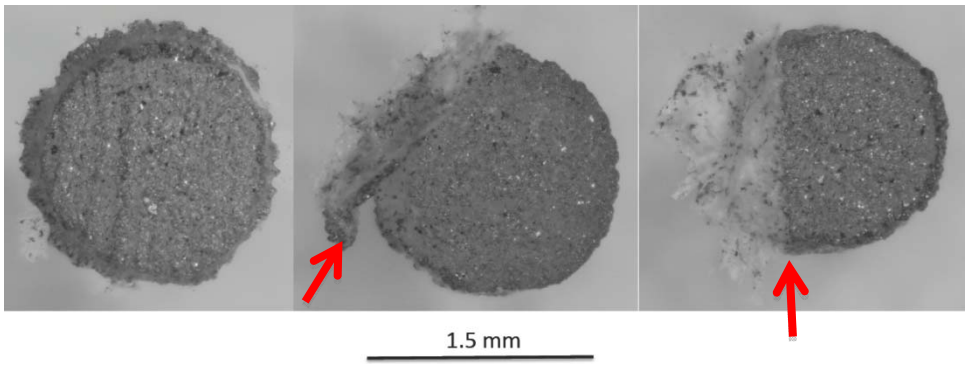

Figure 9. M9 unfired propellants used in drip tests. Note "skirt" that formed where the propellant contacted the glass frit (arrows).

3.1.2 Thin sections

We microtomed thin sections for optical microscopy and TEM analyses. We found that single- and double-base propellants are transparent to translucent and show signs of having been extruded (Fig. 10).

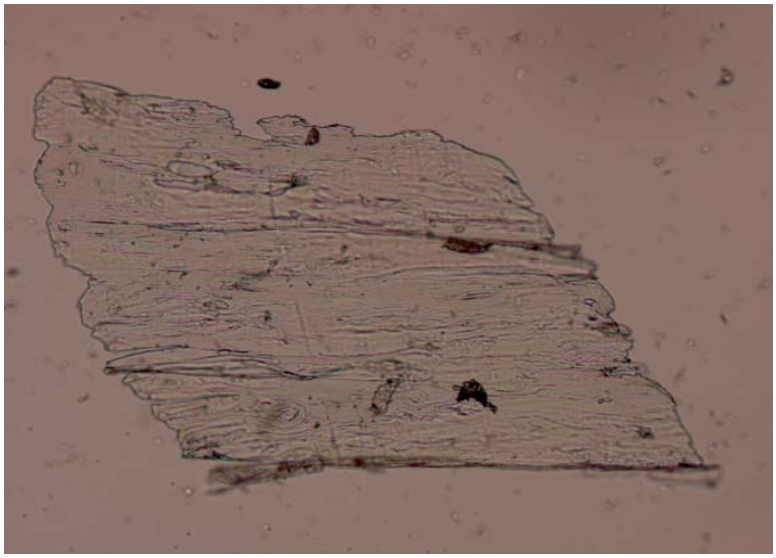

Figure 10. Thin section of M10 propellant viewed in reflected light

The double-base propellants examined (0.50-cal., 9-mm, M2, and M9) contained micron-sized inclusions dispersed throughout (Fig. 11a and c). However, the outer surfaces of these propellants are devoid of inclusions if the propellant has been exposed to water during drip or batch tests (Fig. 11b and d). We think these inclusions are liquid droplets of NG contained within the nitrocellulose matrix. One of the thin sections shows what appears to be a liquid phase exiting the matrix via a crack (Fig. 11b).

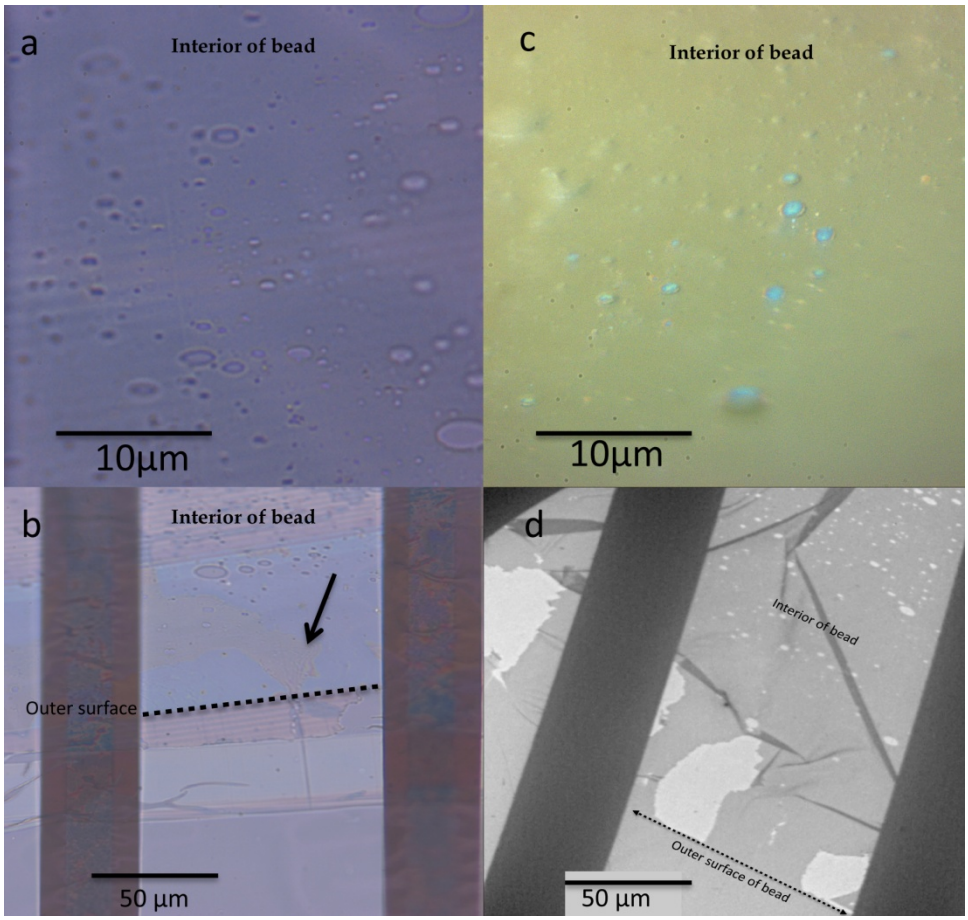

Figure 11. Images of thin sections of an unfired 9-mm propellant placed in water. Optical reflected light images (a, b), optical transmitted light image (c) and transmission electron image (d). The dark bars in b and d are the TEM grids and the white areas near the surface of the propellant in d are rips of the thin section. Note fluid like yellow phase moving toward propellant surface (arrow). Note also that areas close to the marked surfaces of the propellants do not have droplet-like features like those seen in the interior of the grain.

The triple-base propellants we examined, M31, M31A1, and M31A2, were cylindrically shaped grains with one (M31) or seven perforations (M31A1 and M31A2) (Fig. 12a). Unlike the single- and double-base propellants, which contain no visible crystals, the triple-base propellants have crystals

of NQ (~5 μm in diameter) running parallel to the long axis of the cylinder (Fig. 12b).

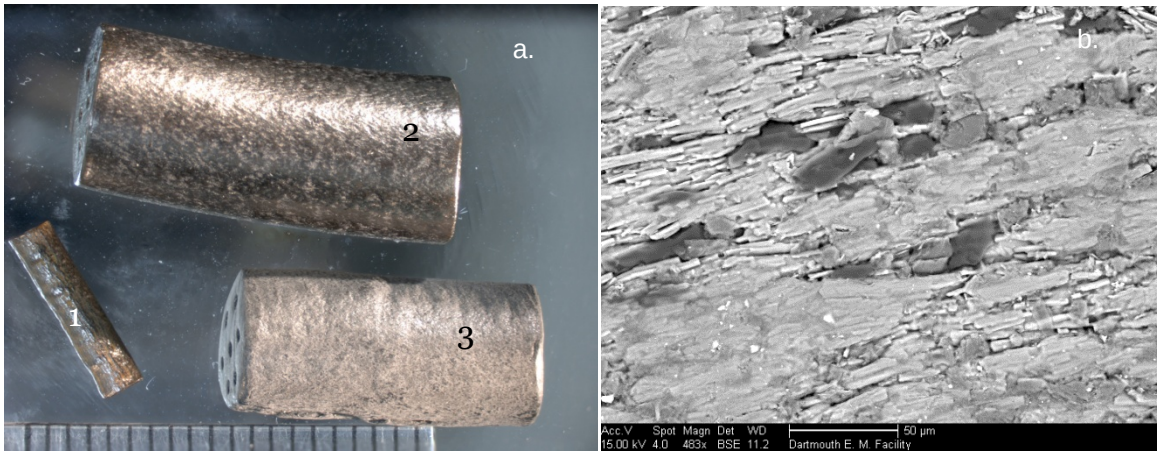

Figure 12. Triple-base propellants studied, (a) 1. M31, 2. M31A1 and 3. M31A2. (b) SEM image of M31A2 surface. Dark patches are the graphite coating, long crystals are NQ and the light grey smooth looking material is the NC and NG mix.

Thin sections cut perpendicular to the long axis of the propellants show that triple-base propellants are heterogeneous in appearance and brown to orange in color (Fig. 13a). The color is produced by 2-nitrodiphenylamine, a minor ingredient (1.5% by mass). The visual heterogeneity results because the 2-nitrodiphenylamine stains NC but not NQ. The NQ crystals look like round, grey circles at high magnification (Fig. 13b).

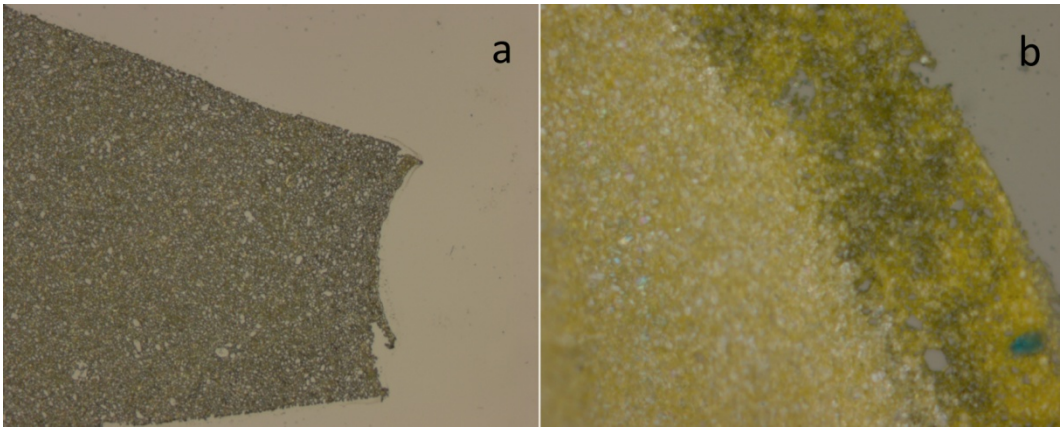

Figure 13. Thin section of M31 triple-base propellant viewed in reflected light.

We sectioned two unfired M31 propellants, one used in the drip tests and the second stored dry. Images of the sections in reflected, darkfield, and transmitted light (Fig. 14) show that the propellant used in the drip test appear to have lost mass; they have a raggedy looking interior surface. We think holes around the exterior surfaces of M31 grains formed when NQ

crystals dissolved during the drip tests (Fig. 15a). NQ readily dissolves as evidenced by transparent NQ crystals that form on a glass slide where water, that had wet the triple-base propellant, had evaporated (Fig.15 b and c).

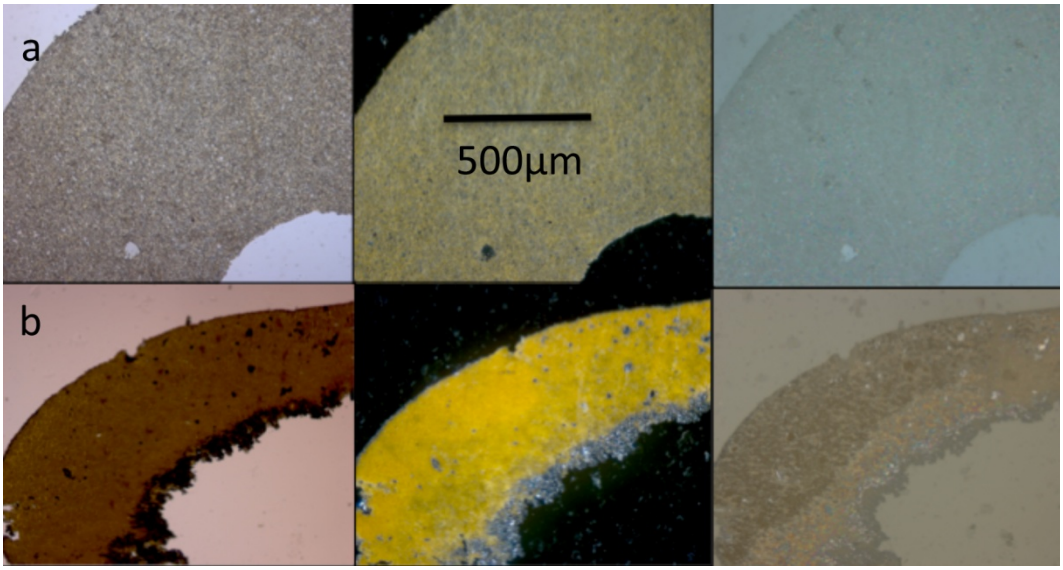

Figure 14. Reflected, dark field and transmitted light of (a) thin section of an M31 not exposed to water and (b) thin section of an M31 used in drip test.

Figure 15. Appearance of M31 thin section exposed to water: (left) dark field view of yellow NC+NG and missing NQ crystals; (center) image showing wetting front and NQ crystals that formed from water; and (right) close up of NQ crystals.

3.1.3 Scanning electron microscopy images

SEM images of propellant residues show that the residues have been heated to different degrees (Fig. 16). These images show two interesting things. First, during heating, the formation and release of gas creates pits on the residues surface (Fig. 16 and 17). Second, submicron metal grains, present in the propellant, become concentrated on the surface of the residue (Fig. 16 and 17).

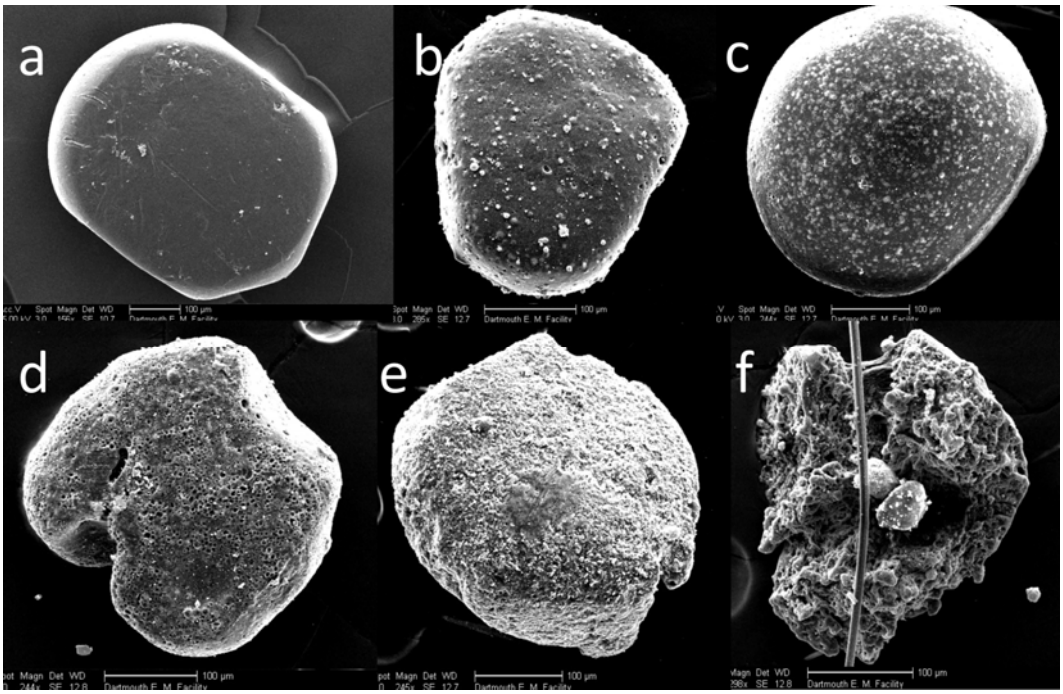

Figure 16. Images of a series of 9-mm propellant grains showing how the grains change with increased heating; (a) an unfired grain; (b) pits visible on surface; (c) surface has begun to bubble; (d) gas bubbles have opened larger holes on surface; (e) metals and other elements contained within the propellant are concentrated at the surface as the propellant burns; (f) breakdown of nitrocellulose structure.

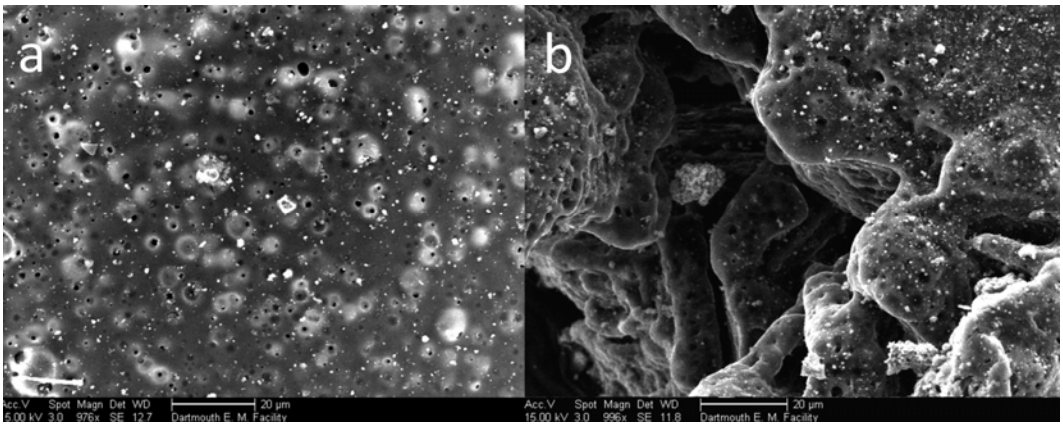

Figure 17. High magnification images of surfaces showing (a) the initiation of pits and (b) the bright metal particles that are concentrated on the residue surface.

SEM images of small arms' unfired propellants immersed in water for 5 months (batch test 1) showed little difference from those stored dry (Fig. 18) despite the loss of between 7 and 21% of their NG. The only difference was slightly smoother surfaces attributable to dissolution of constituent salts (e.g., sodium sulfate, calcium carbonate, potassium nitrate) present on their surfaces (Fig. 18).

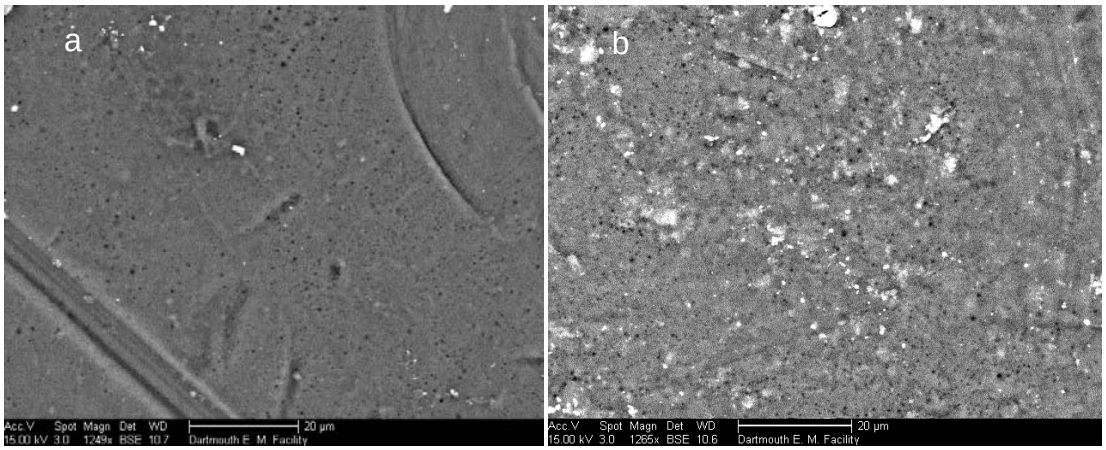

Figure 18. SEM image of WPR289 propellant used to fire 9-mm pistol: (a) surface of grain immersed in water for 5 months, (b) surface of a propellant grain not placed in water.

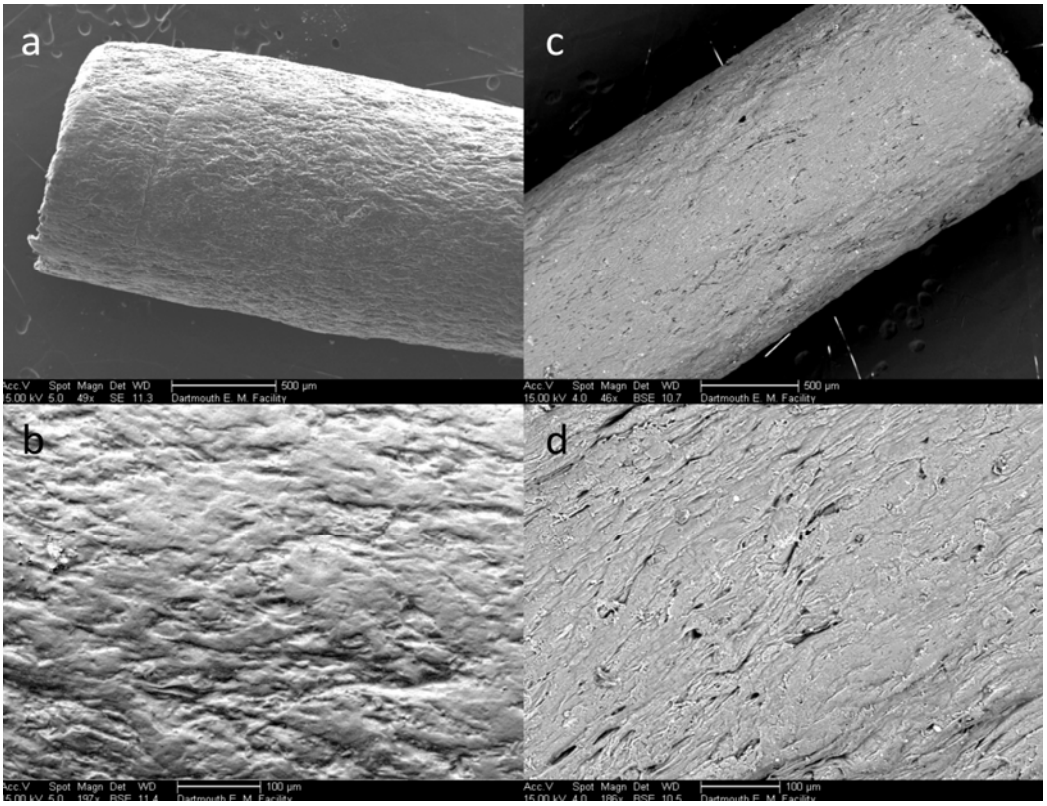

Figure 19. Images of the M1 propellant: (a) and (b) were not wetted; (c) and (d) were immersed in water for 500 days.

However, SEM images of propellants after they were immersed in water for 500 days (batch test 2) show clear changes to the surfaces of the grains. For example, the wet M1 single perforation grain had hollows between the ropey strands of NC, features not seen on dry grains (Fig. 19). The surface of the submerged 0.50-cal. grain had rough sections that look sponge-like and appear to extend into the grain (Fig. 20), features not seen on dry

grains. The M9 grain had deep holes in its surface where material was missing (Fig. 21). The M31 surface had lost much of its carbon coating and the outlines of dissolved NQ crystals could be seen over the entire surface of the grain (Fig. 22).

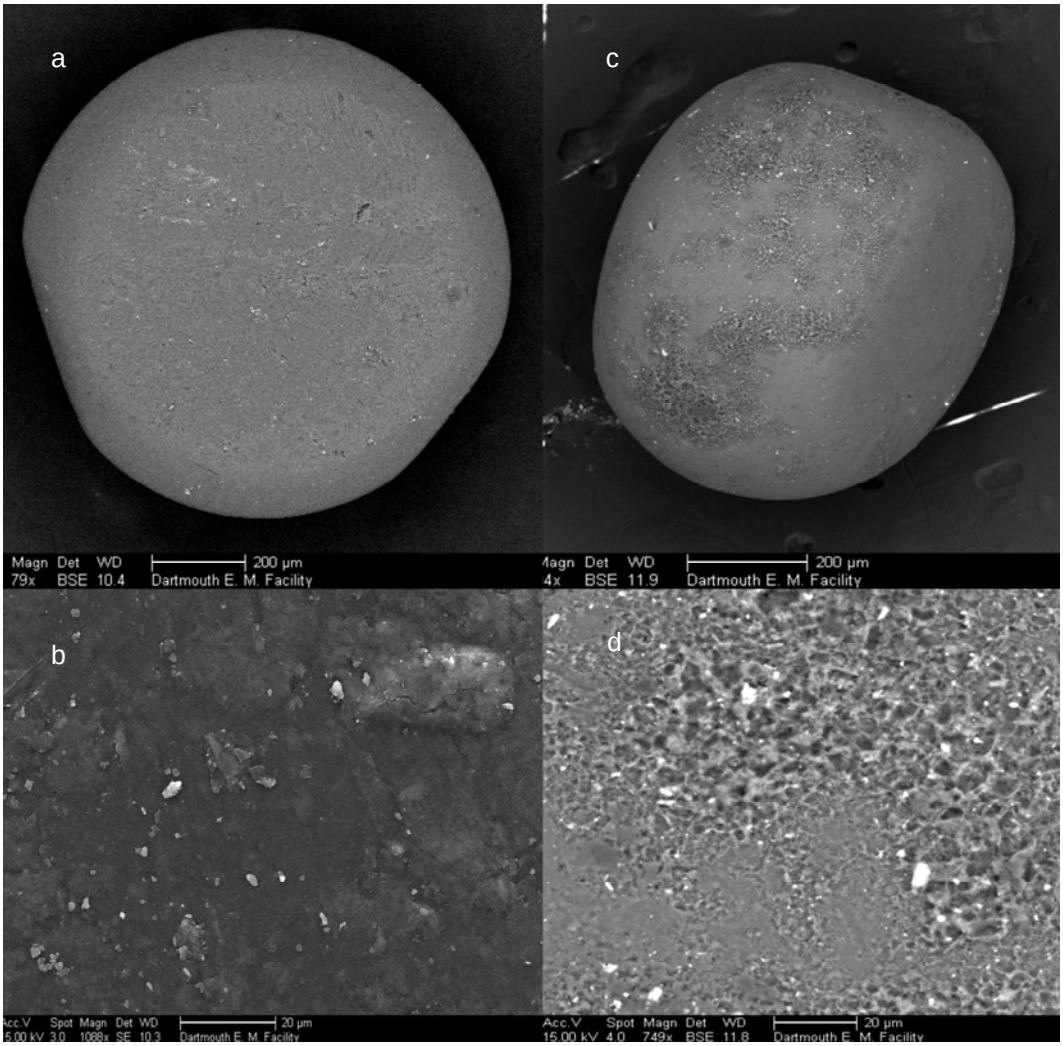

Figure 20. Images of unfired 0.50-cal. propellants; not wetted (a and b) and immersed in water for 500 days (c and d).

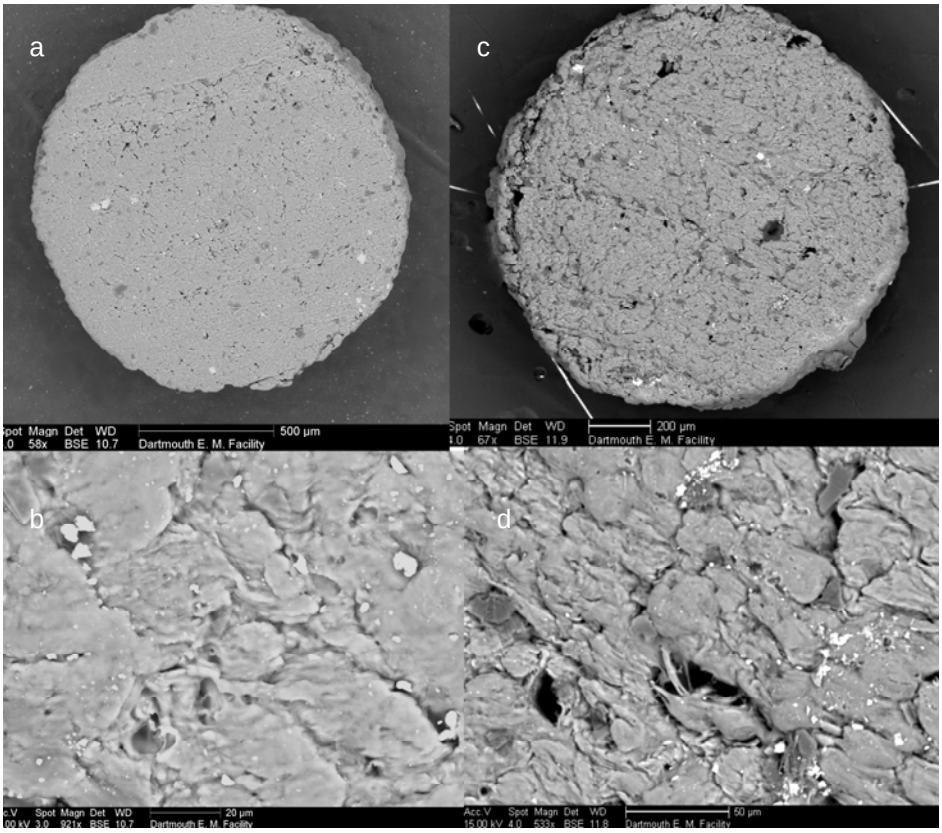

Figure 21. Images of unfired M9 propellants; not wetted (a and b) and immersed in water for 500 days (c and d).

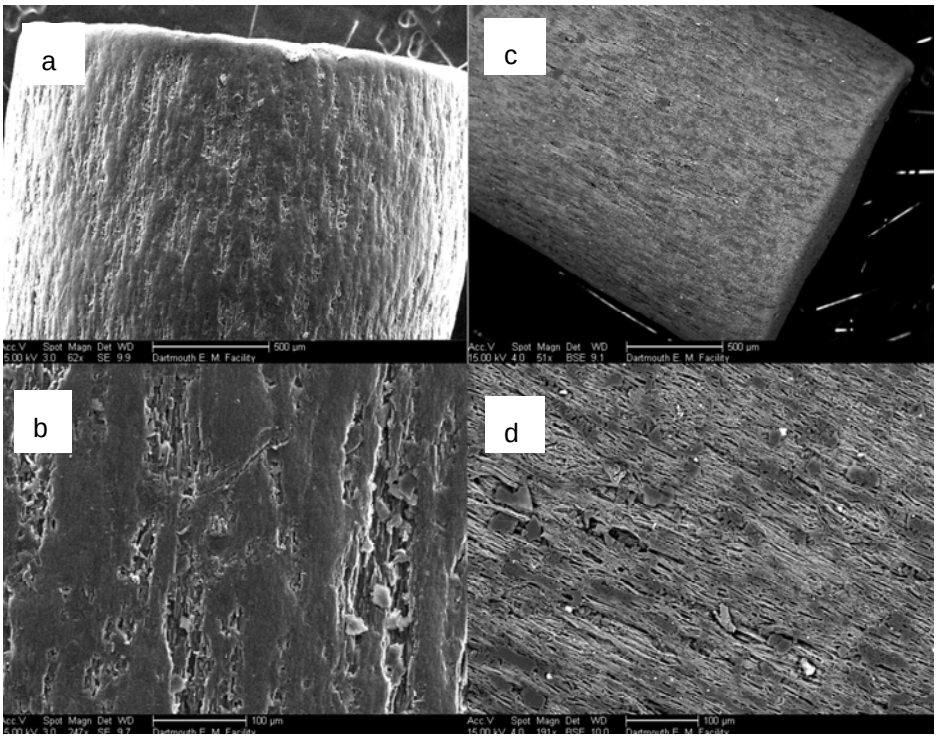

Figure 22. Images of unfired M31 propellants; not wetted (a and b) and immersed in water for 500 days (c and d).

3.1.4 Scanning transmission electron imaging and spectroscopy

We selected WPR289 (9-mm pistol) and M2 propellants for study because of their different NG content: WPR289 had 10% NG and 90% NC and M2 had 20% NG and 80% NC.

Energy-filtered images of WPR289 show a distinct, lighter colored zone near the graphite coated surface in an unfired grain used in the drip tests (Fig. 23). The width of this zone is ~10 µm. The propellant rim has a lower N/C ratio than the interior, consistent with the loss of nitroglycerin. The sharp boundary is also consistent with the behavior of NG in NC and in polymers, generally (Levy 1955). A study of diffusion of NG into NC propellants, a process used to manufacture extruded impregnated (EI) propellants, showed a sharp diffusion front (Levy 1955).

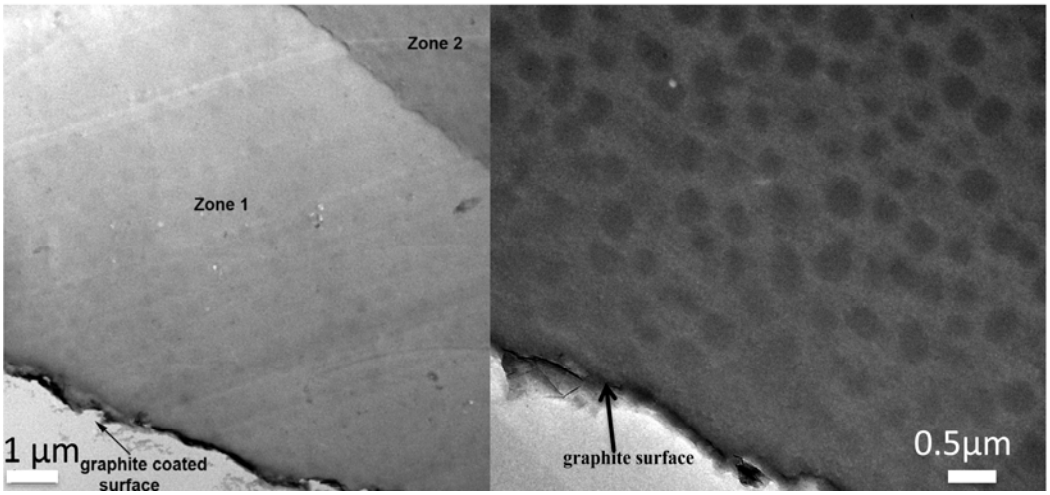

Figure 23. Energy loss image of sectioned unfired WPR289 propellant immersed in water (left) and not wetted (right). The thin graphite layer marks the surface of the propellant. Zones 1 and 2 seen in the left image are interpreted as a sharp diffusion boundary between NC lacking NG (1) and NC containing NG (2). We think the stippled pattern seen in both sections, but prominent in the right image, results from the manufacture of grains and is not NG.

Electron energy-loss spectroscopy (EELS) and energy-filtered images of the M2B HEDP propellant (Fig. 24) show compositional heterogeneities in C, N, and O abundances and distributions. The surface regions appear more homogenous than the interior. The images suggest that the interior of the propellant has two different and well-mixed phases with essentially identical compositions but slightly different densities. We also noted the presence of tiny bright spots in energy-filtered image that exhibit strong UV absorption at 207 nm (Fig. 25). Although NG absorbs well at 207 nm,

it also absorbs at shorter wavelengths and we suspect these spots may be constituent salts in the propellant.

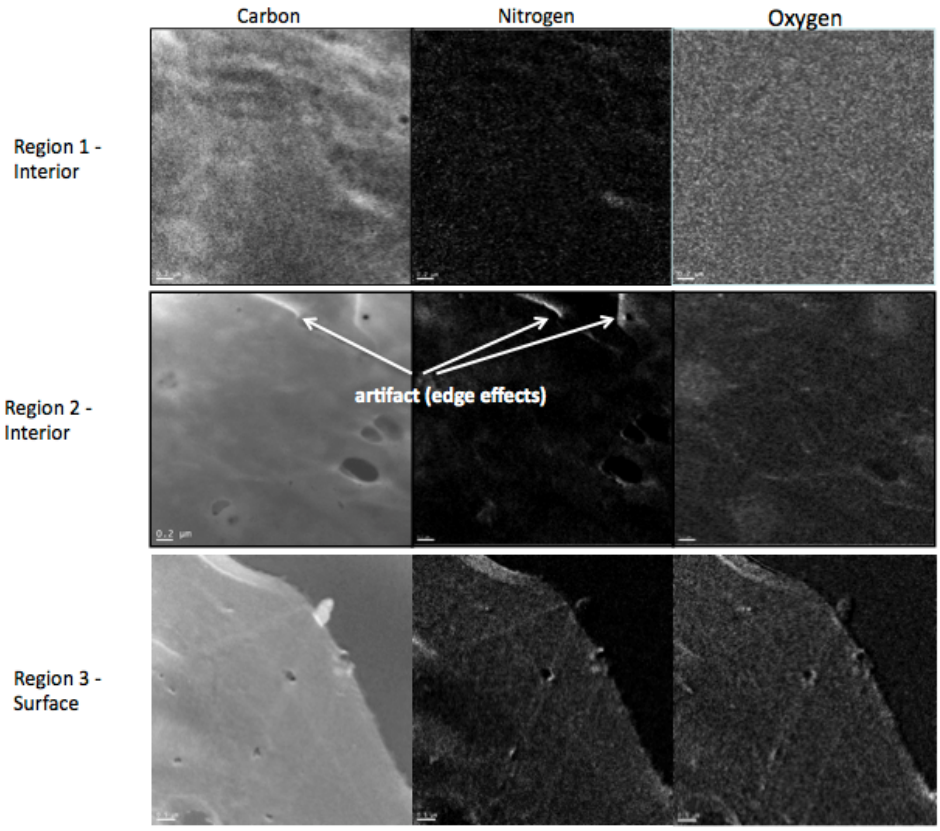

Figure 24. Energy loss maps made of the surface and interior regions of a sectioned M2 propellant.

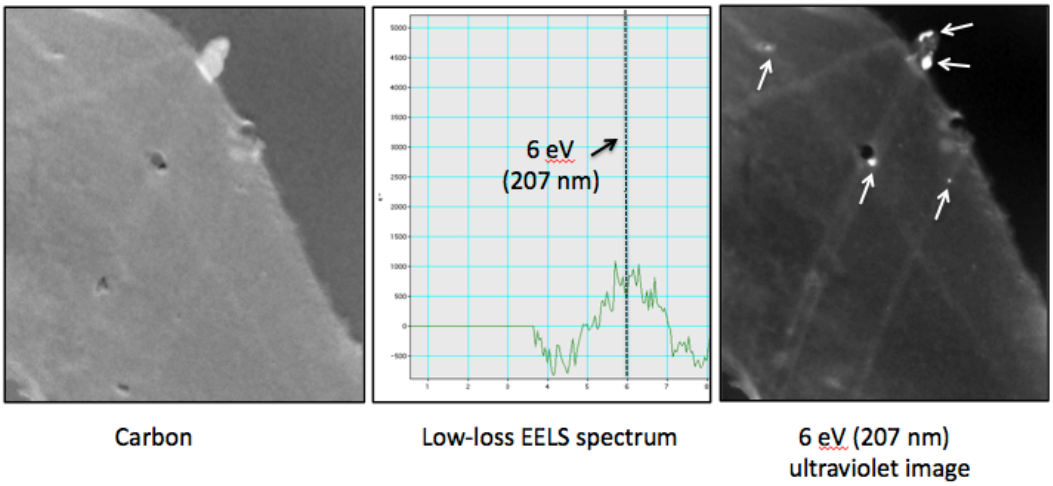

Figure 25. Figure showing an energy loss map for carbon (left), an EELS spectrum (center), and a map of the sample at 6eV showing very bright regions (right).

3.2 Laboratory drip and batch tests

The laboratory drip tests mimic field conditions on training ranges, where propellant residues are scattered on the soil surface and whose constituents are dissolved by precipitation. Here, the propellants were generally wet but could experience drying during the weekends when the syringe pumps stopped. The tests were similar to those successfully used to measure dissolution of explosives (Lever et al. 2005). We also ran batch dissolution tests on individual, unfired propellant grains (Table 2). These tests allowed us to investigate energetic loss from individual propellants, as compared to the multiple grains needed for the drip tests. The fixed water volume and weeklong sampling intervals allowed the dissolved energetic concentrations to build up sufficiently to measure. The tests also let us study many different types of propellants simultaneously.

Table 2. Solubility (mg L^{-1} at 20 to 25 °C) and molecular formulae for energetic compounds studied.

	Solubility	Mol. formula	O/C	N/C
Cellulose	NA	$C_6H_{10}O_5$	0.83	0
Nitrocellulose	NA	$C_6N_8H_2O_9$	1.5	1.33
2,4-DNT	270[1]	$C_7H_6N_2O_4$	0.57	0.29
Nitroglycerine	1500[2]	$C_3H_5N_3O_9$	3	1
Nitroguanidine	2600[3]	$CH_4N_4O_2$	2	4

[1]Phelan and Barnett (2001); [2]Yinon (1999); [3]Haag et al. (1990).

3.2.1 Single-base propellants

Single-base propellants containing 2,4-DNT are used to fire artillery, mainly 105- and 155-mm rounds from howitzers. Figure 26 shows the percentage of DNTs dissolved during drip and batch tests on a variety of M1 propellants. Note that for the unfired grains, the dissolution rate was quite linear and that even after 500 days the maximum DNT loss is only 10%. The larger propellant grains lost more DNT than the smaller grains but a smaller percentage of what they contained (Table 3). The residues from M1 seven-perforation propellant (12 fibers) lost the highest percentage of their 2,4-DNT owing the their large surface to volume ratios, although the total mass was small. The mass loss curve for the residues was not linear—it rose rapidly initially, but after day 20 it becomes more linear, still having a positive slope (Fig. 26).

Table 3. Mass balance calculations for single-based propellants used in the drip and batch experiments.

Propellant single-base-2,4-DNT 10±2 % DNT	Mass initial (*I*) (mg)	Mass final (*F*) (mg)	Initial – final (*I*–*F*) (mg)	Mass diss. (*D*) (mg)	Mass ext. (*E*) (mg)	% Mass balance ([*F*+*D*]/I)× 100	% 2,4-DNT Recovered ([*D*+*E*]/*Exp*) ×100	%2,4-DNT Measured* 2,4-DNT /*Prop* ×100
M1-seven perforations								
M1-7 unfired extracted	115.3				11.21			9.72
M1-7 fired extracted	3.74				0.30			8.01
M1-7 (drip)	113.3	112.9	0.4	0.20		100		
M-7 fired (drip)	3.9			0.07	0.17		75.38	
Weathered-A (batch)	245.6	243.5	2.1	0.43		99		
Weathered-B (batch)	238.6	237.3	1.3	0.34		100		
Weathered-C (batch)	238.4	237	1.4	0.12		99		
M1-one perforation								
M1 unfired extracted	30.7				2.78			9.06
M1-1A (batch-unfired)	10.7	10.5	0.2	0.10		99		
M1-1B (batch-unfired)	10	9.8	0.2	0.11		99		
M1-1C (batch-unfired)	10	9.8	0.2	0.10		99		

From Technical manuals, * analyzed at CRREL. *F* = final mass, *D* = dissolved mass, *I* = initial mass, *Exp* = expected, *Prop* = mass of propellant.

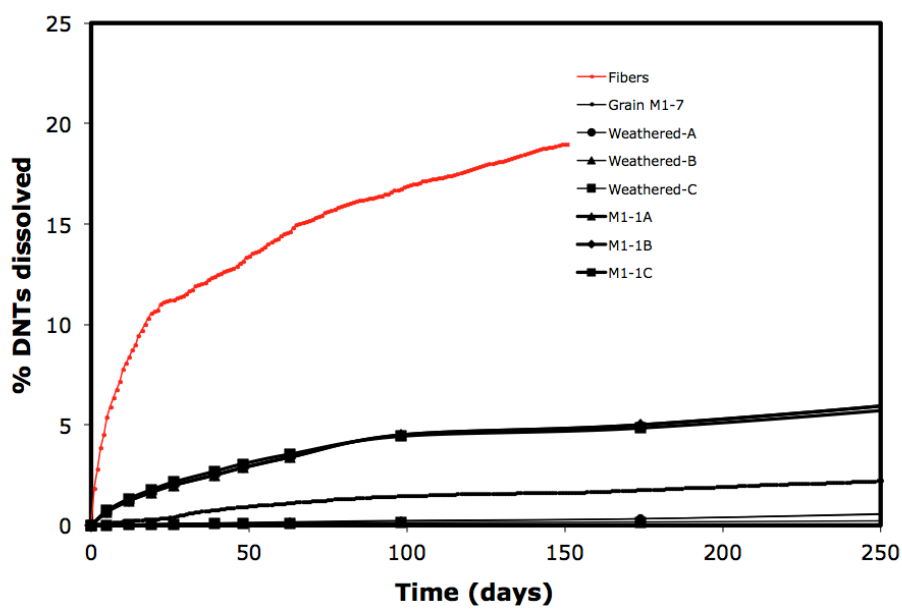

Figure 26. Percentage of 2,4-DNT and 2,6-DNT dissolved into water from unfired seven perforation M1 propellant grains (black) and from fired residues (red).

3.2.2 Double-base propellants

Double-base propellants are the most common and are used to fire small arms, mortars, and rockets. In both drip and batch tests, unfired double-base propellants show initial rapid dissolution of NG followed by much slower dissolution. Most double-base propellants lost NG in proportion to how much NG they contained. For example, the M9 propellant with 40% NG lost a greater percentage of its NG than a propellant that contained less (Fig. 27). We found that the amount of NG dissolved was a function of the NG/NC ratio in the propellant (Fig. 28). Clustering of the data using this normalization suggests that NC binds 10 to 20% of the NG and that any extra NG is not well retained.

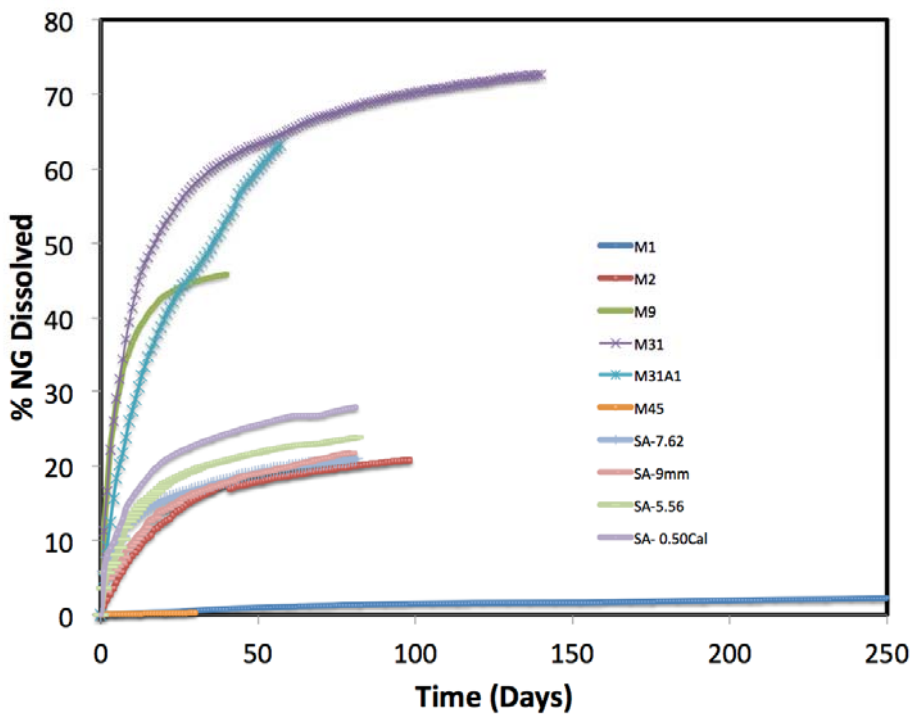

Figure 27. Percentage of NG dissolved (mg dissolved/mg present in propellant) for a variety of double-based propellants. We show the single-base M1 for comparison.

Exceptions from this trend are the ball propellants, used to fire small arms, and the M45 propellant, used to fire mortars from the Stryker. The ball propellants all contain ~10% NG, yet variable amounts of NG are dissolved independent of their NC content. The M45 propellant also contains 10% NG, yet it loses less than 1% during both the drip and batch tests (Table 4, Fig. 28). The M45 is a squat grain with a central perforation. We expected the central perforation to increase its surface area and, therefore,

increase its NG loss. In the case of M45, we speculate that the nitrocellulose was not fully nitrated when it was manufactured so that the NG effectively binds to the NC.

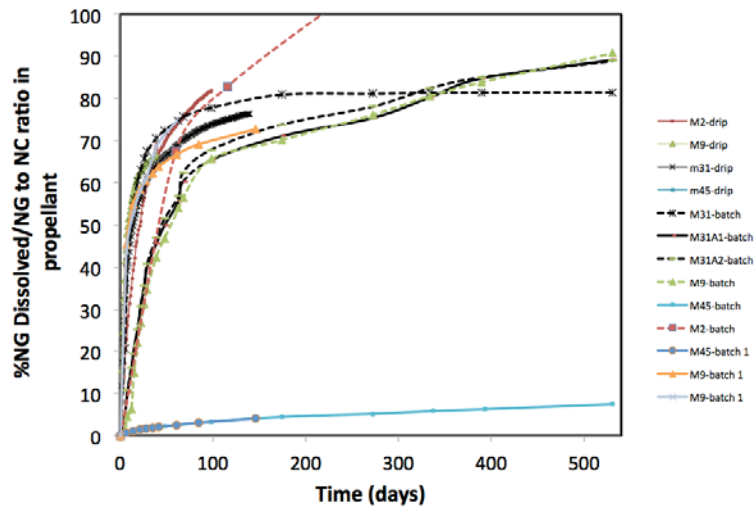

Figure 28. Plot showing the % NG dissolved normalized by the NG/NC ratio versus time. All of the data from NG containing propellants, except for the small arms, are plotted on this figure.

Table 4. Mass balance calculations for double-based propellants used in the drip and batch experiments.

Propellant-NG Double–base NG	Mass initial (*I*) (mg)	Mass final (*F*) (mg)	Initial–final (mg)	Mass diss. (*D*) (mg)	Mass ext. (*E*) (mg)	% Mass balance ([*F*+*D*]/I)× 100	% NG recovered ([*D*+*E*]/Exp)× 100	% NG measured† (*NG/I*) ×100	% NG expected**
M2-one perforation									19.5±1
M2 extracted (F)	3.33				0.64			19.25	
M2C (drip-F)	29.49	24.55	4.94	1.13	3.58	87	83		
M2D (drip-F)	4.56	3.97	0.59	0.19	0.61	91	91		
M2A (batch-F)	0.3	0.2	0.1	0.01	0.03	71	76		
M2B (batch-F)	0.4	0.3	0.1	0.02	0.05	80	86		
M2C (batch-F)	0.3	0.3	0	0.02	0.04	106	106		
M9 solid grain									40 ± 1.5
M9 extracted (U)	117.3				46.00			39.22	
M9 extracted (F)	7.3				1.47			20.14	
M9 (drip-6-U)*	7.2	3.53	3.67	1.39	0.71	68	73		
M9 (drip-2-U)	2.6	2.08	0.52	0.49	0.46	99	91		
M9 (batch-U) A	1.3	1.07	0.23	0.32		107	sent to LLNL		
M9 (batch-U) B	1.3	1.13	0.17	0.33	0.20	112	101		
M9 (batch-U) C	1.1	1.05	0.05	0.28	0.18	121	105		

Propellant-NG Double–base NG	Mass initial (*I*) (mg)	Mass final (*F*) (mg)	Initial–final (mg)	Mass diss. (*D*) (mg)	Mass ext. (*E*) (mg)	% Mass balance ([*F*+*D*]/I)× 100	% NG recovered ([*D*+*E*]/Exp)× 100	% NG measured† (*NG*/*I*) ×100	% NG expected**
M45-one perforation									**10 ± 2**
M45 extracted (U)	4.47							9.95	
M45 extracted (U)	4.79							10.25	
M45 extracted (U)	3.85							9.57	
M45 extracted (F)	4.1				0.36			8.89	
M45 extracted (F)	13.71							8.9	
M45 (drip-F)	14	13.71	0.29	0.01	0.85	98	61		
M45 (batch-5 U)	19.3	19.3	0	0.02	1.88	100	98		
WPR289 (9-mm)									**12–18**
WPR289 (ext. U)								12.20	
WPR289 (ext. F)	48.75				6.24			12.80	
WPR289 (drip-F)	38.6	30.6	8	0.22	5.94	80	125		
WPR289 (drip-U)	14.5	11.1	3.4	0.29	1.07	79	77		
WC844 (5.56mm)									**8–11**
WC844 (ext. U)								9.90	
WC844 (ext. F)	54				4.4			8.10	
WC844 (drip-F)	68.2	62	6.2	0.33	5.62	91	97		
WC844 (drip-U)	32.8	31.2	1.6	0.65	2.09	97	103		
WC846 (7.62mm)									**8–11**
WC846 (ext. U)								10.20	
WC846 (ext. F)	47				3.70			7.90	
WC846 (drip-F)	17.9			0.10	lost				
WC846 (drip-U)	17.7			0.34	1.27		89		
WC860 (0.5 cal)									**8–11**
WC860 (ext. U)								9.70	
WC860 (ext. F)	61.5				4.80			7.80	
WC860 (drip-F)	57	49.8	7.2	0.27	4.72	88	112		
WC860 (drip-U)	20.2	19.1	1.1	0.47	1.21	97	86		
WC860 (batch-U)	2.1	2.1	0	0.08	0.12	104	97		
AT-4-sheet									**36.5–39.5**
AT-4 ext. F	0.45				0.16			35.56	
AT-4 ext. F	71				26.00			36.62	
AT-4 drip F&W	3.84	3.52	0.32	0.40	0.63	102	75		
AT-4 drip F	7.97	5.31	2.66	1.78	0.86	89	92		
AT-4 drip F	6.4	4.21	2.19	1.09	0.80	83	82		

*Four of 6 initial grains recovered. E = extracted, U = unfired, F = fired, W = weathered, *F* = final mass, *D* = dissolved mass, *I* = initial mass, *Exp* = expected mass, †measured at CRREL, ** from propellant manual.

We collected both fired residue and unfired grains from all the small arms propellants. Concentrations of NG in the unfired grains were within the variability given in the technical manual, whereas the fired residues contained about 80% of the NG on a mass basis (Table 3). Figure 29 shows that more NG was dissolved from the unfired propellants (15–20%) than from their residues (3–7%). For the unfired propellants, the shape of the cumulative mass loss versus time curves were consistent with rapid loss of the NG from the surface of the grain, followed by slower diffusion of the NG from the interior of the grain. The high aqueous solubility of NG suggests that NG could be rapid dissolved by contact with water. If NG existed as fine liquid droplets within an NC matrix rather than as dispersed molecules, droplets at the grain surface would be in direct contact with water whenever the grain was wet. Once this outer layer of liquid NG was depleted, NG would need to diffuse through the NC matrix to reach the water, with considerably lower diffusivity (~10–14 $cm^2 s^{-1}$). Late time dissolution would thus be limited by molecular diffusion.

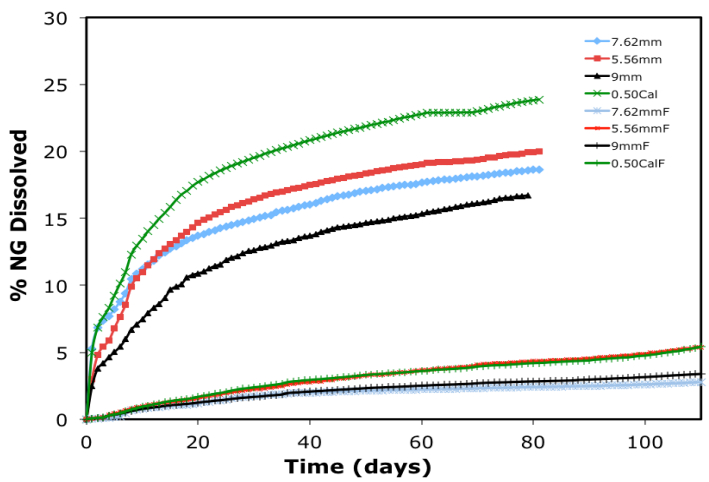

Figure 29. Percent NG dissolved versus time for unfired and fired (F) small arms propellants.

This concept also qualitatively accounts for the much lower dissolution rates observed for fired grains. Firing likely burns or volatilizes surface NG droplets, and we estimate that volatilizing NG from a surface layer about 5% of the thickness of the fired particle would lower the NG concentration by 20%, the difference we measured between fired and unfired propellants. SEM images of the small arm propellants show pits that are about 5 µm in diameter and similarly deep (Fig. 16), consistent with the depth needed to produce the drop in concentration. All dissolution of NG from fired grains would thus be limited by molecular diffusion. Indeed the data

for fired grains did not show the abrupt roll-off characteristic of the unfired grains, but were similar to the latter's late-time dissolution rates. The linear shape of the cumulative mass loss curves, the slower dissolution rate of NG from the fired residues, and their 20% lower NG concentration compared to unfired grains are explained if NG near the surface is burned during firing.

The shapes of the mass loss curves for most unfired double-base propellants were different from those seen for single-base, DNT-containing propellants: they were much steeper initially and then flattened out. We think that this results because NG is added as a liquid to the NC during manufacture. Depending on the nitration level of the NC, variable amount of NG are attached to the NC. Any excess NG migrates toward the surface of the grain where water contacting the liquid NG removes it from the propellant.

Dissolution from fired versus unfired are also very different for single and double-base propellants. For the single-base propellants, the fired residues lose a larger percentage of 2,4-DNT than do the unfired grains. Furthermore, the %mass loss for the residues was much higher at the beginning of the tests than at the end. We think this occurred because the residues were small and had much larger surface to volume ratios, allowing the 2,4-DNT to diffuse to the surface. For double-base propellants, except for the M45 whose mass loss was similar to single-base propellants, the unfired double-base propellants lost a higher percentage of their energetics (15–20%) than their fired residues (3–7%). This suggests that the NG from the outer surface of the double-base propellants is easily lost relative to 2,4-DNT, and that once lost, the rate at which NG diffuses out to the surface is slower than the 2,4-DNT diffusion rate.

3.2.3 Triple-base propellants

Like the single-base propellants, triple-base propellants are also used to fire artillery. We ran drip tests for 140 days on eight individual M31 grains, four at 0.5 mL hr^{-1} and four at 1.0 mL hr^{-1} flow rates. During this time the M31 propellants lost an average of 6.32±0.22 mg of NG (or ~73%) and 3.23±0.55 mg of NQ (or ~13%). The mass loss scaled linearly with the drip rate, so the data from the 0.5 and 1.0 mL hr^{-1} flow rates were plotted together (Fig. 30). Batch tests run on three M31 grains showed similar mass losses, 6.87 ± 0.23 mg NG and 3.03 ± 0.38 mg NQ (Fig. 31—black curves), although the batch tests ran for almost four times as long. Note that most

of the NG was dissolved rapidly, as was seen in the double-base propellants. The NQ also dissolves rapidly initially but the late time dissolution for the NQ was smaller than that for NG.

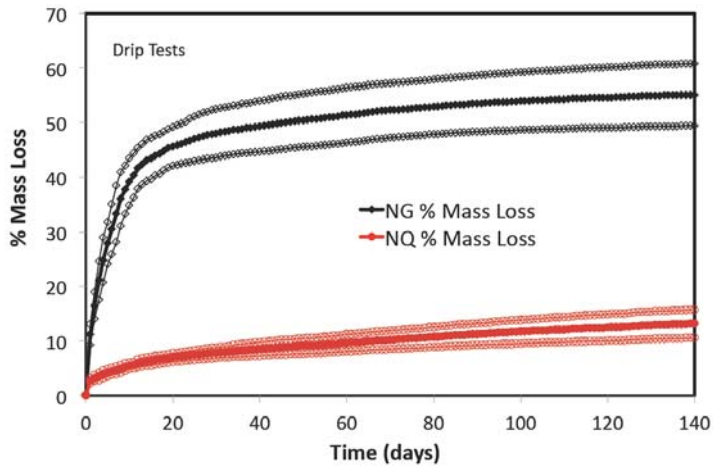

Figure 30. Drip test results showing the percent NG and NQ dissolved (Ave. ± 1 sigma, *n* = 8) versus time for unfired M31 single-perforation propellants.

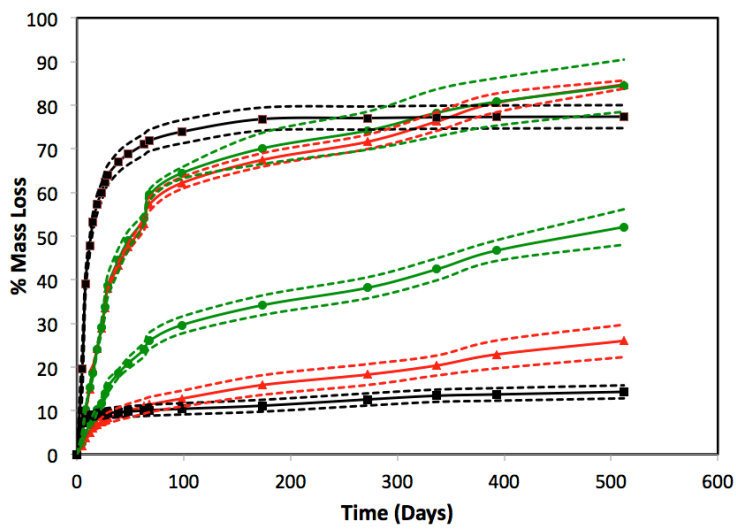

Figure 31. Batch tests results showing the percent NG and NQ dissolved (Ave. ± 1 sigma, *n* = 3) versus time for unfired M31 (black), M31A1 (red) and M31A2 (green) triple-base propellants. The lower of the pair of curves is always NQ.

Although there is more NQ than NG in the M31 propellant (55 vs. 20%), and NQ is more soluble than NG (2600 vs. 1500 mg L^{-1} at 20° C, Haag et al. 1990; Yinon 1999), both by mass and by percentage, more NG was dissolved than NQ. We think this is because, during manufacture of the propellant, NG is added as a liquid, whereas NQ is mixed in as a solid. Tests to

measure how well the components in triple-based propellants were mixed (Yazici and Kalyon 1998) showed that NG is not as well mixed as NC and NQ and that there is more NG near the surface and less in the interior of the grain. These authors suggest that, after a certain threshold (27%NG for a 12.2% nitrated NC), the NG does not effectively bond to the NC and it migrates to the propellant surface as a low viscosity fluid. This migration would make liquid NG available near the surface of the propellant where it would be removed when in contact with water. The NQ on the other hand would have to dissolve to leave the propellant.

The M31A1 and M31A2 propellants are similar in composition to the M31 (54% NQ and 20% NG) but are larger, cylindrically shaped grains with seven perforations (Fig. 12a). Drip and batch tests run on M31A1 again showed higher losses of NG (80%) than NQ (20%) (Fig. 31). The multi-perforated grains showed a different dissolution pattern in that the original loss of NG and NQ was less abrupt and the late time dissolution rates for both NG and NQ were higher than for the single-perforation grains. Both these multi-perforated grains were large (1.4- and 0.87-g masses; Table 4) and had lower surface to volume ratios.

3.2.4 Mass balance

Tables 3–5 list the initial and final masses of the propellants tested in the drip and batch tests along with the masses of energetic compounds dissolved and extracted at the ends of the tests. The masses of propellants or residues extracted to determine the percentage of energetics initially present in the propellant are underlined. We calculated a percent mass balance for all the propellants by summing the final mass and the dissolved mass and dividing by the initial mass. For the double-base and triple-base propellants, we also calculated an energetics percent mass recovery by adding the dissolved and the extracted energetic compounds and dividing by the initial mass of energetics. The latter value was determined by multiplying the initial mass of the propellant or residue by the fraction of energetic extracted from a similar sample.

Table 5. Mass balance calculations for triple-based propellants used in the drip and batch experiments.

Propellant— Triple Base NQ+NG	Mass initial (*I*) (mg)	Mass final (*F*) (mg)	Initial – final (mg)	Mass diss. (*D*) (mg)	Mass ext. (*E*) (mg)	% Mass balance ([*F*+*D*]/*I*)× 100	% NG recovered ([D+E]/*Exp*)× 100
M31-one hole				NG+NQ	NG+NQ		NG
M31-1 (drip-U)	45.61	35.2	10.41	9.90	9.40	99	90
M31-2 sent to LLNL							
M31-3 (drip-U)	45.9	35	10.9	9.54	9.34	97	85
M31-4 (drip-U)	45.56	34.6	10.96	9.52	9.35	97	80
M31-5 (drip-U)	42.7	30.9	11.8	10.68	8.98	97	84
M31-6 (drip-U)	44.24	34.4	9.84	8.74	9.42	98	87
M31-7 (drip-U)	45.21	34.8	10.41	9.18	9.68	97	86
M31-8 (drip-U)	43.28	32.3	10.98	9.84	9.53	97	88
M31-A (batch-U)	46	35.1	10.9	10.04		98	76
M31-B (batch-U)	46.1	35.2	10.9	10.39		99	80
M31-C (batch-U)	48.2	36.3	11.9	11.19		99	76
M31A1-seven holes							NG
M31A1-A (drip-U)	1450	1351.4	98.6	198.94		107	65
M31A1-B (drip-U)	1400	1261.3	138.7	242.64		107	80
M31A1-C (drip-U)	1430	1308.6	121.4	242.17		108	78
M31A1-D (drip-U)	1320	1203.9	116.1	215.22		108	74
M31A1-A (batch-U)	1392.2	1119.1	273.1	424.16		111	85
M31A1-B (batch-U)	1417.8	1164	253.8	394.17		110	84
M31A1-C (batch-U)	1404.5	1104.3	300.2	449.07		111	86
M31A2-seven holes							
M31A2-A (batch-U)	875.3	510.1	365.2	413.25		105	87
M31A2-B (batch-U)	866.2	526	340.2	380.40		105	89
M31A2-C (batch-U)	879.3	530.1	349.2	365.39		102	78

The percent mass balances for the single-base propellants average 99±1% (Table 3), for the double-base propellants 93±13% (Table 4), and for the triple-base propellants 103±5% (Table 5). The percent mass balances are generally good. Low mass balances resulted if either water or propellant samples were lost. For example, the glass frit in our drip tests clogged from time to time, causing the funnels to overflow, thereby losing both water and propellant grains. Small propellants were subject to loss in this manner, which resulted in low percent mass balances (e.g.. the M9 sample where six grains were tested but only four recovered). High mass balances also were measured and these occurred mainly for large propellants. For example, the M31A1 propellants are ~10% high. Although we waited to

mass the grains for about a week after the end of the tests, we think the perforations in these grains still contained some residual water. Owing to the residual water, their final masses were high and their initial minus final mass was smaller than it should have been.

For the double-base propellants, the %NG balance average is 91±15%, a value that seems reasonable given that we do not know the exact concentration of NG in our starting materials. For example, for the sample that had the highest value, 125% (WPR289, fired-9mm residue), the %NG would vary between 133 and 89% depending on if 12 or 18% where used as the starting composition—the range given for this propellant.

We calculated the %NG and NQ balance for the single perforation M31 grains but had difficulty extracting these samples. The energetic balance for the seven M31 grains averaged 78±4%, the NG recovered was 86±3%, and the %NQ 47±3%. As the NQ is not as soluble as NG in ACN, we think that the transparent NQ crystals remained unnoticed in the bottom of the vial. A better extraction method is needed for triple-base propellants.

3.3 Diffusion modeling of NG from small arm propellants

Lever et al. (2005) and Taylor et al. (2009a, b) showed some success in modeling dissolution of particles of high explosives exposed to rainfall. In those cases, explosive at a particle's surface are in direct contact with liquid water, and as they dissolve the particle becomes smaller. However, dissolution of 2,4-DNT, NG, and NQ from propellant grains is quite different. The NC is not soluble and we needed to learn if the energetic components were transported via molecular diffusion through an effectively solid NC matrix or whether water can penetrate the matrix allowing the NG to diffuse through tortuous water channels to the grain's surface. Our laboratory data on cumulative dissolved mass loss versus time cannot differentiate between these two mechanisms and we found no data on these processes in the literature. We focused our modeling effort on understanding NG loss, as NG is present in many propellants, including triple-base propellants. For simplicity we chose the small arms propellants and we modeled diffusion through a solid matrix. We modeled both constant diffusion and variable diffusion.

First, we modeled propellant dissolution as diffusion through a solid matrix, using simple grain geometries and a constant diffusion coefficient. Figure 32 shows model results for the solid diffusion model applied to

small arms propellants, both from batch tests on single grains and drip test on many grains.

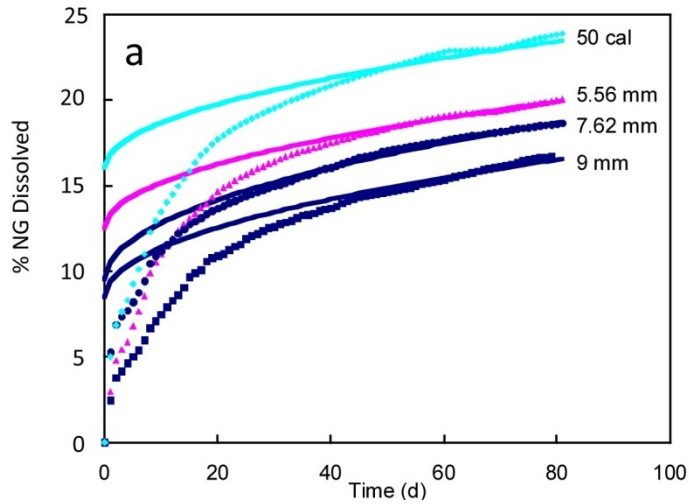

a. Batch tests (single grain).

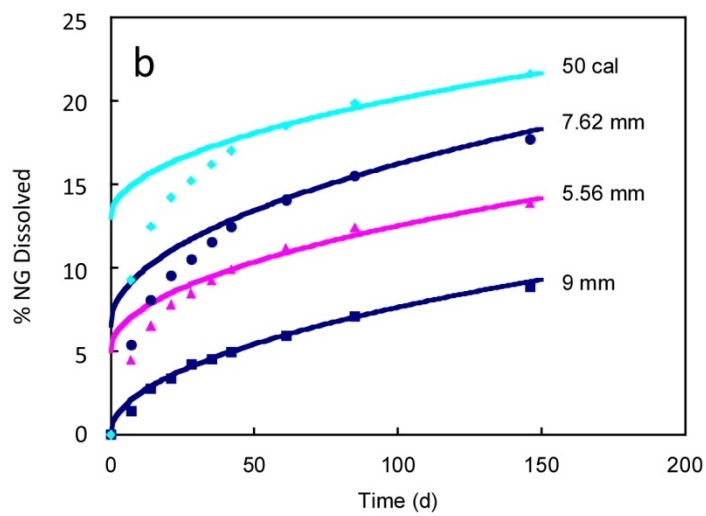

b. Drip tests (many grains).

Figure 32. Laboratory data from batch tests (single grain) and drip tests (many grains) compared with model predictions (solid lines) of solid-phase diffusion of NG from spherical NC grains. We fit the model results to the long-term trends in the data to obtain diffusion coefficients. Initial dissolution rates are higher than predicted for spherical particles, and we are investigating effects of grain shape and surface roughness.

The model assumes spherical particles of equal mass to that of the propellant grains. We fit the model results to the long-term trends (tail slopes) in the data to obtain diffusion coefficients. The diffusion coefficients are dif-

ferent for each propellant type (9 mm = 3.20×10^{-14} cm² s⁻¹; 5.56 m = 5.90×10^{-14} cm² s⁻¹; 7.62 = 1.00×10^{-13} cm² s⁻¹; and 0.50 cal = 1.20×10^{-13} cm² s⁻¹) but the same for the two tests on the same propellants. The results suggest that dissolution is similar to diffusion from a sphere as time progresses. However, dissolution rate is higher at early times than diffusion from a sphere.

The results found by Levy (1955) suggested that concentration-dependent diffusion of NG from the NC matrix could control the NG dissolution rate. To test this, we examined the effect of concentration-dependent diffusivity compared with constant diffusivity, the role of grain geometry (spherical vs. cylindrical), and the influence of wet/dry cycling compared with constant wetting.

The governing diffusion equation is

$$\frac{\partial c}{\partial t} - \nabla \bullet (D\nabla c) = 0 \tag{3}$$

where $c(x,t)$ is the time-dependent NG concentration within the grain and D is diffusivity (possibly concentration dependent).

We assume that the NC matrix is isotropic with respect to NG diffusion. We also assume that the initial concentration within the grain is uniform, $c(x,0)=c_0$, and that diffusion of NG into the surrounding water is rapid relative to diffusion through the solid NC matrix. This latter condition is equivalent to specifying $c = 0$ on the grain boundary when seeking analytical solutions (e.g., spherical grain immersed in water). However, for stable numerical solutions and to examine the role of wet/dry cycling, we found it best to prescribe the flux, $q(x,t)$, along the boundary:

dry grain
$$q = -D\nabla c \bullet \mathbf{n} = 0 \tag{4}$$

wet grain
$$q = -D\nabla c \bullet \mathbf{n} = h(c - c_w) \tag{5}$$

The condition set up in eq 4 prevents NG from leaving the grain when it is dry, although NG can still diffuse within the grain. We may simplify the condition set up in eq 5 by assuming NG concentration in the water is

small relative to the surface concentration, $c_w << c$, and that the mass-transfer coefficient, h, is large such that diffusion within the grain controls the mass flux into the water.

Crank (1975) and Skelland (1974) present analytical solutions for unsteady, one-dimensional diffusion through spheres, slabs, and cylinders with constant diffusivity, D_o, uniform initial concentration, c_o, and constant surface concentration. These all take similar form as infinite series for concentration profiles and cumulative mass fluxes. We focus on the latter because they equate to the cumulative dissolved NG mass measured during dissolution experiments. For a sphere of radius a, the fractional mass loss to time t is given by

$$\frac{M_l}{M_\infty} = 1 - \frac{6}{\pi^2}\sum_{n=1}^{\infty}\frac{1}{n^2}\exp\left(-D_0 n^2 \pi^2 t / a^2\right) \tag{6}$$

where M_∞ is the ultimate mass loss, where the total NG mass within the grain is M_0. A two-term expansions of eg 6 converges well for short dimensionless time, $\tau = D_{ot}/a^2$:

$$\frac{M_l}{M_0} = \frac{6}{\sqrt{\pi}}\tau^{1/2} - 3\tau \tag{7}$$

Truncation error in eq 7 is less than 0.1% for $\tau \leq 0.15$ or equivalently $M_l/M_0 \leq 0.86$, which exceeds the fractional mass loss encountered for all grains tested. Equation 7 approximates the fractional mass loss for a spherical grain with constant diffusivity immersed continuously in water.

To investigate the roles of gain shape, concentration-dependent diffusivity, and wet/dry cycling, we discretized eq 3–5 using the finite element method (FEM) for the spatial variables and the finite difference method for time. The simple geometries reduce the problem dimensions. Pitt (2011) describes the numerical approach and its validation; we summarize the key points here.

We apply to eq 3 the standard Ritz-Galerkin approximation (e.g., Brenner and Scott 1994) and arrive at a system of ordinary differential equations in time:

$$[M]\frac{\partial C}{\partial t} + [K(C)]C + h[M_{\partial\Omega}]C = 0 \tag{8}$$

where

$[M]$ = mass matrix
$[M_{\partial\Omega}]$ = mass matrix for the boundary terms
$[K(C)]$ = concentration-dependent system matrix
$C(t)$ = vector of time-dependent nodal unknowns.

Note we have assumed that $c_w = 0$ and can switch between no-flux and flux boundary conditions (eq 4, 5) by simply setting h to zero or some large value.

For time integration, we use a standard second-order Crank-Nicholson scheme:

$$\begin{aligned}&\left([M]+k[K(C^{n+1})]+kh^{n+1}[M_{\partial\Omega}]\right)C^{n+1}\\&=\left([M]-k[K(C^{n})]-kh^{n}[M_{\partial\Omega}]\right)C^{n}\end{aligned} \tag{9}$$

where n denotes solution vector at previous time step, h can change due to wet/dry cycling, and $k = \Delta t/2$ is half the fixed time step.

Equation 9 has a nonlinearity in $[KC^{n+1}]$ to allow for concentration-dependent diffusivity. We wanted to explore this possibility because early work on the formation of double-base propellants revealed that NG diffusion into NC decreased with decreasing concentration, producing a sharp-edge penetration front (Levy 1955). Unfortunately, we have not found information on the form of this dependence, so as a first approximation use a simple linear dependence:

$$D(c) = D_0 \frac{c}{c_0} \tag{10}$$

To solve for the required $[KC^{n+1}]$, we use a semi-implicit scheme to determine $D(C^{n=1})$:

$$D(C^{n+1}) \approx D(C^{n}) + \frac{D_0}{c_0}\left(C^{n} - C^{n-1}\right) \tag{11}$$

We implemented the numerical algorithm in C++ utilizing the deal.ii differential equation solver library (Bangerth et al. 2007). The symmetry simplifications allow use of a desktop computer to run the simulations. Using the method of manufactured solutions (Roach 2002), the code shows at least second-order convergence with grid refinement (Pitt 2011).

FEM predictions also agreed within 0.1% with analytical predictions for a spherical grain with constant diffusivity (eq 7).

3.4 Model and experiment comparison

We focused our attention on modeling the experiments that used unfired propellants owing to the complex geometries of the fired grains. The batch tests represent the simplest case, with single grains in a stirred bath satisfying our modeling assumptions of $c_w \sim 0$ and high surface mass-transfer coefficient h. Figure 33 compares data from the batch tests with analytical predictions based on spherical grains with constant diffusivity (eq 7).

All grains have mass density $\rho \sim 1.6$ g cm^{-3} from which we calculated equivalent spherical radii. This leaves diffusivity D_0 as the only tuning parameter, and we fit the curves to the data for the first 3–4 measurements to estimate it for each propellant type. Table 6 summarizes the parameters used. Note that best-fit diffusivities are orders-of-magnitude lower than that of NG diffusing into water at similar temperature ($D_0 \sim 6\times10^{-6}$ cm^2 s^{-1}, Wilke 1949). This satisfies a modeling requirement that NG mass transfer from a grain's surface is high relative to its diffusion rate through the NC matrix.

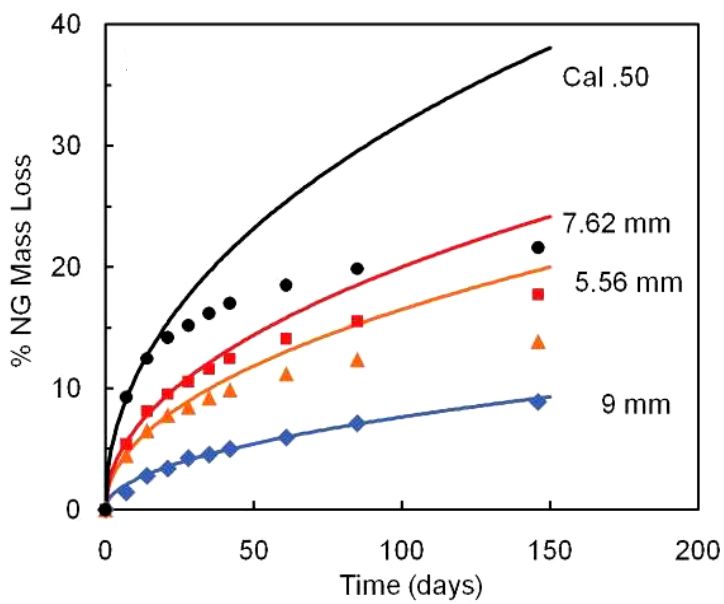

Figure 33. Analytical model for spherical grains and constant diffusivity compared with data from batch tests using single, unfired grains. Analytical curves were fit to initial portion of the experimental data and yield different diffusivities for each propellant type.

Table 6. Parameters used in analytical model, eq 7 derived for spherical grains with constant diffusivity, using radius for grain of equivalent mass (r = 1.6 g cm^{-3}). To simulate drip tests on multiple grains, model uses average grain mass and diffusivity obtained from best fit to single-grain data.

Propellant type	Single grain batch tests				Multiple grain drip tests			
	Grain mass (mg)	Radius a (μm)	Diffusivity* D_0 (cm²/s)		Grain mass (mg)	Radius a (μm)	Diffusivity** D_0 (cm²/s)	Diffusivity*** D_0 (cm²/s)
9-mm	0.080	229	3.2×10^{-14}		0.050	195	3.2×10^{-4}	3.2×10^{-14}
5.56-mm	0.210	315	3.0×10^{-13}		0.157	286	3.0×10^{-13}	5.9×10^{-14}
7.62-mm	0.210	315	4.5×10^{-13}		0.179	299	4.5×10^{-13}	1.0×10^{-13}
0.50-cal	0.720	475	2.8×10^{-12}		0.455	408	2.8×10^{-12}	1.2×10^{-13}

* Best fit to first 3-4 data points.

**Used same diffusivities as those estimated for single grains.

***Best fit to tail slope.

The model produces reasonable agreement with the data, particularly given its simplicity. However, Figure 33 reveals two important concerns: except for the 9-mm propellant, the model over-predicts mass loss at later times, and the best-fit diffusivities span two orders-of-magnitude although propellant formulations are all similar (double-base, NG within NC matrix).

Figure 34 compares data from drip tests on multiple grains with the same analytical model. We retained the best-fit diffusivities determined from the batch tests but used the average mass of each group to calculate equivalent spherical radius. Figure 34 reinforces our concerns that a simple diffusion model might not capture key physics of NG dissolution from the propellants. Except for the 0.50-cal. results, model agreement worsens, failing to track even short-time NG dissolution from the grains. Interestingly, the dissolution rates during the drip tests were all higher than those from the corresponding batch tests. Given that mass-transfer from the surface into the water is high in both cases, the net diffusion rates were somehow higher for drip tests per day of wetting.

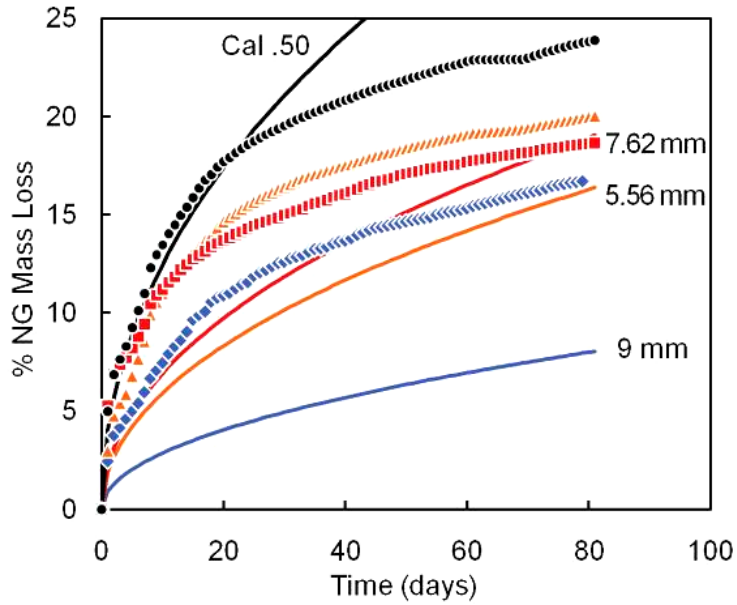

Figure 34. Analytical model for spherical grains and constant diffusivity compared with data from drip tests using multiple, unfired grains. The analytical curves used the same diffusivities determined from best fit to single-grain batch tests.

We formulated the FEM simulations to assess whether some straightforward additional physics would improve model predictions. For example, grain geometries are more cylindrical than spherical. Initial NG loss from grain edges should boost dissolution rates relative to long-term rates. Additionally, if diffusivity decreases with concentration, NG loss could drop off rapidly as it is depleted from the outer layers. Lastly, because the drip tests were stopped each weekend, internal diffusion would steepen NG concentration profiles, leading to higher dissolution rates when the tests resumed. This could account for higher drip-test dissolution rates compared with batch tests.

We limited the FEM study to a single propellant type—unfired 5.56 mm. The model parameters were the same as the analytical study (Table 6) with the addition of the initial concentration, c_0 = 0.158 g cm^{-3}, and the measured dimensions of the cylindrical grain, radius and height, both 347 μm.

Figure 35 compares FEM predictions for continuous wetting with data from the batch test. Modeling the grain as a cylinder indeed increases dissolution rate, owing to an increase in surface area. However, dimensionless time is too small ($\tau < 0.01$) to reveal a reduced rate after depletion of NG along the grain edges. Rescaling based on surface area would essentially collapse the cylinder and sphere results.

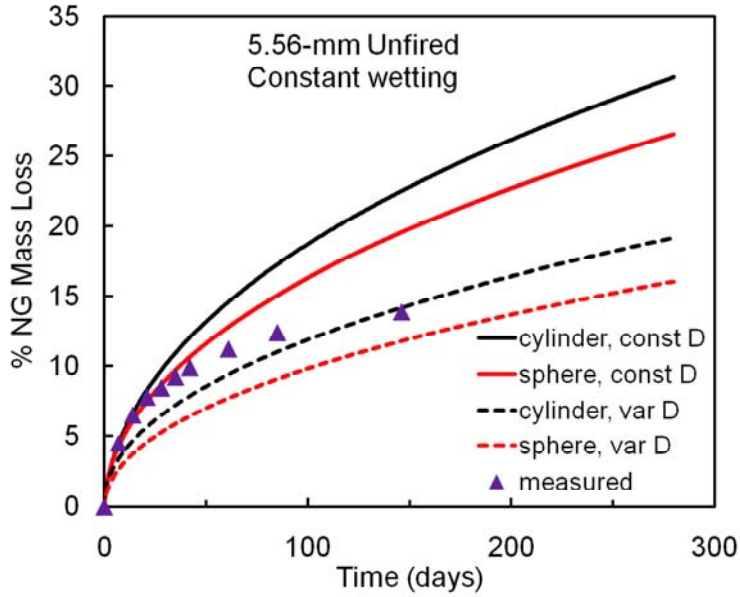

Figure 35. FEM predictions compared with data for 5.56-mm unfired grains in batch test (constant wetting).

Figure 36 does reveal the expect influence of concentration-dependent diffusivity as modeled via eq 8: dissolution rates decrease much more rapidly with time than for constant diffusivity as concentration (and hence diffusivity) decreases in the outer layers. However, the predicted curves (sphere and cylinder) do show as abrupt a roll-off as the data do, suggesting that the concentration dependence might be higher order than linear.

As noted, the FEM simulations can mimic the cyclic wetting pattern of the drip tests, namely 5 wet days followed by 2 dry days. Figure 36 shows the results along with the data from the drip tests on 5.56-mm propellant grains. The data show a stronger roll-off than the FEM predictions, even for variable diffusivity. As with the simulations of the batch test (Fig. 35), the results suggest a stronger dependence of diffusivity on concentration than the linear dependence modeled here.

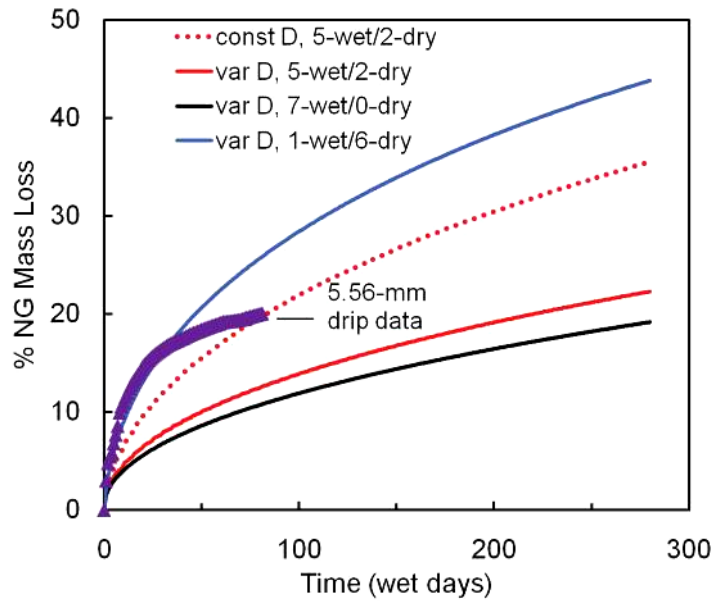

Figure 36. FEM predictions for constant and variable diffusivity with 5-day wet/2-day dry cyclic wetting (red curves) compared with data for 5.56-mm unfired grains in drip test and FEM predictions for variable diffusivity and continuous wetting 7-day wet/0-day dry and cyclic 1-day wet/6-day dry.

Figure 36 also shows FEM results for continuous wetting and 1-day wet/6-day dry cyclic wetting, both for variable diffusivity. All results are plotted against the number of wet days to demonstrate that wet/dry cycling increases the dissolution rate per wet day owing to steepening of concentration gradients at the grain boundaries. This effect would occur in the field, as rainfall days would generally be less frequent than dry days.

We modeled easiest cases first to determine whether molecular diffusion could account for observed dissolution of NG from small arms propellants. The analytical model using constant diffusivity and continuous wetting has only diffusivity as a tuning parameter. Results show roll-off with time is not as abrupt as data and require best-fit diffusivities that vary by two orders of magnitude.

FEM extension to more realistic cylindrical grain shape did not improve agreement, indicating that the abrupt roll-off is not due to depletion of NG near grain edges with constant diffusivity. FEM simulations using linear concentration-dependent diffusivity show a more abrupt roll-off but still not as abrupt as the data.

The FEM simulations of wet/dry cycling demonstrate the expected effect that dissolution rate per wet day increases. Although the results did not substantially improve agreement with data from drip tests with similar wet/dry cycling, this effect would occur for in-field dissolution of propellant grains caused by intermittent rainfall.

The FEM model has two major tuning parameters: the scale and concentration dependence of NG diffusivity through NC. We resisted the urge to fit the data by varying these independently for each propellant type. Rather, we implemented a series of simple diffusion models to understand the effects of geometry, concentration dependence, and wet/dry cycling on dissolution rate. We prefer to wait for additional investigations into the physical and chemical structure of these propellant grains and use that information to guide future modeling.

The analytical and FEM results presented above show that if we fit diffusivities to the initial portions of our mass loss curves we cannot account for the abrupt decrease in mass loss rates, even using concentration dependent diffusivities and different grain geometries. However, if dissolution of near surface NG droplets is driving initial dissolution rates (as suggested by our microscopic results), then the long-term trends in the data (tail slopes) may represent diffusion-controlled dissolution. The diffusivities obtained by fitting the tail slopes of the drip and batch tests differ by less than a factor of four among the propellants tested compared with two order of magnitude differences seen when the initial slopes are fitted (Table 6). Furthermore, the diffusivities for the batch tests and the drip tests are the same for each propellant.

3.5 Propellant–soil interactions

3.5.1 Batch soil studies

We performed kinetic batch adsorption studies on 2,4-DNT, NG, and NQ in three different soils to determine adsorption and transformation rates for these compounds. Detailed information on the soils is given in Appendix B. Treatments without soils (blanks) exhibited no change in their concentration during the 120-h experiment (Fig. 37). In the presence of soil, both adsorption and transformation of these compounds occurred (Fig. 37). The initial decrease in concentration, 1st time point at 1 h, was attributed to adsorption, while further, generally more gradual, decrease in concentration was attributed to transformation (Fig. 37). When the con-

centration of energetic compounds is expressed as a natural logarithm and plotted as a function of time, the slope of the line can be used to determine transformation rate (k) (Fig. 38).

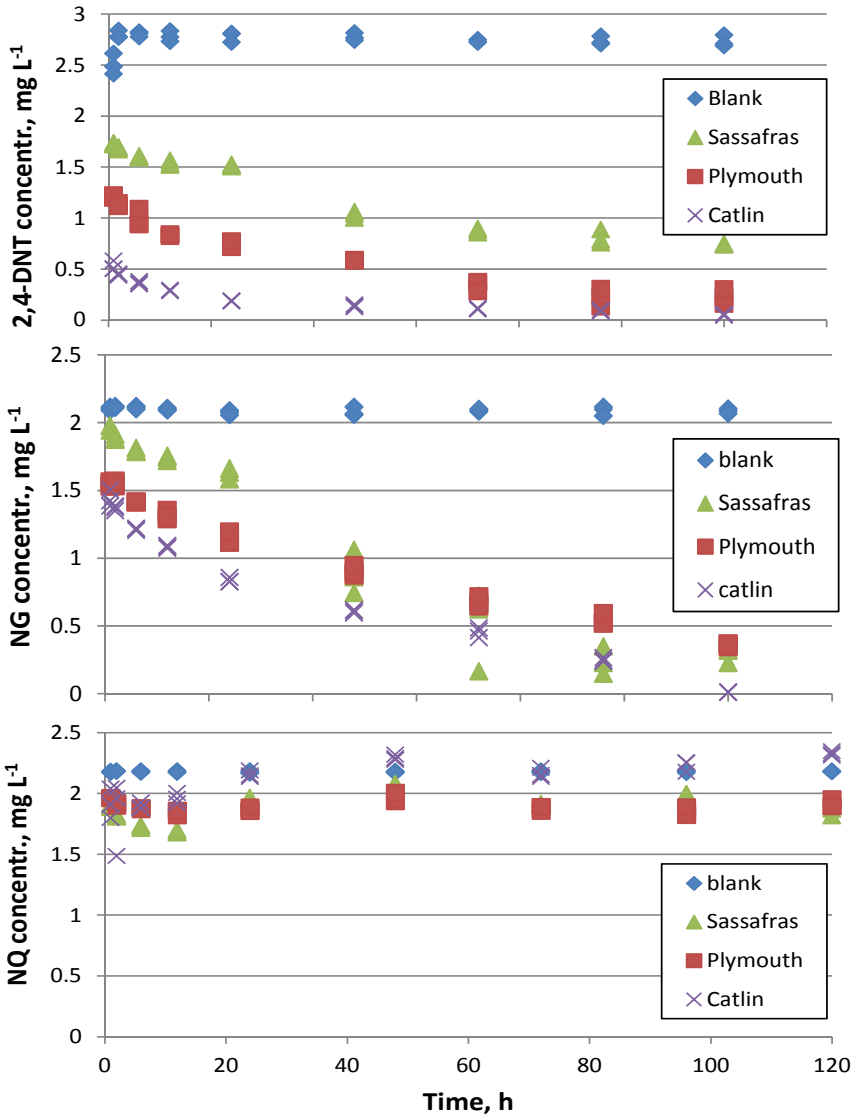

Figure 37. Concentrations of 2,4-DNT (top), NG (center), and NQ (bottom) found in suspensions of Sassafras, Plymouth, and Catlin soils as a function of time. Our control sample that contained no soil is also plotted.

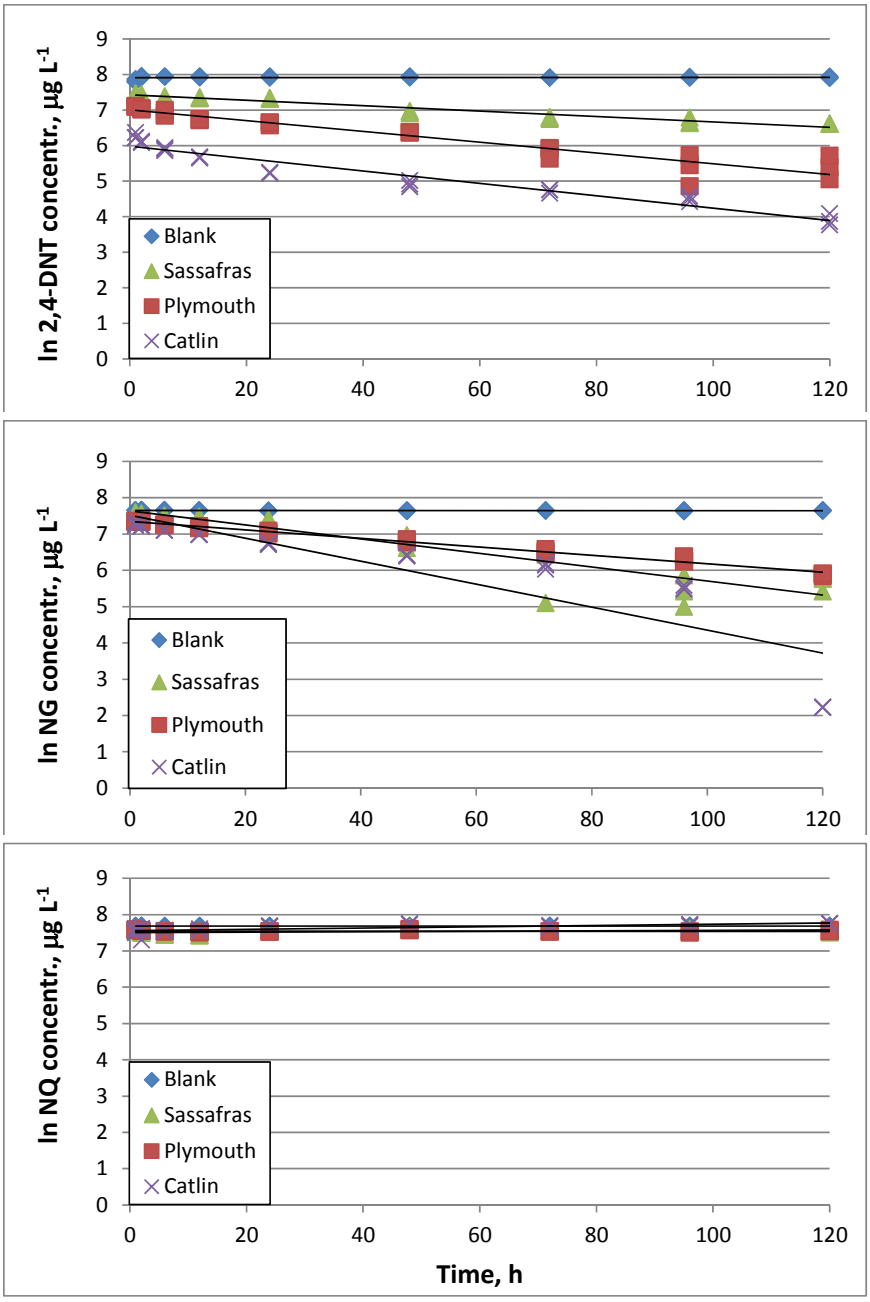

Figure 38. The natural logarithm of 2,4-DNT (top), NG (center), and NQ (bottom) in suspensions of Sassafras, Plymouth, and Catlin soils concentrations plotted as a function of time. Also plotted is our control that contained no soil. The slope of regression line is the transformation rate (*k*) (Table A2).

Kinetic batch soil experiments showed that 2,4-DNT, NG, and NQ had different behaviors when in contact with soil. For 2,4-DNT and NG, there was an initial drop and a steady decrease in solution concentration, indicating adsorption and degradation in the three soils tested (Fig. 37 top and center). This resulted in measurable adsorption and transformation constants

(Table 7) that were influenced by soil type. Nitroguanidine, on the other hand, showed minimal interaction with soils and appeared not to have degraded during the experiment (Fig. 37 bottom).

Table 7. Fate and transport parameters for propellant constituents in soils determined in batch adsorption studies.

Compound	Soil	*C* %	K_d cm³ g⁻¹	K_{OC}	log K_{OC}	*k* hour⁻¹	$t^{1/2}$ d	R^2
NG	Sassafras	1.30	0.26	20	1.30	0.0193	1.49	0.86
NG	Plymouth	1.72	1.41	82	1.91	0.0117	2.48	0.99
NG	Catlin	3.75	1.27	34	1.53	0.0317	0.91	0.78
NQ	Sassafras	1.30	0.60	46	1.66	−0.0006	−48.14	0.18
NQ	Plymouth	1.72	0.44	26	1.41	0.0001	458.43	0.01
NQ	Catlin	3.75	0.24	7	0.82	−0.0018	−16.37	0.53
2,4−DNT	Sassafras	1.30	2.34	180	2.26	0.0076	3.80	0.95
2,4−DNT	Plymouth	1.72	5.06	294	2.47	0.0152	1.90	0.91
2,4−DNT	Catlin	3.75	15.30	408	2.61	0.0174	1.66	0.93

*Transformation constant (*k*) and $t^{1/2}$ values for NQ are not significantly different from zero.

The 2,4-DNT adsorption coefficients ranged from 2.34 cm³ g⁻¹ for Sassafras soil to 15.3 cm³ g⁻¹ for high organic matter Catlin soil. The Plymouth soil adsorption coefficient was between these two values (5.02 cm³ g⁻¹). Lower 2,4-DNT coefficients (0.28 and 3.3 cm³ g⁻¹) were measured for Plymouth soil using column studies (Yamamoto et al. 2004; Dontsova et al. 2009). The difference between values from our batch studies and the column studies is that batch tests measure irreversible and reversible adsorption together, while column studies measure irreversible adsorption with transformation. Because 2,4-DNT transformation products experience irreversible adsorption (Pennington et al. 2003; Thorn et al. 2008), a systematic bias exists between these two methods.

Adsorption coefficients determined for 2,4-DNT showed a strong correlation with organic carbon (OC) content (R^2 = 1.00) (Fig. 39a), a trend also true for K_{ds} published in the literature (Fig. 39b). The slope of our regression function (5.21) was similar to the slope obtained for published data (4.84), confirming 2,4-DNT's affinity for organic matter. Our 2,4-DNT transformation rates ranged between 0.0076 and 0.0174 h⁻¹ and increased

with soil organic matter OM content (Table 7). The measured transformation rate for 2,4-DNT in Plymouth soil was 0.0152 h^{-1} within the range previously determined for this soil, 0.002–0.0238 h^{-1} (Dontsova et al. 2009).

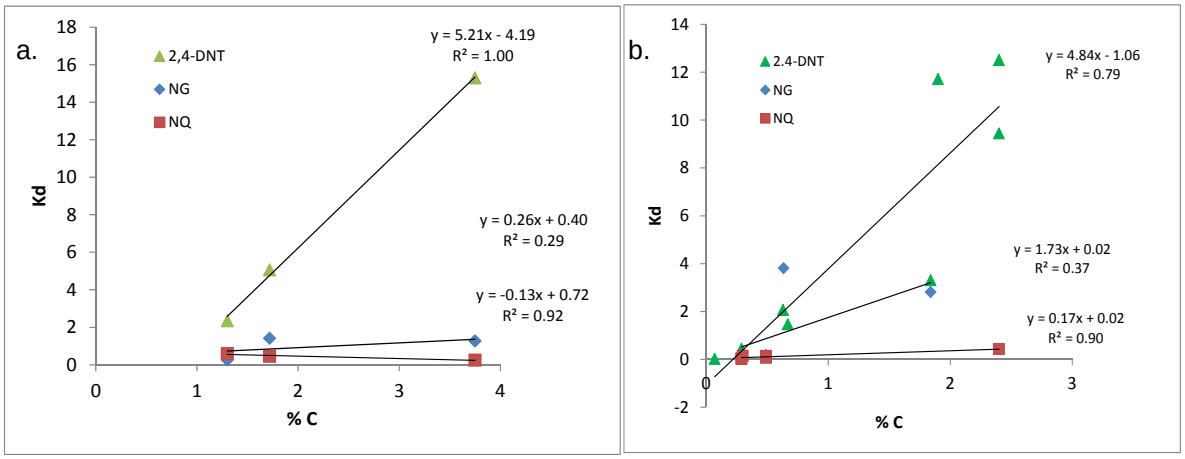

Figure 39. Adsoprtion coefficints (K_d) plotted as a function of carbon content for: (a) the soils we studied and (b) literature values (Table A2).

Nitroglycerin adsorption coefficients ranged from 0.26 to 1.41 $cm^3\ g^{-1}$ for the soils studies (Table 7). These are lower than the ones determined for 2,4-DNT but significantly different from zero. Our values are similar to literature-reported values (Dontsova et al. 2007, 2008; Table A1). NG adsorption coefficients did not exhibit a strong relationship with organic matter content (Fig. 39a), indicating that other mechanisms are responsible for adsorption. NG is a polar molecule (Winkler 1985) and may form dipole-dipole and hydrogen bonds with polar moieties in the soils. Reported K_{ow} values for NG (1.62–1.77) (Mirecki et al. 2006) vary depending on the method used to estimate them, but generally indicate a preference for non-polar interactions. Transformation/degradation rates determined for NG were high, with half-life of only 0.91 days for Catlin to 2.48 days for Plymouth soils (Table 7). Similar to adsorption rates, there was no trend in NG transformation rates as a function of soil OC content.

Nitroguanidine did not show the steady decrease in solution concentrations that was observed for 2,4-DNT and NG. For all three soils, the slopes of the regressions lines in plot of ln NQ concentration vs. time (transformation rates) were not significantly different from zero (Fig. 38 bottom, Table 7) illustrating its conservative behavior. This finding is consistent with observations for similar soils (Dontsova et al. 2007; Table A2). NQ adsorption coefficients (Table 7, Fig. 39a) were all less than one and tend-

ed to increase with decreases in soil organic carbon content (R^2=0.92), indicating repulsive rather than attractive interactions with soil carbon. This is likely related to the polar nature of the NQ molecule with log K_{ow} values between −0.89 and 0.156 (Mirecki et al. 2006), which results in low affinity for non-polar organic matter in the soils.

Based on high adsorption and transformation coefficients determined for Catlin soil in batch studies, as well as preliminary column experiments using 2,4-DNT, 2,6-DNT, NG, and NQ in solution, which indicated high retention of all measured compounds in this soil, we decided to not use Catlin soil in the column experiments. Instead, we focused on Plymouth and Sassafras soils, which provided a more conservative estimate of soil retention for 2,4-DNT, NG, and NQ and allowed us to measure their transport through the soil columns.

3.5.2 Soil column studies

We completed a total of 31 individual column dissolution and transport experiments (Table 8). We used two soils, Sassafras loam from Aberdeen Proving Ground and Plymouth sandy loam from Massachusetts Military Reservation, two flow rates, 0.01 and 0.02 mL min^{-1}, and three different propellant compositions: M1, WC 860 and M31. For two of the propellants, M1 and WC 860, we also studied fired residues (Fig. 40). The main energetic component of M1 propellant was 2,4-DNT, while WC 860 contained NG, and M31 had both NG and NQ (Table 9). Each experiment was conducted twice, with and without flow interruption. The 0.01 mL min^{-1} flow rate corresponded to a 0.55 cm h^{-1} flux, and the 0.02 mL min^{-1} flow rate to 1.1 cm h^{-1} flux. The water fluxes used in this study were about 12 and 25% of the average 1-year rainfall intensity (4 cm h^{-1}) for the eastern U.S. At the end of the soil column tests we extracted the propellants and the soil.

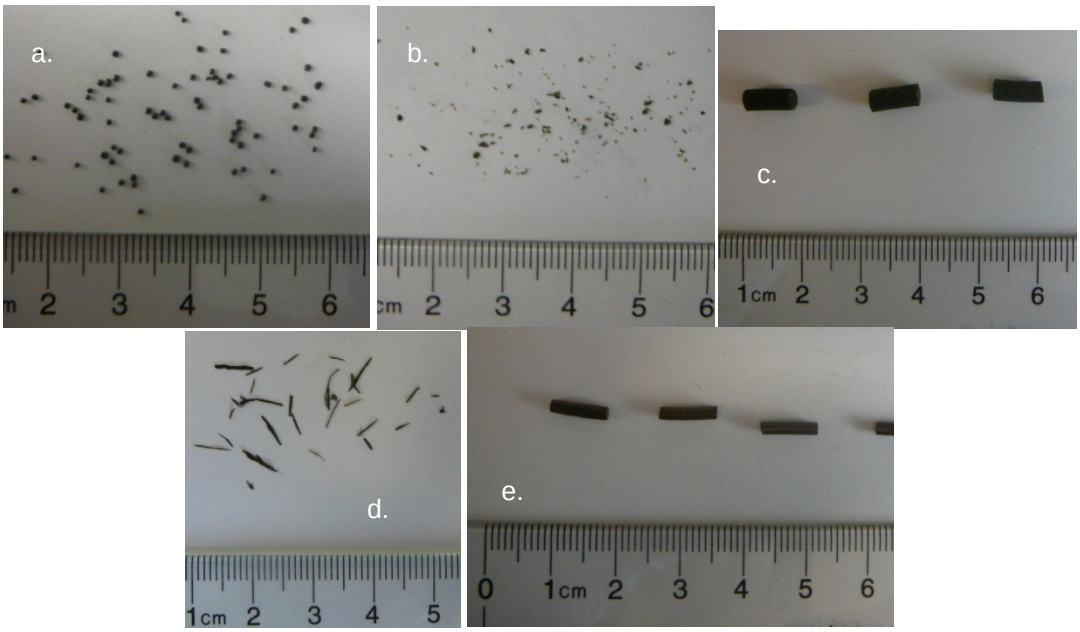

Figure 40. Unfired propellants and residues used in the column study: (a) unfired WC 860; (b) WC 860 residues; (c) unfired M1; (d) M1 residues; and (e) unfired M31 propellant.

Table 8. Soil column experiments.

Propellant		Energetic compounds	Flow rate, mL min^{-1}	Soil	Set	Number of columns
WC 860	fired+unfired	NG	0.01	Plymouth	I	4
			0.01	Sassafras	III	4
			0.02	Plymouth	II	4
			0.02	Sassafras	IV	4
M31	unfired only	NG, NQ	0.01	Plymouth	III	2
			0.01	Sassafras	III	2
			0.02	Plymouth	IV	2
			0.02	Sassafras	IV	1
M1	fired+unfired	2,4-DNT	0.01	Plymouth	V	4
		2,6-DNT	0.01	Sassafras	V	4
			0.02	Plymouth	*	4
			0.02	Sassafras	*	4

*No detectable 2,4-DNT and 2,6-DNT in outflow for 0.01 mm h^{-1} flow rate so higher flow rate tests were cancelled.

Table 9. Composition of propellants used in column experiments (Defense Ammunition Center 2006).

Function	Compound	WC 860 (%)	M1 (%)	M31 (%)
Energetic plasticizer and binder	Nitrocellulose	78.7 ± 6.5	85 ± 2	20 ± 1.3
	Nitroglycerin	9.5 ± 2.1		19 ± 1
	Dinitrotoluene		10 ± 2	
Oxidizer	Nitroguanidine			54.7 ± 1
Plasticizer	Dibutylphthalate	8 ± 2.8	5 ± 1	1.5 ± 0.1
Stabilizer	Diphenylamine	1.1 ± 0.5	1 ± 0.1	
	2-nitrodiphenylamine			1.5
Flash reducer	Potassium nitrate	0.8 ± 1		
	Sodium sulfate	0.5		
	Calcium carbonate	1		
	Lead carbonate		1 ± 0.3	
	Potassium sulfate			
	Cryolite			0.3±0.1
Antistatic coating	Graphite	0.4		

3.5.2.1 Column outflow

No 2,4-DNT was detected in the M1 0.01 mL min^{-1} column outflow. This is reasonable given the slow 2,4-DNT dissolution rates from M1 propellants (Fig. 26, 27; Dontsova et al. 2009), and the strong interaction between 2,4-DNT and the soil matrix, particularly the irreversible adsorption of amino products produced by reductive transformation (Thorn et al. 2008). Because we found no 2,4-DNT in the M1 column outflow at 0.01 mL min^{-1} flow rate, we did not run the M1 experiments at 0.02 mL min^{-1} flow; larger water fluxes always resulted in smaller outflow concentrations of energetics in the other experiments.

A comparison of the column experiments using fired and unfired WC 860 showed that the residues had lower outflow NG concentrations than the unfired propellants (Fig. 41 and 42, Table 10). Part of the reason was that we used a smaller amount of fired residues (0.016 g) than unfired propellant (0.1 g), because we had only a small amount of the fired residues. The fired residues, however, also had less dissolution per unit mass than the unfired particles (Table 10). The ratio between dissolution per unit mass of NG in unfired and fired particles was 3.9 for the 0.01 mm h^{-1} flow rate and

1.9 for the 0.02 mm h^{-1} flow rate. We think that partial burning of the NG in the residue resulted in lower total concentration of NG (Table 3) and decreased the NG concentration in the rim close to the surface of the residue (e.g., Fig. 11). These results are similar to what we found in the drip tests where the unfired propellants lost 15–20% and their residues lost 3 to 7%, also resulting in ~4 per unit mass ratio for unfired and fired propellants for the equivalent flow rate.

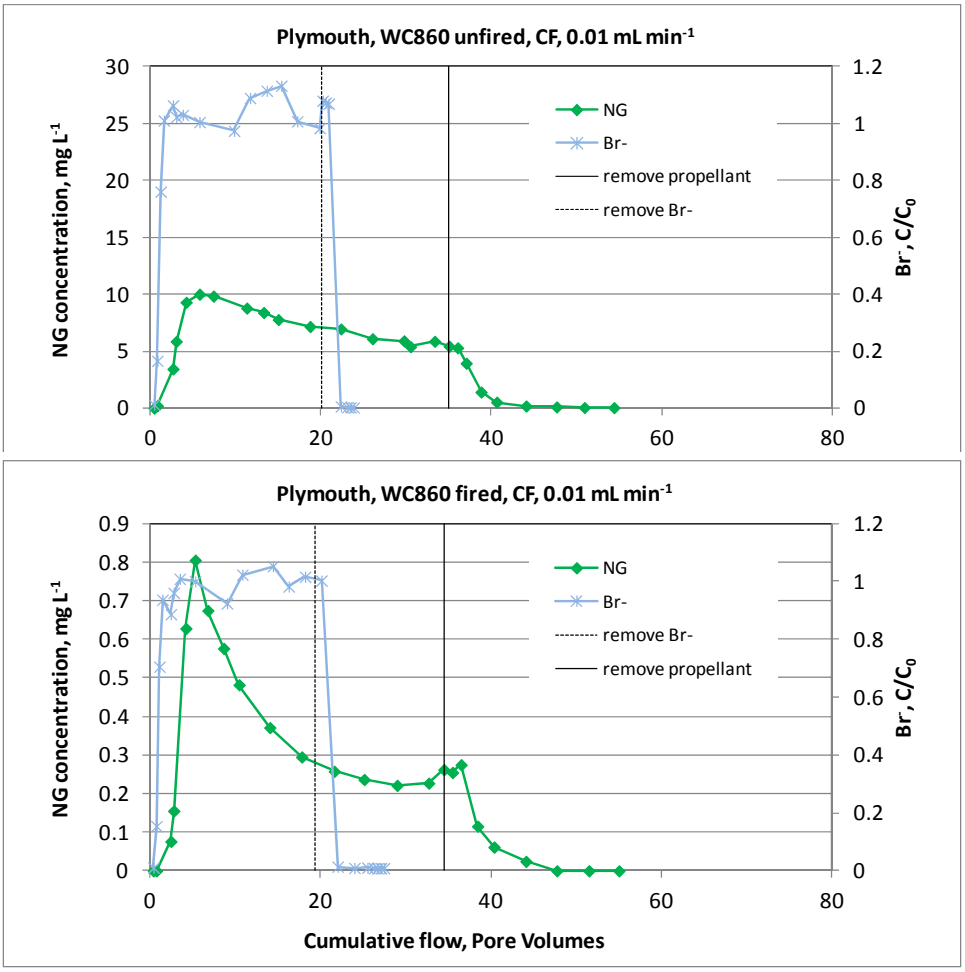

Figure 41. Breakthrough curves for continuous water flow onto unfired and fired 0.50-cal. (WC 860) propellants. The solid vertical line indicates when the propellant was removed from the soil surface. Greater outflow concentrations were observed in unfired propellants indicating greater dissolution per unit mass of propellant.

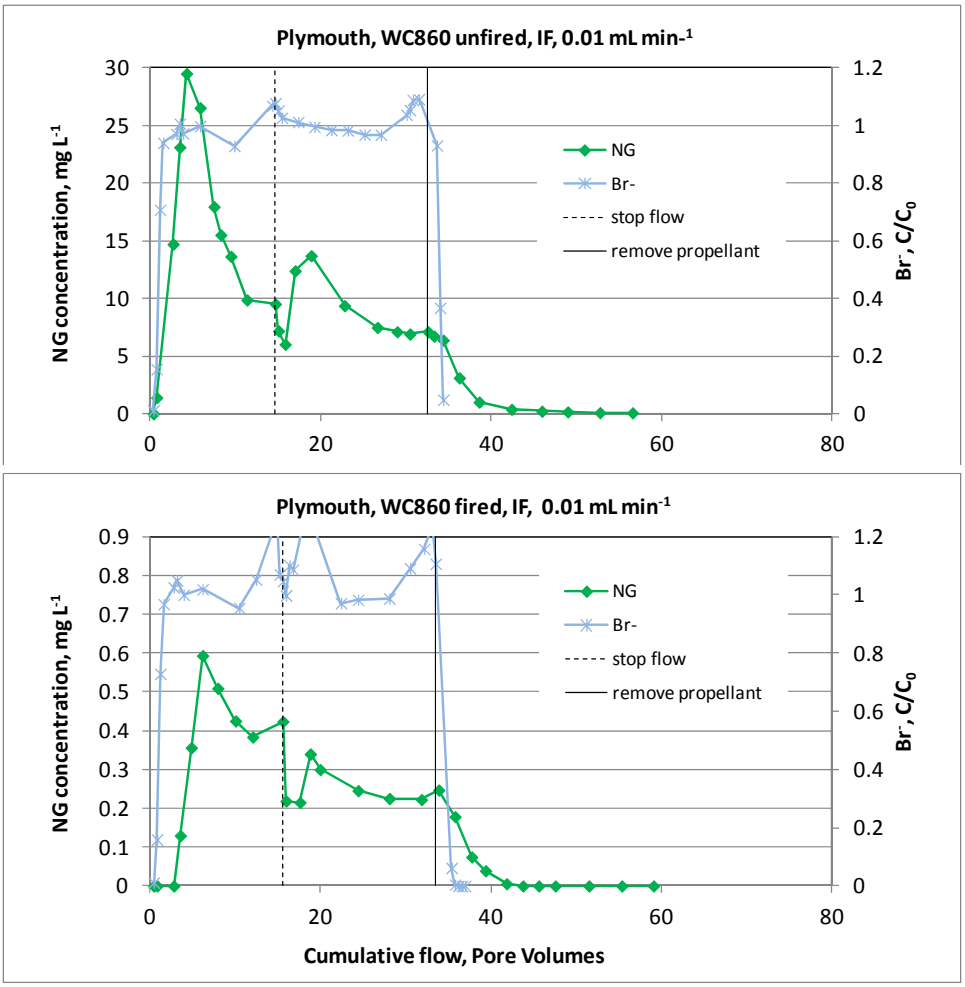

Figure 42. Breakthrough curves for interrupted water flow onto unfired and fired 0.50-cal. (WC 860) propellants. The solid vertical line at ~13 pore volumes indicates when the flow was interrupted. The solid vertical line at ~30 pore volumes shows when the propellant was removed from the soil surface.

The M31 propellant, which contains 19.5% NG and 55% NQ, initially showed more NQ in the outflow than NG as expected given its higher content in the M31 grain. NQ, however, had a lower steady-state concentration than NG (Fig. 43), suggesting that less NQ leaves the propellant than NG. The ratio of NG to NQ in the outflow was 4.57 for 0.01 mm h^{-1} flow rate and 2.52 for 0.02 mm h^{-1} flow rate.

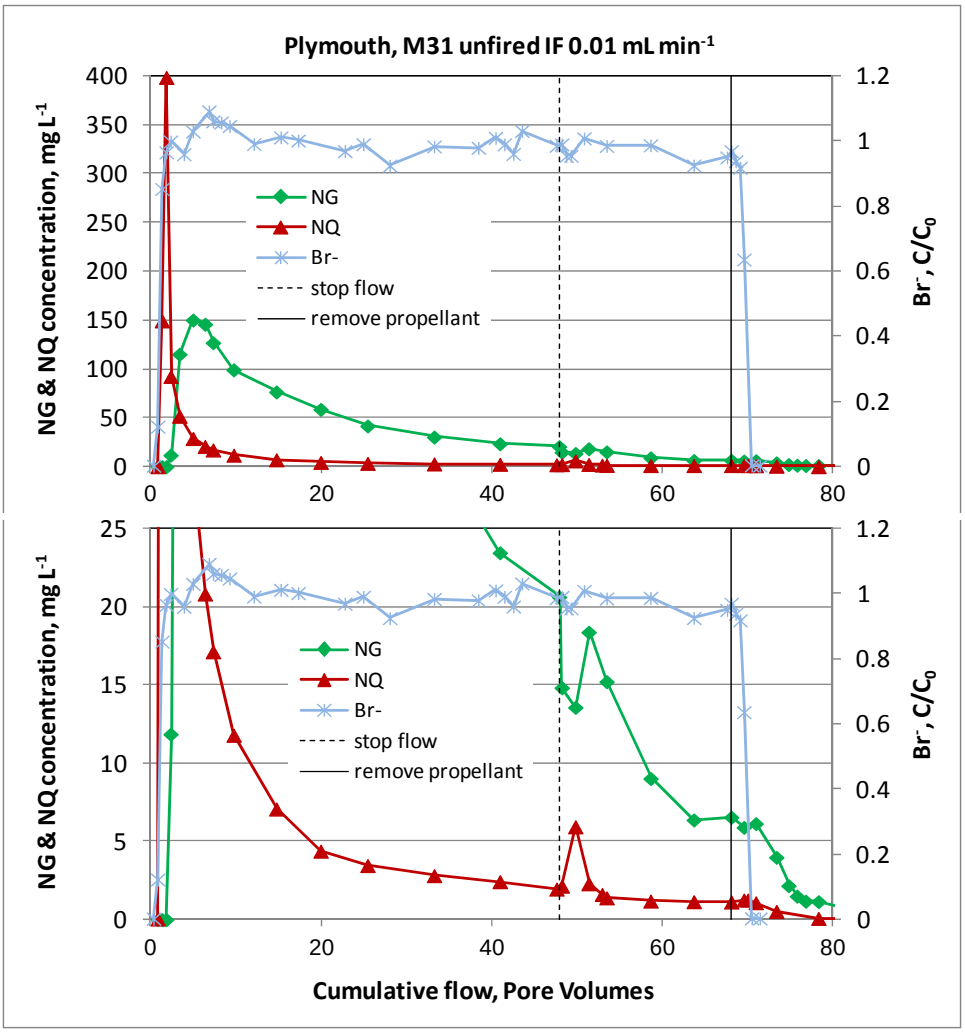

Figure 43. Breakthrough curves for interrupted water flow onto unfired M31 propellant. The second plot shows a detailed view of the initial decrease in concentration for NG after flow interruption. No decrease is observed for the NQ, indicating it does not degrade or transform in soil. The vertical line at ~45 pore volumes indicates when the flow was interrupted. The solid vertical line at ~70 pore volumes shows when the propellant was removed from the soil surface.

By multiplying the degradation rate by the pore volume and then dividing by the flow rate, we calculated the fraction of NG that degraded as the NG-laden water moved through the soil column. We expected and saw a larger fraction of the NG degrade for the lower, 0.01 mL min^{-1}, flow rate tests because it took longer for one pore volume (PV) to get through the soil. We saw this effect in both the Sassafras and Plymouth soils, although the degradation did not significantly change the total NG in solution (Tables 10 and 11).

The soil column tests showed that NQ experienced limited adsorption in the studied soils, while NG had larger adsorption coefficients, indicating

natural attenuation of this compound in soils (Fig. 44), results similar to our batch studies (Fig. 37, Table 7). NG experienced retardation due to adsorption, as demonstrated by delay in NG breakthrough, while there was little delay in NQ breakthrough relative to the conservative tracer, Br– (Fig. 44). NG breakthrough also happened later in Plymouth soil than in Sassafras soil, consistent with their measured adsorption coefficients (1.41 $cm^3\ g^{-1}$ for Plymouth and 0.26 $cm^3\ g^{-1}$ for Sassafras) (Table 7).

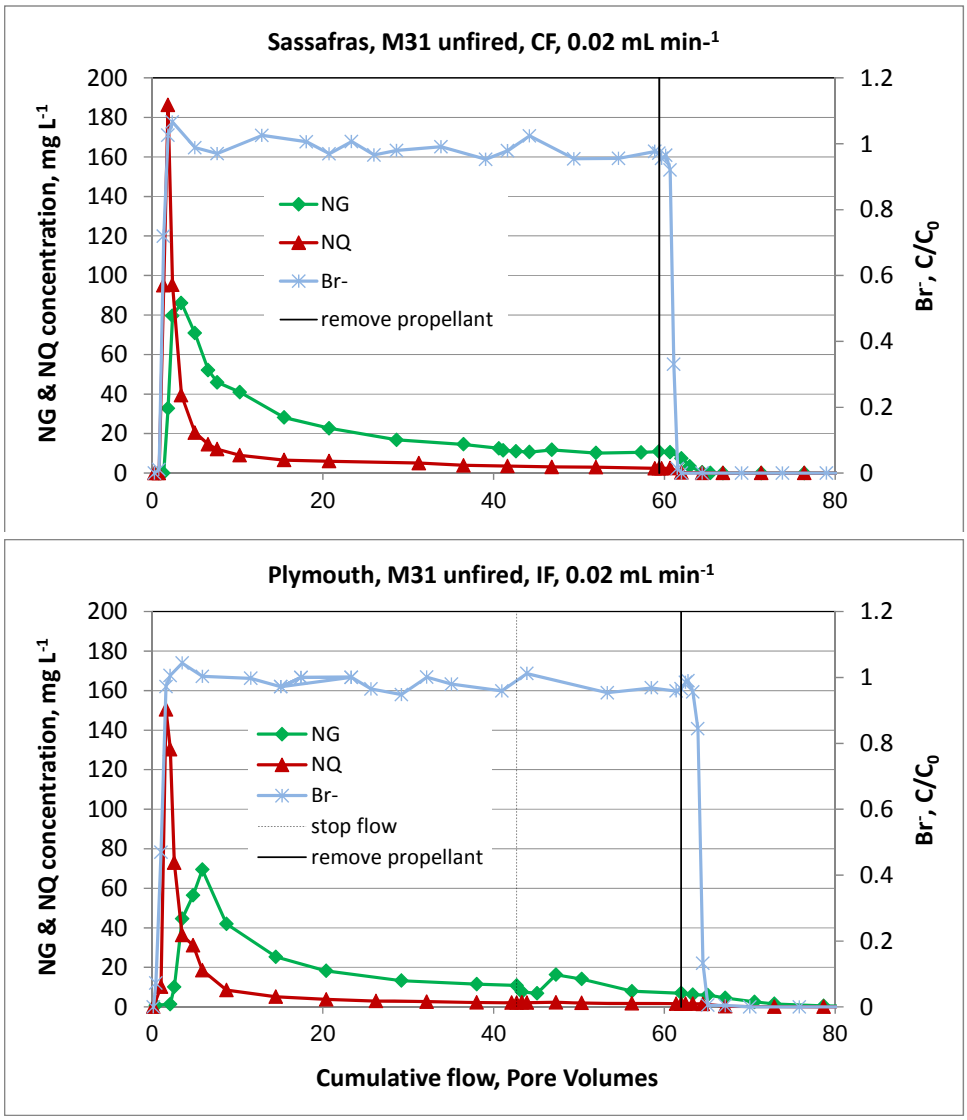

Figure 44. Breakthrough curves for continuous (CF) and interrupted (IF) water flow at 0.02 mL min^{-1} rate onto unfired M31 propellant in Sassafras and Plymouth soils. Breakthrough of NG happened later in Plymouth compared to Sassafras soil indicating greater adsorption of NG.

Table 10. NG loss from unfired and fired WC860 propellant tested in column experiments at 0.01 and 0.02 mL min^{-1}.

Soil	U/F	CF/IF	Set	Col.	Cum. NG outflow (µg)	PV (mL)	Flow rate (mL min^{-1})	Fraction trans-formed	Cum. NG* outflow (µg)	Cum. soln. flow PV	WC860 mass (g)	NG (%)	NG (µg)	Loss (%)	Loss* (%)
0.01 mL min^{-1}															
Sassafras	U	IF	III	c1	606.1	2.95	0.0093	0.1023	675.2	61.8	0.1021	9.7	9904	6.12	6.82
Sassafras	U	CF	III	c2	568.1	2.77	0.0087	0.1023	632.8	49.8	0.1009	9.7	9787	5.80	6.47
Plymouth	U	IF	I	c3	1360.6	3.49	0.0088	0.0777	1475.1	14.7	0.1000	9.7	9700	14.03	15.21
Plymouth	U	CF	I	c4	854.2	3.44	0.0083	0.0810	929.4	35.1	0.1000	9.7	9700	8.81	9.58
Average ± SE				847±182					928±194	40±10				9±2	9±2
Sassafras	F	IF	III	c3	42.1	2.87	0.0091	0.1012	46.9	59.5	0.0165	7.8	1287	3.27	3.64
Sassafras	F	CF	III	c4	19.5	2.88	0.0090	0.1026	21.8	50.5	0.0167	7.8	1303	1.50	1.67
Plymouth	F	IF	I	c5	36.5	3.55	0.0093	0.0744	39.4	33.5	0.0166	7.8	1295	2.82	3.04
Plymouth	F	CF	I	c6	44.0	3.57	0.0087	0.0797	47.8	34.5	0.0166	7.8	1295	3.40	3.69
Average ± SE					35±6				39±6	45±6				3±0.4	3±0.5
0.02 mL min^{-1}															
Sassafras	U	IF	IV	c1	385.1	3.03	0.0171	0.0571	408.4	46.3	0.1000	9.7	9700	3.97	4.21
Sassafras	U	CF	IV	c2	401.8	3.01	0.0180	0.0538	424.6	51.4	0.1003	9.7	9729	4.13	4.36
Plymouth	U	IF	II	c1	718.0	2.96	0.0181	0.0319	741.7	41.2	0.1004	9.7	9739	7.37	7.62
Plymouth	U	CF	II	c2	687.2	2.65	0.0197	0.0263	705.7	52.4	0.1002	9.7	9719	7.07	7.26
Average ± SE					548±89				570±89	48±3				6±0.9	6±0.9
Sassafras	F	CF	IV	c3	34.9	2.76	0.0177	0.0502	36.7	55.0	0.0166	7.8	1295	2.69	2.84
Plymouth	F	CF	II	c3	55.7	2.84	0.0183	0.0302	57.5	39.3	0.0157	7.8	1225	4.55	4.69
Plymouth	F	IF	II	c4	50.0	2.85	0.0177	0.0315	51.6	49.6	0.0160	7.8	1248	4.00	4.13
Average ± SE					47±6				49±6	48±5				4±0.5	4±0.5

U=Unfired, F= Fired; SE = Standard error; CF=continuous flow; IF=interrupted flow; PV = pore volume; *=Accounting for transformation. Transformation rate (k) used to calculate this value was determined in batch experiments and equaled 0.0193 h^{-1} in Sassafras soil, and 0.0117 h^{-1} in Plymouth soil (Table 7)

Table 11. NG and NQ loss from unfired M31 propellant in column experiments conducted at 0.01 and 0.02 mL min^{-1} flow.

Soil	CF/ IF	Set	Col.	Cum NG or NQ outflow (µg)	PV (mL)	Flow rate (mL min^{-1})	Fraction trans-formed	Cum. NG* outflow (µg)	Cum. soln. flow PV	NG/NQ	NG*/ NQ	M31 (g)	NG or NQ (%)	NG or NQ (µg)	Loss (%)	Loss* (%)
0.01 mL min^{-1} NG																
Sassafras	IF	III	c5	7990	2.82	0.0096	0.0945	8824	63.3	4.46	4.92	0.0918	19	17442	45.81	50.59
Sassafras	IF	III	c6	6250	2.85	0.0097	0.0949	6905	61.3	4.23	4.67	0.0885	19	16815	37.17	41.07
Plymouth	IF	III	c7	5169	2.85	0.0093	0.0598	5497	52.0	4.42	4.70	0.0884	19	16796	30.77	32.73
Plymouth	CF	III	c8	7662	2.84	0.0096	0.0579	8133	68.2	3.77	4.00	0.0935	19	17765	43.13	45.78
Average ± SE			6768 ± 653				7340 ± 731		61±3	4±0.2	5±0.2				39±3	43±4
0.01 mL min^{-1} NQ																
Sassafras	IF	III	c5	1793									54.7	50215	3.57	
Sassafras	IF	III	c6	1477									54.7	48410	3.05	
Plymouth	IF	III	c7	1169									54.7	48355	2.42	
Plymouth	CF	III	c8	2032									54.7	51145	3.97	
Average ± SE			1618±188												3±0.3	
0.02 mL min^{-1} NG																
Sassafras	IF	IV	c5	2735	2.77	0.0197	0.0451	2864	60.2	2.75	2.87	0.0905	19	17195	15.91	16.66
Sassafras	CF	IV	c6	3400	2.70	0.0183	0.0474	3569	59.4	2.39	2.51	0.0929	19	17651	19.26	20.22
Plymouth	IF	IV	c7	2840	2.43	0.0182	0.0261	2916	62.0	2.04	2.09	0.0896	19	17024	16.68	17.13
Plymouth	CF	IV	c8	2676	2.59	0.0188	0.0269	2750	62.1	2.54	2.61	0.0890	19	16910	15.82	16.26
Average ± SE				2913±166			3025±185		61±0.7	2±0.1	3±0.2			17±0.8		18±0.9
0.02 mL min^{-1} NQ																
Sassafras	CF	IV	c5	996									54.7	49504	2.01	
Sassafras	CF	IV	c6	1423									54.7	50816	2.80	
Plymouth	IF	IV	c7	1392									54.7	49011	2.84	
Plymouth	CF	IV	c8	1052									54.7	48683	2.16	
Average ± SE				1216±111											2.5±0.2	

SE = Standard error; CF=continuous flow; IF=interrupted flow; PV = pore volume; *=Accounting for transformation. NG transformation rate (k) used to calculate this value was determined in batch experiments and equaled 0.0193 h^{-1} for Sassafras soil and 0.0117 h^{-1} for Plymouth soil. Transformation rate for NQ was not significantly different from zero in both soils (Table 18).

For experiments using double and triple-based propellants we observed a set of common features. Both NG and NQ had high initial dissolution fol-

lowed by near exponential decrease in concentration (Fig. 41, 42, 43, and Appendix C). The peak concentrations were always lower than the solubilities of these compounds (Table 2). For experiments where the flow was interrupted (a period of 24 h of no flow), NG concentration in the leachate decreased after flow interruption. We think that NG continued to transform, and that the increased residence time during no flow resulted in lower leachate concentrations. For NQ, there was no decrease when the flow was stopped, confirming no NQ degradation in our soils. After flow was resumed and one or more PV passed through the column, however, both NG and NQ concentrations increased to levels similar or higher than before flow interruption.

The energetic dissolution patterns observed from propellants provide clues about the mechanisms involved in dissolution. Decreased energetic concentrations over time (as well as increases in dissolution following flow interruption) indicated that dissolution was limited by the rate of diffusion of these compounds through nitrocellulose (Dontsova et al. 2009). It took longer for NG or NQ to reach the surface as the distance between the surface of the particle and energetic front increased over time. Interrupting the flow provided additional time for the energetics to reach the surface and be dissolved by the water. This idea was supported by the time- but not flow-dependent dissolution rate of both NG and NQ in M31 propellant that was seen both in the drip and the soil column tests. In M31, NG concentrations in the outflow were higher at the 0.01 mL min^{-1} flow rate than at the 0.02 mL min^{-1} (Fig. 45) and more NG mass was dissolved (Table 11). As the same cumulative amount of water was supplied in both flow rate treatments, about 2.4 times more NG was dissolved at 0.01 mL min^{-1} flow rate. A similar trend was observed for NQ but the differences were not statistically significant at the 95% confidence level. If the measured outflow concentrations (adjusted for transformation) were the same, independent of the flow rate, we would conclude that propellant dissolution was limited by removal of dissolution products with the flow, as observed for explosives (Taylor et al. 2009b). However, because concentrations decreased with increase in the flow, it is likely that dissolution was limited by the supply of NG from the propellant.

In addition, we observed that the percentage of NG dissolved was lower for the WC 860 compared to M31. For similar flow, the unfired WC 860 lost 5.9-9.5% NG, while the M31 lost 17.6–42.5% (Table 11), similar to what observed in drip dissolution studies (Fig. 27). The difference in mass loss be-

tween the two propellants cannot be explained by the total surface area available for dissolution, as WC 860 are small particles (Fig. 40) and have greater surface area per unit mass. However, NG/NC ratio, the parameter used to normalize dissolution in drip studies, can explain the differences. M31 has equal amounts of NG and NC, each at about 20% (Table 9), while in WC 860 has about 10 NG% and 90% NC. If NG is being adsorbed and held by NC, as we concluded from the drip studies, then an increased NG to NC ratio would result in greater NG dissolution, as observed here.

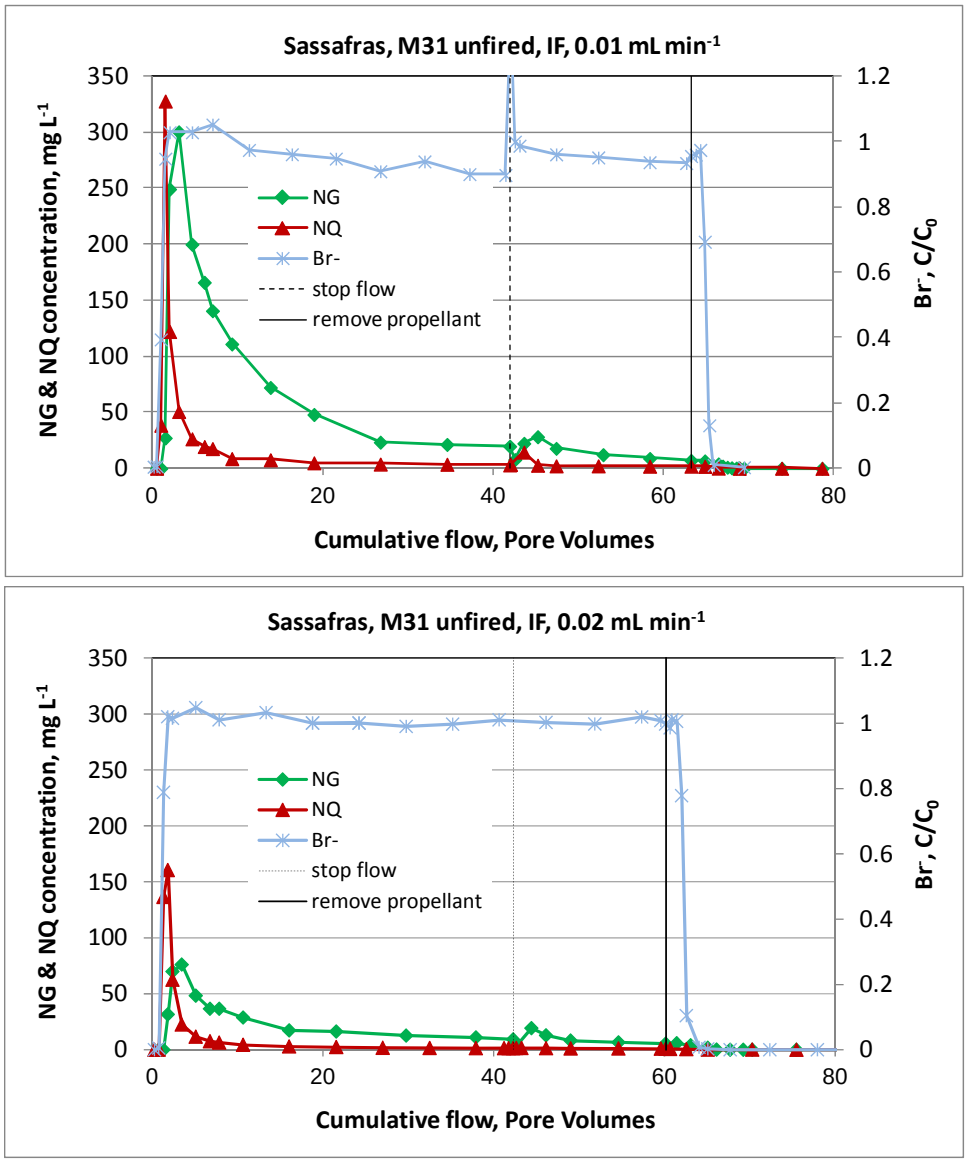

Figure 45. Breakthrough curves for interrupted (IF) water flow onto unfired M31 propellant in Sassafras soil at two different flow rates, 0.01 and 0.02 mL min^{-1}. Greater outflow concentrations of both NG and NQ were observed at the slower flow rate.

3.5.2.2 Mass balance

At the end of the column tests, we extracted the propellants and the soils (Table 12). We recovered about 55% of 2,4-DNT in the M1 residues and 93% from the M1 unfired propellants (Table 12). Differences between fired and unfired particles were similar to ones observed in the drip tests (Fig. 26). We were able to recover only small fraction of the original 2,4-DNT (up to 2% for some columns) when we extracted the soil (Table 12 and Table B2). The 2,4-DNT concentrations were highest in the top layers of the soil and decreased with depth (Table B2). The unfired WC860 propellant lost 21% of its original NG and the fired residues 18% (0.02 mL min^{-1} flow rate). Of the NG originally in the M31, between 49 and 61% was not in the extracted propellants and larger losses occurred at lower flow rates.

When we added the mass of energetic extracted from the propellants to the mass analyzed in solution, we did not recover the original mass of energetics. This was true even when transformation in the soil was taken into account and when the energetics remaining in the soil were included. Although soil extractions indicated that there was some 2,4 DNT and NG in the soil even if these were absent in the outflow (Table 12, Appendix B), the soil concentrations were small and did not close the mass balance. No NQ was detected in the extracted soils.

Less 2,4-DNT was recovered in the fired (54.2%) than in the unfired (93.3%) M1 propellants. This can be explained by non-linear irreversible adsorption of 2,4-DNT. If adsorption decreases with increase in concentration, fired propellant with lower dissolution rates would result in more adsorption and smaller 2.4-DNT concentrations. Non-linear adsorption can happen if there are a limited number of sorption sites in the soil. Energetic compounds can have liner sorption over most concentrations, but exhibit decreased sorption during initial peak concentrations in propellants. For the WC860 propellant, the total NG recovery was 83.5±3.0% and was similar for unfired and fired particles and for both flow rates. This was within the range of what was observed in the drip studies (86–112%) (Table 4).

In drip studies, NG recoveries for M31 were 83±5% (Table 5), while in the soil column studies they were 81.6% (0.01 mL min^{-1} flow) and 68.7% (0.02 mL min^{-1} flow).

Table 12. Enrgetic compounds recovered in leachate, extracted from the soil and extracted from propellants at end of column experiments: data for 2,4-DNT in the M1, NG in the WC860, and NG the unfired M31 propellant.

Soil	U/F	CF/ IF	Set	Col.	%Orig. conc.	% in leach.*	%in soil	%Extracted propellant	%Energetics recovered
M1 0.01 mL min^{-1}									
Sassafras	U	IF	V	c1	9.7	ND	0.01	87.63	87.64
Sassafras	U	CF	V	c2	9.7	ND	ND	92.78	92.78
Plymouth	U	IF	V	C5	9.7	ND	0.07		
Plymouth	U	CF	V	C6	9.7	ND	0.08	99.38	99.46
Average±SE								93.3±3.4	93.3±3.4
Sassafras	F	IF	V	c3	9	ND	ND	54.44	54.44
Sassafras	F	CF	V	c4	9	ND	ND	52.00	52.00
Plymouth	F	IF	V	C7	9	ND	ND	57.78	57.78
Plymouth	F	CF	V	C8	9	ND	2.18	50.33	52.51
Average±SE								53.6±1.6	54.2±1.3
WC860 0.01 mL min^{-1}									
Sassafras	U	IF	III	c1	9.7	6.82	0.44	70.21	77.47
Sassafras	U	CF	III	c2	9.7	6.47	0.44	77.01	83.92
Plymouth	U	IF	I	c3	9.7	15.21	NA		
Plymouth	U	CF	I	c4	9.7	9.58	NA		
Average±SE						9.5±2.0		73.6±3.4	80.7±3.2
Sassafras	F	IF	III	c3	7.8	3.64	5.89	69.49	79.02
Sassafras	F	CF	III	c4	7.8	1.67	2.65	74.87	79.19
Plymouth	F	IF	I	c5	7.8	3.04	NA		
Plymouth	F	CF	I	c6	7.8	3.69	NA		
Average±SE						3.0±0.5		72.2±2.7	79.1±0.1
WC860 0.02 mL min^{-1}									
Sassafras	U	IF	IV	c1	9.7	4.21	ND	81.96	86.17
Sassafras	U	CF	IV	c2	9.7	4.36	ND	82.89	87.25
Plymouth	U	IF	II	c1	9.7	7.62	ND	67.53	75.15
Plymouth	U	CF	II	c2	9.7	7.26	ND	81.86	89.12
Average±SE						5.9±0.9		78.6±3.7	84.4±3.2
Sassafras	F	CF	IV	c3	7.8	2.84	ND	78.97	81.81
Plymouth	F	CF	II	c3	7.8	4.69	ND	103.85	108.54
Plymouth	F	IF	II	c4	7.8	4.13	2.69	63.59	70.41
Average±SE						3.8±0.5		82.1±11.7	86.9±11.3
M31 0.01 mL min^{-1}									
Sassafras	U	IF	III	c5	19	50.59	ND	31.89	82.48
Sassafras	U	IF	III	c6	19	41.07	ND	40.89	81.96
Plymouth	U	IF	III	c7	19	32.73	0.16	47.95	80.84
Plymouth	U	CF	III	c8	19	45.78	0.17	35.11	81.06
Average±SE						42.5±3.8		39.0±3.5	81.6±0.4

Soil	U/F	CF/ IF	Set	Col.	%Orig. conc.	% in leach.*	%in soil	%Extracted propellant	%Energetics recovered
M31 0.02 mL min^{-1}									
Sassafras	U	CF	IV	c5	19	16.66	ND	49.79	66.45
Sassafras	U	CF	IV	c6	19	20.22	ND	46.11	66.33
Plymouth	U	IF	IV	c7	19	17.13	0.09	58.95	76.17
Plymouth	U	CF	IV	c8	19	16.26	0.10	49.63	65.99
Average±SE						17.6±0.9		51.1±2.7	68.7±2.5

ACN=acetonitrile; SE = Standard error; CF=continuous flow; IF=interrupted flow; PV = pore volume; *=Accounting for transformation, NA=not analyzed, ND=not detected. The NG transformation rate (k) was calculated from batch experiments and equaled 0.0193 h^{-1} for Sassafras soil and 0.0117 h^{-1} for Plymouth soil (Table 7).

One reason for incomplete mass balance may be irreversible adsorption or degradation in the soil not accounted for by batch-determined degradation and adsorption parameters. However, should adsorption or degradation contribute, they would influence concentrations at slower flow rates and we see the opposite.

3.5.2.3 Risk to groundwater

Because 2,4-DNT was not detected in the column outflow, we think it unlikely that 2,4 DNT will reach groundwater unless the source concentrations are high (1–10 mg/L) and the depth to groundwater small, less than 3 m. This agrees with studies of training ranges where no 2,4-DNT was found in groundwater even if it was detected in firing point soils (Clausen et al. 2004). NG experienced both adsorption and transformation in the soils, resulting in retardation of the breakthrough curve and decrease in eluted concentrations. Given the rate of transformation over short flow paths, we think that the majority of NG will be transformed before reaching groundwater. As NQ does not significantly degrade in the soil, it is likely to persist and eventually reach groundwater. Fortunately, it appears to be less toxic than 2,4-DNT or NG (Nipper et al. 2009). Triple-base propellants are also not as widely used as double-based propellants and the field test we witnessed deposited no measurable residues. Because NQ is not one of the analytes quantified by Method 8330B, it has not been routinely sought in the groundwater. We know of no instances of NQ in groundwater.

3.6 HYDRUS modeling

Computational models such as HYDRUS-1D, a widely used, one-dimensional water flow and solute transport code, use transport parameters, such as the adsorption coefficients, K_d, and the transformation rates, k, to predict transport of solutes through soils and into groundwater. In inverse mode, HYDRUS-1D fits the transport equations to the experimental breakthrough curves like ones obtained in our column experiments to determine values for the transport parameters (Šimunek et al. 2005).

HYDRUS-1D has been modified by Dr. Šimunek, its developer, to also estimate dissolution rate of energetics in the solid form, such as explosive particles (Dontsova et al. 2006) or propellant grains (Dontsova et al. 2008, 2009). To predict the dissolution of 2,4-DNT from M1 propellant, HYDRUS-1D used an empirical model that assumed exponential decrease in energetic dissolution with time. This resulted in very good agreement with experimental dissolution curves for M1; however, it did not work as well for NG and NQ dissolution from M9 and M30 propellants (Dontsova et al. 2008). Observed dissolution rates for NG and NQ did not decrease to zero but approached a steady rate that continued with little change. Therefore, in the current study, the HYDRUS was expanded to include a steady-state dissolution rate. This version was used to analyze all the breakthrough curves for the soil column studies. However, even with the changes implemented, the model did not explicitly address the processes that cause the exponential decrease in dissolved energetics.

To describe dissolution more mechanistically, and to link dissolution experiments conducted with and without soil, we also performed 2-D simulations of NG and NQ dissolution from M31 propellant in the drip studies and created a framework for modeling both dissolution and transport of energetics in soil.

3.6.1 1-D HYDRUS studies of propellant dissolution and transport in the soil columns

3.6.1.1 Dissolution

For propellants, the NG and NQ dissolution rate, γ [μg g^{-1} h^{-1}] was defined as follows:

$$\gamma_w = \max\left(\xi e^{-\chi t}, a\xi\right) \tag{12}$$

Where

ξ = initial dissolution rate [μg L^{-1} h^{-1}]

χ = decay constant [h^{-1}]

a = dimensionless constant that defines the minimum or steady-state dissolution rate ($a\xi$) as a fraction of the initial (maximum) dissolution rate (ξ)

t = time [h].

If a is larger than 1, a constant dissolution rate is used. When presenting the results, dissolution rate was recalculated relative to mass of propellant added to the column [μg g^{-1} h^{-1}].

3.6.1.2 Transport

The transport of the Br^{-1} tracer can be described using the convection-dispersion equation for constant water content, flux density, and dispersion coefficient:

$$\theta \frac{\partial c}{\partial t} = \theta D \frac{\partial^2 c}{\partial z^2} - q \frac{\partial c}{\partial z} \tag{13}$$

Where

c = solute concentration (μg cm^{-3})

q = convective flux (cm h^{-1})

θ = water content (cm^3 cm^{-3}) equal to porosity for saturated experiments

z = spatial coordinate (cm)

t = time (h)

D = dispersion coefficient (cm^2 h^{-1}) equal to the product of the longitudinal dispersivity, λ (cm), and q divided by θ.

3.6.1.3 Equilibrium sorption model (with decay)

The full model for soil transport implemented in HYDRUS includes two-site sorption (Selim et al. 1976; van Genuchten and Wagenet 1989) and non-equilibrium adsorption–desorption reactions. In the simulations presented in this report, we used only equilibrium sorption. Here, sorption, s (μg g^{-1}) is assumed to be instantaneous

$$s = K_d c \tag{14}$$

where K_d is the linear distribution coefficient (cm^3 g^{-1}), and c is the solute concentration (μg cm^{-3}). The governing transport equation is then as follows for constant water content, flux density, dispersion coefficient, bulk density, and distribution coefficient:

$$\frac{\partial \theta c}{\partial t} + \frac{\partial \rho s}{\partial t} = \frac{\partial}{\partial z}\left(\theta D^w \frac{\partial c}{\partial z}\right) - \frac{\partial q c}{\partial z} - \mu_w \theta c - \mu_s \rho s + \gamma_w \theta \tag{15}$$

where

ρ = bulk density (g cm^{-3})
μ_w = first-order rate coefficient in the liquid phase (h^{-1})
γ = dissolution rate as described in Eq. 12 (μg L^{-1} h^{-1}).

First-order rate coefficients in liquid and solid phase were set to be equal.

3.6.1.4 Parameter estimation

The numerical analysis of experimental data was carried out as follows. First, the conservative tracer breakthrough curves were used to estimate the longitudinal dispersivity, λ (cm). Then the longitudinal dispersivity was fixed at a value determined for the tracer and the chemical equilibrium model was then used to analyze energetic breakthrough curves. While it has been shown before that chemical non-equilibrium may play a role in adsorption and transport of explosives in soils at similar fluxes and for the same soils as used in this study (Dontsova et al. 2006), kinetic sorption has been not as important for NG and NQ (Dontsova et al. 2008). The following parameters were estimated for energetics: adsorption coefficient, K_d (g^{-1} cm^3), and three parameters that describe dissolution: initial dissolution rate ξ [μg L^{-1} h^{-1}], decay constant χ [h^{-1}], and constant, a, that multiplied by ξ gives the steady-state dissolution rate [μg L^{-1} h^{-1}]. Transformation rate coefficients (μ_w, same as k) determined in batch studies were used to account for transformation of solute in the soil.

The R^2 values and confidence intervals for fitted parameters were obtained by analyzing the correspondence between measured and fitted breakthrough concentrations and the behavior of the objective function around its minimum, respectively (Šimunek and Hopmans 2002). Parameter estimates were considered significant if they were different from zero (confidence intervals did not intersect with zero). For comparison between treatments, differences were considered significant when greater than the

sum of standard errors of the means multiplied by 1.96 (for 95% probability).

3.6.2 2-D HYDRUS simulations of energetic dissolution from M31 propellants

To model dissolution of energetics from propellant particles (a necessary step needed to compare experiments that were conducted with and without soil and to be able to model dissolution in soil columns mechanistically), we performed HYDRUS-2D simulations for dissolution curves from the drip studies of M31 propellants (Fig. 30). The two kinetic sorption sites model was applied to the data. This model was similar to the one used for soil transport, but looked at the condition where there is no flow within the particle and the only way for energetics to reach the surface is through diffusion. The model was run in axi-symmetrical 2-D; equations here are shown in 1-D to simplify them:

$$\frac{\partial\theta}{\partial t} + \rho\frac{\partial s_1}{\partial t} + \rho\frac{\partial s_2}{\partial t} + \rho\frac{\partial s_3}{\partial t} = \frac{\partial}{\partial z}\left(\theta D\frac{\partial c}{\partial z}\right) \tag{16}$$

$$s_1 = K_D c \tag{17}$$

$$\rho\frac{\partial s_2}{\partial t} = \theta k_{a2} c - k_{d2}\rho s_2 \tag{18}$$

$$\rho\frac{\partial s_3}{\partial t} = \theta k_{a3} c - k_{d3}\rho s_3 \tag{19}$$

$$\frac{\partial\theta}{\partial t} + \rho\frac{\partial s_1}{\partial t} + \rho\frac{\partial s_2}{\partial t} + \rho\frac{\partial s_3}{\partial t} = \frac{\partial}{\partial z}\left(\theta D\frac{\partial c}{\partial z}\right) \tag{16}$$

which leads to

$$\frac{\partial\theta R c}{\partial t} + \rho\frac{\partial s_2}{\partial t} + \rho\frac{\partial s_3}{\partial t} = \frac{\partial}{\partial z}\left(\theta D\frac{\partial c}{\partial z}\right) \tag{20}$$

$$R = 1 + \frac{\rho K_D}{\theta} \tag{21}$$

There was an equilibrium phase (characterized by the retardation factor R) and two kinetic sorption sites, one with faster release and one with slower release (basically irreversible). For the kinetic sites with rates of attachment and detachment, the equilibrium state is characterized as:

$$K_{D*} = \frac{\theta k_a}{\rho k_d} \tag{22}$$

This model assumes that dissolution of energetics from propellant particles is influenced by diffusion and equilibrium, kinetic and irreversible adsorption of NG to the NC matrix. The model assumes presence of the water phase inside the propellant particle.

3.6.3 Axi-symmetrical 2-D HYDRUS simulations of propellant in soil column

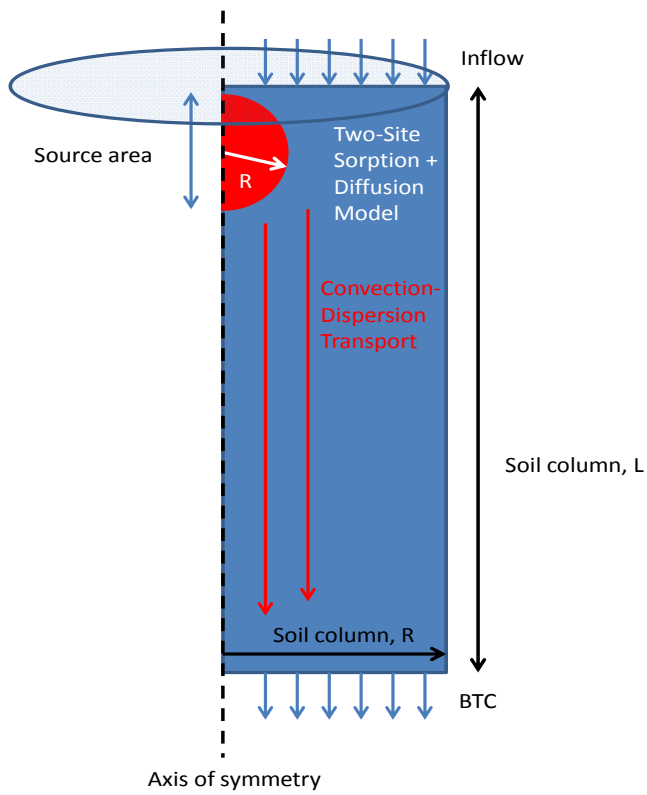

Figure 46. HYDRUS-2D axi-symmetrical domain showing modeled processes for dissolution of energetic from propellant particles and their transport in soil. The image is not done to scale to show detail.

The two models discussed above, one for energetic movement through propellant particle interior to the surface and another for its reactive transport in the soil, were then combined to characterize energetic dissolution and transport in the column. We set up the experimental domain (propellant particle on the surface of soil column) in 2-D to simulate axi-symmetrical (radial) 3-D. We multiplied each element by $2\pi \times R$ (circumference) (i.e., distance from the center of symmetry) to achieve axi-

symmetrical 3-D and relate this to propellant flux in the column outlet. HYDRUS-2D simultaneously solved the transport within the grain (on the scale of 1 mm or less, *R*) and then within the column (on the scale of about 10 cm, *L*) (Fig. 46). We tested this method using one sample dataset.

3.7 HYDRUS model and experiment comparisons

3.7.1 Propellant dissolution and transport in the soil columns

HYDRUS-1D simulations using a steady-state dissolution rate (eq 12) resulted in good agreement between observed and fitted breakthrough curves (Fig. 47, Table 13). In the majority of the cases, parameter *a*, which defines steady-state dissolution rate as a fraction of original dissolution rate, was significantly contributing to the objective function. Generally, better fit was produced for NG than for NQ (Fig. 47) and determined dissolution and transport parameters for NQ were largely non-significant. The reason the new model did not accurately describe NQ breakthrough curves is that NQ generally had a high initial peak followed by a fast decrease and then a slower decrease in dissolution rate over a long time period. An exponential decrease in dissolution rate that we modeled could describe the sharp peak, but not gradual decrease at the same time, so HYDRUS fitted a steady-state dissolution rate to the second half of the breakthrough, when concentration in reality changed over time. There were some potential issues with modeling NG dissolution, as well. In particular, the behavior of the actual and modeled breakthrough cures during flow interruption indicated that transformation rates determined in the batch experiments might have underestimated transformation rates of NG in soils. If this is true, it would be consistent with irreversible adsorption disproportionally contributing to transformation in columns studies and would also help close the mass balance. However, there was not enough evidence to support deriving transformation rates from interrupted flow experiments. While increasing the transformation rate improved fit for several simulations, this was not consistent across experiments, and for some it decreased the R^2.

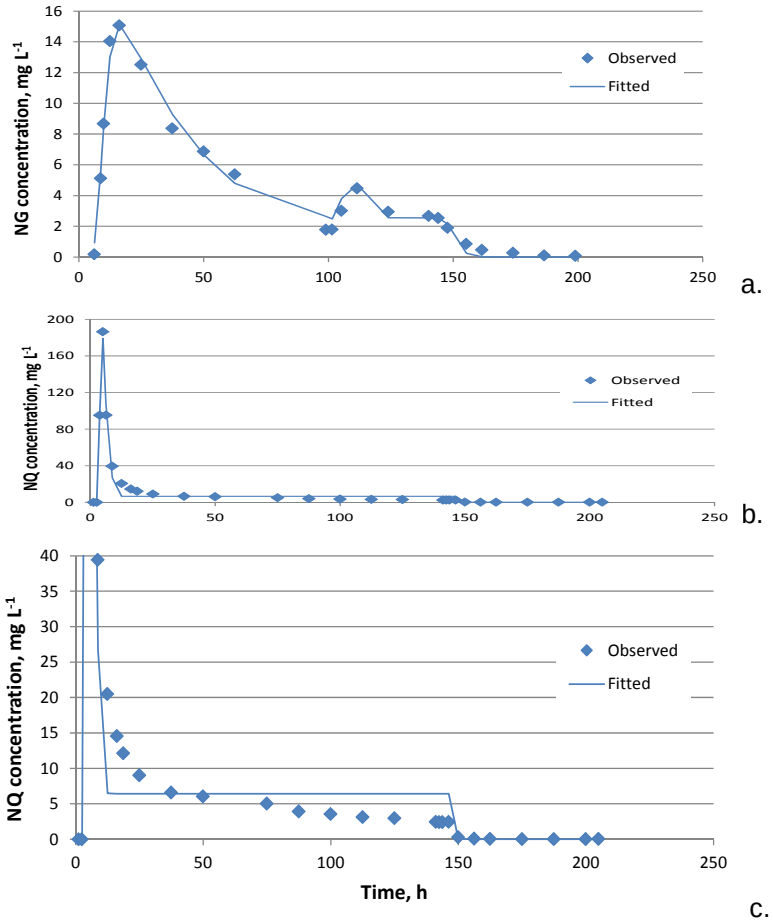

Figure 47. Observed and HYDRUS-1D generated breakthrough curves for NG (a) and NQ (b and c). (a) Unfired WC 860 propellant in Plymouth soil, interrupted flow experiment, 0.02 mL min^{-1} flow rate, set II, c_1, obtained parameters: χ =0.026±0.001; ξ =189± 6 µg g^{-1} h^{-1}; a = 0.136±0.017; K_d = 0.79±0.02 cm^3 g^{-1}; R^2=0.99. (b) and (c) (detail) unfired M31 propellant in Sassafras soil at continuous 0.02 mL min−1 flow rate, set IV, c_6, χ =0.56±0.06; ξ =3376±233 µg g^{-1} h^{-1}; a =0.018±0.004; K_d = 0.16±0.01 cm^3 g^{-1}; R^2 =0.98.

Table 13. Solute transport parameters obtained by HYDRUS-1D for column saturated flow experiments involving Br^{-1} and WC 860 and M31 propellants in Plymouth and Sassafras soils. λ was estimated from Br^{-1} breakthrough and characterizes water flow in the column, while χ, ξ, a, and K_d were determined from NG breakthrough. NQ transport parameters were not significantly different from zero and are not presented.

Treatment					Water parameters			NG parameters								
					λ		R^2	χ		ξ		a		K_D		R^2
					Est.	SE		Est.	SE	Est.	SE	Est.	SE	Est.	SE	
Soil	Prop.	F/U	CF/IF	Col.	(cm)			(h^{-1})		($\mu g\ g^{-1}\ h^{-1}$)				($cm^3\ g^{-1}$)		
Set I																
Plymouth	WC 860	U	IF	c3	0.734	0.014	0.83	0.052	0.010	367	55	0.124	0.020	0.93	0.07	0.98
Plymouth	WC 860	U	CF	c4	0.176	0.012	0.99	0.003	0.000	53	1	0.050	0.000	0.60	0.01	0.99
Plymouth	WC 860	F	IF	c5	0.237	0.015	0.96	0.011	0.002	26	2	0.288	0.028	1.17	0.05	0.95
Plymouth	WC 860	F	CF	c6	0.117	0.015	0.99	0.007	0.001	26	2	0.050	0.000	0.83	0.06	0.94
Set II																
Plymouth	WC 860	U	SF	c1	0.329	0.016	0.93	0.026	0.001	189	6	0.136	0.017	0.79	0.02	0.99
Plymouth	WC 860	U	CF	c2	0.983	0.021	0.79	0.051	0.016	277	58	0.109	0.036	1.33	0.16	0.90
Plymouth	WC 860	F	CF	c3	0.975	0.012	0.92	0.023	0.003	95	10	0.050	0.000	1.18	0.13	0.93
Plymouth	WC 860	F	SF	c4	0.010	0.297	0.95	0.024	0.002	65	3	0.164	0.030	0.88	0.02	0.96
Set III																
Sassafras	WC 860	U	SF	c1	0.513	0.013	0.81	0.055	0.006	228	18	0.014	0.008	0.18	0.04	0.96
Sassafras	WC 860	U	CF	c2	0.243	0.032	0.88	0.065	0.016	325	57	0.023	0.018	0.52	0.05	0.93
Sassafras	WC 860	F	IF	c3	0.031	0.117	0.87	0.035	0.006	85	9	0.015	0.011	0.02	0.01	0.90
Sassafras	WC 860	F	CF	c4	0.100	0.033	0.91	0.040	0.003	70	3	0.000	0.000	0.34	0.01	0.98
Sassafras	M31	U	IF	c5	0.945	0.014	0.65	0.025	0.008	1947	453	0.050	0.035	0.44	0.06	0.86
Sassafras	M31	U	IF	c6	0.212	0.014	0.90	0.029	0.004	1809	158	0.049	0.017	0.34	0.02	0.96
Plymouth	M31	U	CF	c7	0.100	0.033	0.93	0.008	0.001	540	21	0.050	0.000	0.66	0.02	0.98
Plymouth	M31	U	IF	c8	0.255	0.009	0.88	0.012	0.001	1039	34	0.053	0.015	0.62	0.02	0.98
Set IV																
Sassafras	WC 860	U	IF	c1	0.198	0.013	0.95	0.049	0.005	155	9	0.033	0.008	0.37	0.02	0.97
Sassafras	WC 860	U	CF	c2	1.238	0.015	0.71	0.055	0.007	213	16	0.067	0.020	0.62	0.04	0.93
Sassafras	WC 860	F	CF	c3	0.100	0.019	0.99	0.039	0.002	84	2	0.001	0.000	0.37	0.01	0.99
Sassafras	M31	U	IF	c 5	0.541	0.007	0.91	0.091	0.017	1290	156	0.099	0.019	0.40	0.04	0.93
Sassafras	M31	U	CF	c6	0.100	0.024	0.91	0.042	0.003	1015	36	0.127	0.012	0.29	0.01	0.98
Plymouth	M31	U	IF	c7	0.891	0.005	0.92	0.080	0.023	1582	347	0.073	0.018	1.38	0.15	0.95
Plymouth	M31	U	CF	c8	1.577	0.009	0.86	0.014	0.002	503	68	0.050	0.000	0.66	0.18	0.80

CF=continuous flow; IF=interrupted flow; F=fired; U=unfired; λ =longitudinal dispersivity, cm; kd = adsorption coefficient ($cm^3\ g^{-1}$); χ = exponent, h^{-1}; ξ = maximum (initial) dissolution rate, $\mu g\ g^{-1}\ h^{-1}$; a = constant, dimensionless; $a\xi$ = minimum (steady-state) dissolution rate, $\mu g\ g^{-1}\ h^{-1}$. NG transformation rate (k) was determined in batch experiments and equaled 0.0193 h^{-1} in Sassafras soil, and 0.0117 h^{-1} in Plymouth soil (Table 7). Shaded parameter estimates were not statistically significant.

Much higher NG dissolution rates, both maximum (1216 ± 192 μg g^{-1} h^{-1} vs. 226 ± 35 μg g^{-1} h^{-1}) and steady-state (83 ± 15 μg g^{-1} h^{-1} vs. 17 ± 6 μg g^{-1} h^{-1}) were calculated for M31 than for WC860 propellant, in agreement with drip studies. In M31 propellant, steady state rates were higher for higher flow velocity (99 vs. 67 μg g^{-1} h^{-1}) but the differences were not significant at 95%. Flow rate did not significantly influence WC860 dissolution. Soil did not affect dissolution rates for either propellant, as expected. Determined adsorption coefficients were 0.92 ± 0.02 cm^3 g^{-1} for Plymouth and 0.35 ± 0.05 cm^3 g^{-1} for Sassafras, in general agreement with batch numbers (1.41 cm^3 g^{-1} and 0.26 cm^3 g^{-1} for Plymouth and Sassafras, respectively). High initial concentrations of energetics dissolving from propellant particles can result in non-linear adsorption and lower measured K_{ds}.

Initial NG dissolution rate, calculated for the unfired WC860 propellant (226 μg g^{-1} h^{-1}), was lower than one previously calculated for the similarly sized M9 (1583 μg g^{-1} h^{-1}) (Dontsova et al. 2008). The difference can be explained by the lack of graphite on the surface of M9 but more likely by the much higher NG to NC ratio in this propellant (0.667 for M9 and 0.125 for WC860) further supporting conclusions made in drip studies about the importance of how NG adsorbs to NC and the NG/NC ratio.

At the same time, M31 had similar NG to NC ratios to previously studied M30 (1 and 0.8, respectively), but much higher initial dissolution (1216 μg g^{-1} h^{-1} in M31 and 60 in μg g^{-1} h^{-1} in M30). A lower dissolution rate of NG from M30 propellant may be explained by the very large size of M30 particles (2.2 cm in length and 1.05 cm in diameter) and their smaller surface area to mass ratio.

3.7.2 2-D HYDRUS simulations of energetic dissolution from M31 propellants

HYDRUS-2D simulations of NG and NQ dissolution from M31 propellant in drip studies indicated that diffusion only did not adequately describe experimental results (Fig. 48a). This agrees with diffusion modeling of NG dissolution from small arms propellants done in this project. To improve the fit, we included an interaction term between NG, NQ, and NC matrix in our simulations. Adding equilibrium absorption (eq 17) did not improve the agreement between experiment and simulation (not shown). However, adding kinetic adsorption (eq 18 and 19) significantly improved the fit (Fig. 48b).

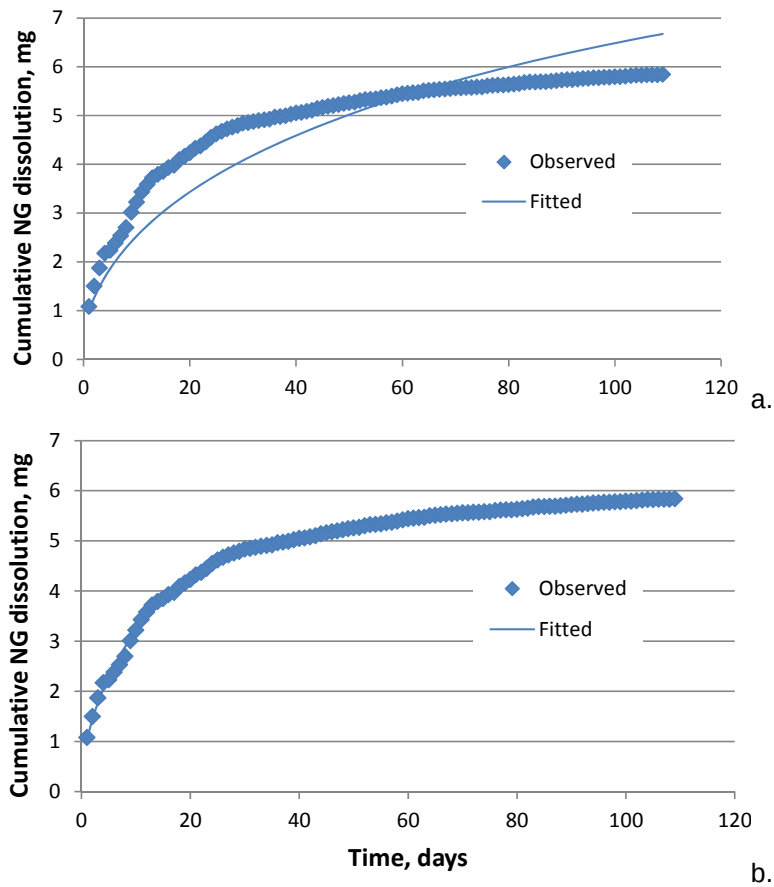

Figure 48. Observed and HYDRUS-1D generated cumulative dissolution curves for NG from M31 propellant particle in drip studies without soil. (a) Diffusion only: D = 1.81x10^{-10} ± 4.82x10^{-5}, cm^2 s^{-1}; R^2 = 0.91; (b) Diffusion and adsorption on two kinetic sites in NC: D = 6.63x10^{-9} ± 1.06 x10^{-9} cm^2 s^{-1}; adsorption rate for fast sites, k_{a1} = 0.1775 ± 0.0172 day^{-1}; desorption rate for fast sites, k_{d1} = 0.1163 ± 0.0110 day^{-1}; adsorption rate for slow sites k_{a2} = 0.0050 ± 0.0008 day^{-1}; desorption rate for slow sites k_{d2} = 0.0024 ± 0.0003 day^{-1}; R^2 = 1.00.

For NG, adsorption on two types of kinetic sites (one slow and one fast) better described the data than one adsorption site only, but for NQ one kinetic site was sufficient. In fact, adsorption and desorption rates for a second site were not significant (Table 14), and removing this second kinetic site did not change other parameters. For NG one kinetic site resulted in a good fit, though not as good as two sites. The diffusion coefficient, however, was an order of magnitude lower if only one sorption site was modeled. This indicates that both sites were contributing to NG adsorption. The fact that kinetic sorption is needed to describe dissolution of energetics from propellant particles indicates that slow release of solute from the sorption sites slows NG and NQ dissolution.

Table 14. HYDRUS 2D-determined parameters for dissolution of NG and NQ from M31 particles in drip studies in the absence of soil: diffusion coefficient, adsorption and desorption rates for two different kinetic adsorption sites, adsorption coefficient calculated for these sites.

Parameter	NG		NQ	
	Average	SE (n=8)	Average	SE (n=8)
Two kinetic adsorption sites				
D, cm^2 s^{-1}	2.09×10^{-8}	4.39×10^{-9}	1.78×10^{-9}	3.74×10^{-10}
k_{a1}, day^{-1}	0.7519	0.1261	0.0203	0.0200
k_{d1}, day^{-1}	0.2953	0.0469	0.2511	0.0193
k_{a2}, day^{-1}	0.0051	0.0007	0.0066	0.0005
k_{d2}, day^{-1}	0.0013	0.0003	0.0005	0.0001
K_{D1*}, cm^3 g^{-1}	0.88	0.16	0.04	0.04
K_{D2*}, cm^3 g^{-1}	1.42	0.17	4.33	0.62
One kinetic adsorption site				
D, cm^2 s^{-1}	2.55×10^{-9}	3.24×10^{-10}	1.89×10^{-9}	3.31×10^{-10}
k_{a2}, day^{-1}	0.0014	0.0006	0.0072	0.0014
k_{d2}, cm^3 g^{-1}	0.0011	0.0003	0.0005	0.0001
K_{D2*}, cm^3 g^{-1}	0.37	0.04	4.07	0.37

SE = standard error of the mean; Shaded numbers were not statistically significant. D = diffusion coefficient, cm^2 s^{-1}; k_{a1}= adsorption rate for fast sites, day^{-1}; k_{d1}= desorption rate for fast sites, day^{-1}; k_{a2} = adsorption rate for slow sites, day^{-1}; k_{d2}= desorption rate for slow sites, day^{-1}; K_{D1*}=adsorption coefficient calculated for fast sites, cm^3 g^{-1}; K_{D2*}=adsorption coefficient calculated for slow sites, cm^3 g^{-1}.

If no adsorption was modeled, fitted diffusion coefficients were lower than determined in simulations that included kinetic adsorption, as slow release was attributed to diffusion. If we included sorption, slow release was explained partially by slow desorption. The diffusion coefficients ($2.09\times10^{-8} \pm 4.39\times10^{-9}$ cm^2 s^{-1} for NG and $1.78\times10^{-9} \pm 3.74\times10^{-10}$ cm^2 s^{-1} for NQ) were higher than found for small arms propellants in this study but in general agreement with numbers reported by Levy (1955) for nitroglycerin in cellulose acetate, 5.2×10^{-9} cm^2 s^{-1}. Lack of contribution from fast sites to NQ adsorption was also confirmed by the low adsorption coefficient, K_{D1*}, for these sites, 0.04 cm^3 g^{-1} (Table 14). The fact that HYDRUS-2D simulations require adsorption term to describe energetic dissolution from propellants, supports observations by Yazici and Kalyon (1998) that NG in propellant particles is adsorbed and held by NC preventing its movement within the particle.

3.7.3 Axi-symmetrical 2-D HYDRUS simulations of propellant in soil column

A domain was set up to characterize dissolution of NQ from M31 propellant and transport in Plymouth soil. The model was run in direct mode using parameters that were determined for M31 particles. The simulated breakthrough curve was similar to the experimental curve. Further work will be needed to develop this capability, but the initial results indicate the potential for using this method to mechanistically describe energetics dissolution and transport in soil. The main challenge now is to describe multiple particles using axi-symmetrical 3-D.

4 Conclusions and Implication for Future Research

We collected single- and double-base propellant residues from live fire training and found that they had energetic contents similar to, but ~20% lower than, their unfired parent. The appearance of the residue was dictated by the shape of the original propellant grain; un-perforated grains yielded smaller versions of themselves, single perforated grains yielded rings, and multiple perforated grains deposited slivers. No residues were found when triple-base propellants were fired. This was also true for collections made when 155-mm mortars were fired using single-perforation M1 propellant.

Microscopically, we were able to distinguish between NC and crystalline NQ but were not able to map the distribution of 2, 4-DNT or NG in the nitrocellulose matrix, information important for understanding how these compounds dissolve out from the nitrocellulose. The different compounds within propellants are difficult to image because they are composed of amorphous organic compounds with very similar compositions. Also, because they are organic, the carbon, nitrogen, and oxygen energy-loss peaks are weak and diffuse instead of sharp, intense peaks seen in inorganic compounds. Nevertheless, our images and data suggest that NG remains a liquid within the NC matrix. We know NG is added as a liquid during manufacture, and others have noted that NG migrates toward the surface when present in concentrations >20%. For propellants with high fractions of NC (80–90%), we saw no change in the propellant grain size or the size of the residues when these were dripped on or immersed in water. As the percentage of NG increased, however, we noted that the structure of the propellant did change. This was especially noticeable for propellants with <60%NC where the grain collapsed leaving only NC.

The dissolution versus time curves for 2,4-DNT, NG, and NQ from unfired propellants show different patterns. Loss of 2,4-DNT is slower than that for NG or NQ. Furthermore, the shapes of the mass loss versus time curves are linear for unfired single-base propellants containing 2,4-DNT, whereas both the NG and NQ in double- and triple-base propellants show a fast initial mass loss rate followed by a slower dissolution rate. We found that the amount of NG dissolved is related to the NG/NC ratio. We think droplets

of NG near the surface are readily dissolved, followed by internal diffusion of NG through the NC matrix. In some cases, such as in triple-base propellants where crystals of NQ are present, dissolution of the crystals may open channels within the propellant.

Acetonitrile is an excellent solvent for extracting 2,4-DNT and NG from nitroglycerin based propellants. NQ, however, is less soluble in ACN and our low mass balance for NQ in our unfired triple-based propellants highlighted this problem. We suggest that a two-step extraction method might work better. If the propellants were crushed and placed in water, the NQ would quickly dissolve in the water and an aliquot could be used to quantify the NQ. The crushed propellant and an aliquot of the water could then be extracted in ACN to quantify the NG.

We implemented a series of simple diffusion models to understand the effects of geometry, concentration dependence, and wet/dry cycling on dissolution rate from propellants. Fitting the initial slopes of the dissolution curves did not yield similar diffusivities for the propellants, even if concentration dependent diffusion, different grain shapes, and wet/dry cycling were taken into account. Fitting the tail slopes of the dissolution curves, however, gave the same diffusivity rates for different data sets of the same propellant and varied by less than a factor of four among the propellant types ($3.2\times10-14$ to $1.2\times10-13$ $cm^2\ s^{-1}$). We think these values measure the long-term diffusion rates of these materials and that a different process, dissolution of near surface NG droplets, is responsible for the initial high NG loss. Once this outer layer of droplets is depleted, however, NG would need to diffuse through the solid NC matrix to reach the water, with considerably lower diffusivity ($\sim10^{-14}$ $cm^2\ s^{-1}$). Late time-dissolution would thus be limited by molecular diffusion.

This concept also qualitatively accounts for the much lower dissolution rates observed for fired grains. All dissolution of NG from fired grains would thus be limited by molecular diffusion. Indeed, the test data for fired grains do not show an abrupt roll-off characteristic of unfired grains and late-time dissolution rates as similar to those of unfired grains. Our microscopy results suggest that NG droplets are being directly dissolved from the surface, a process that would have to be included in future modeling.

Soil column studies using M1, WC 860, and M31 unfired propellants and the fired residues of M1 and WC 860 showed some of the same dissolution trends as the drip and batch tests where no soil was present. For WC 860 and M31, both NG and NQ concentrations in the outflow were initially high and decreased with time. The fired WC 860 residues released a lower percentage of their NG, supporting microscopic observations that the rim of the residues had burned and were depleted in NG.

Different interactions between 2,4-DNT, NG, NQ and the soils were seen in both the soil batch and column studies. The 2,4-DNT interacted strongly with soils and had the highest adsorption and transformation rates measured. There was also a strong correlation between soil adsorption and organic matter content in the soil. As a result, there was no 2,4-DNT in the column outflow. This result is consistent with lack of 2,4-DNT in groundwater under firing points even when it is deposited and detected in soils.

As was found in the drip tests, less NQ than NG was dissolved from triple-base propellants, despite a higher NQ content in the particles. We found that NQ has a low potential for soil adsorption, with adsorption coefficients for a variety of soils all being less than one; and no degradation or transformation. We would expect that NQ dissolved from propellant particles would reach groundwater. Fortunately, NQ appears to be less toxic than 2,4-DNT and NG (Nipper et al. 2009; Table 15).

Table 15. Summary of important characteristics determined for single-, double- and triple-based propellants.

	2,4-DNT	NG	NQ
Propellant	Single-base	Double- and triple-base	Triple-base
Solubility at 25 °C	270 mg/L Phelan and Barnett (2001)	1500 mg/L Yinon (1999)	2600 mg/L Haag et al. (1990)
Fate/Behavior	Strongly sorbed to organic matter	Moves through soil but subject to rapid aerobic biodegradation	Some photo degradation. Little attenuation, no biodegradation
Drinking water screening levels	0.2 µg/L EPA- Region 9	1.5 µg/L EPA- Region 9	1.6×10^3 µg/L EPA- Region 9
Log KOC	0.31 (–0.61 to 0.79)	–0.16 (–.062 to 0.64)	–0.73 (–0.99 to –0.30)
Half life, *h**	85 (29 to 408)	8 (2 to 347)	79 (15 to 56)
Toxicity	Carcinogenic EPA- Region 9, Quigley (1994)	Non carcinogen, EPA- Region 9 Affects the cardiovascular system, blood, and nervous system, Hathaway et al. (1991)	Non carcinogen; non- endocrine disrupter EPA- Region 9, Hiatt et al. (1988)

* Data summarized from Tables A2 and A3; average and range listed.

5 Case Study: Sampling for NG at the Automatic Record Fire (ARF) Range, Florence, AZ

5.1 Introduction

The Automatic Record Fire (ARF) range (Fig. 49) at the Florence Military Reservation was opened for training in October of 2010. The area had not been previously used for military training and hence the soils were devoid of energetic compounds deposited by training. The soils at the AFR are the Gunsight-Pinamt complex (marked on Fig. 50 as 26) and the Laveen loam (marked on Fig. 50 as 28 and 60) both grouped as Aridisols formed from alluvial material (Soil Survey Staff 2012). They have gravely loam to sandy loam textures and are well drained, with hydraulic conductivities between 14.4 and 151.2 mm h^{-1}. These soils have a calcic horizon (commonly called caliche), are alkaline (pH of 7.9–8.4), low in organic matter (less than 0.5% throughout), and contain about 14–28% clay. Total rainfall between the time the range was opened and when we sampled was 116.33 mm or 4.58 in. (Fig. 51).

Figure 49. Automatic Record Fire range at the AZ National Guard Florence Military Reservation.

Figure 50. National Cooperative Soil Survey, Web Soil Survey map (Soil Survey Staff 2012) of the Florence Military Reservation area that includes the Automatic Record Fire range. Black lines show outline of the range itself. Numbers indicate soil groups: 26—Gunsight-Pinamt complex, 28—Laveen loam.

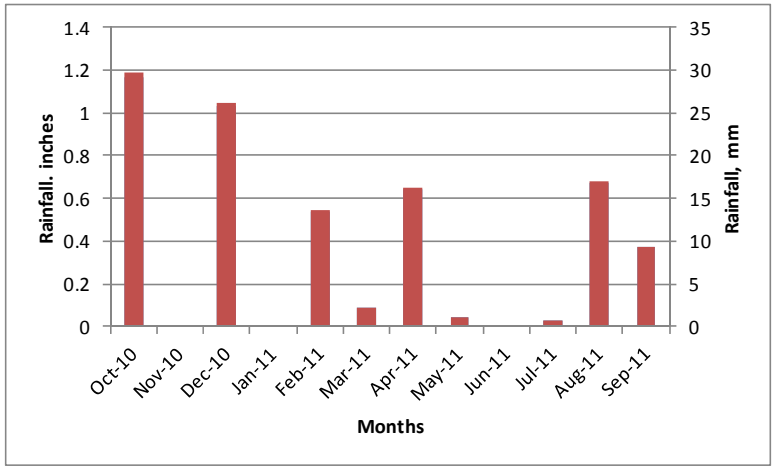

Figure 51. Rainfall record (October 2010 and September 2011) for Florence Military reservation.

Since it opened, the ARF range has been used to fire small arms, including rifles, machine guns, and pistols. The majority of rounds fired were 5. 56-mm, but 0.45- and 0.50-cal., and 9-mm cartridges were also used (Table 16). Because the exact number of rounds fired at the site is known, sampling the range soil provides the first opportunity to relate range usage to energetic compound concentrations in the soil. The propellants WC844 (used in 5.56-mm rounds) and WC 860 (used in 50-cal. rounds) are double-base and contain 8 to 11% nitroglycerin (NG) in an 85% nitrocellulose

matrix (Defense Ammunition Center 2006). All of the propellants fired at this range contained NG.

Table 16. Record of ammunition fired on the Automatic Record Fire (ARF) range between 1 October 2010 and 9 August 2011.

Munition (Mil/DODIC)	Weapon	Propellant	Constituent	No. rounds fired
M855/AA33 Ball	M16A2 Automatic Rifle (5.56-mm)	WC844	NG	34,198
M2 or M33/ A555 Ball Linked	M2 Machine Gun (.50-cal.)*	WC860	NG	250
M1911/A475 Ball	Pistol (.45-cal)**	SR7970	NG	51
M882 /A363 Ball	M9 Pistol (9-mm)	WPR289	NG	23
M856/A063 Tracer	M16A2 Automatic Rifle (5.56-mm)	WC844T	NG	1,200
M855/A062 Ball Linked	M249 Machine Gun (5.56-mm)	WC844	NG	2,400
M855/A059 Ball	M16A2 Automatic Rifle (5.56-mm)	WC844	NG	108,276
Total				146,398

* 12.7-mm, ** 11.4-mm, (Defense Ammunition Center 2006)

5.2 Materials and methods

The ARF range is 240 by 300 m and has 12 firing lanes along its short side (Fig. 52). We sampled soils from decision units that were 8 m wide and approximately 10 m long, about 2 m in front of firing positions 3 through 12. The first two firing lanes were not sampled as they were difficult to access, were overgrown with vegetation, and were not in use. We collected approximately 96 increments, using a 2.5-cm-diameter core pushed 2 cm into the soil, and combined these into one multi-increment sample of about 1-kg size for each decision unit. For three of the decision units (lanes 3, 5, and 9), we collected three multi-increment samples. In addition, we excavated six soil pits in two of the decision units and collected single profile samples to determine if NG was present in the subsoil.

The sizes and locations of the decision units were determined based on the residue distribution pattern found by firing tests of the same munitions (Walsh, M.E. et al. 2007). Walsh et al. found that the majority of the residues were located in a 42-m^2 area immediately in front of the firing point.

We placed our decision units 2 m in front of the firing points, as these were 2 m above ground (Fig. 53), causing the residues to travel a longer horizontal distance before being deposited. Background samples in areas away from the firing range were also collected. The average area of the decision units was 74 m².

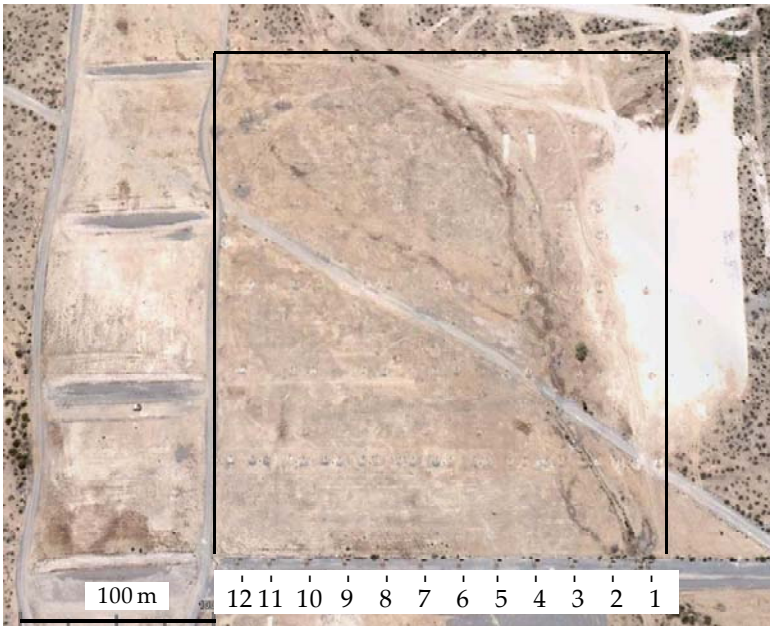

Figure 52. A Google Earth image showing the Automatic Record Fire (ARF) range at National Guard Florence Military Reservation, AZ. Firing positions are numbered, 1 through 12.

Figure 53. Firing position 7.

To measure any NG moving into the subsoil we excavated soil pits in two of the decision units (Fig. 54), three each from firing lanes 5 and 6. We collected discrete soil samples from the surface 0–1 cm and at 1–3, 3–5, 5–10, 10–15, 15–20, and 20–25 cm depth intervals. An impermeable caliche layer limited sampling depth (Fig. 54b). Pits were located about 5 to 6 m from the firing point in the middle of the lanes. These lanes were selected because they were close to the observation tower and are used preferentially (Fielding 2012), so would contain the most propellant residues and a greater potential for subsurface transport.

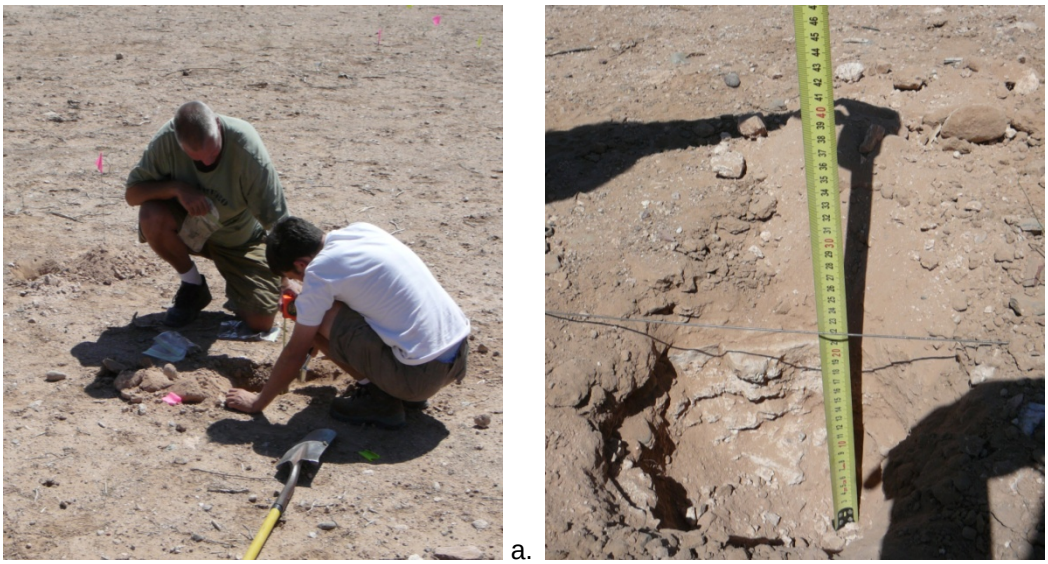

a. b.

Figure 54. Sampling a soil pit (a) and view of pit showing a low permeability white caliche layer (b).

The multi-increment samples were processed and analyzed according to standard procedures (U. S. Environmental Protection Agency 2006). Briefly, samples were air-dried, sieved, and the <2-mm size fraction ground for 90 s, homogenized, and 10-g subsamples were extracted overnight (18 h) using acetonitrile at 1:2, soil:acetonitrile, ratio. The pit samples were dried and sieved and the entire sample extracted. To make the sample mass manageable, we subdivided them into three subsamples, and extracted each subsample using acetonitrile in 1:2 soil to acetonitrile ratio, similar to the multi-increment samples. Acetonitrile extracts were diluted 1:3 with water, filtered through a PTFE filter, and analyzed for NG as described in the *Methods and Materials* section (5.2).

5.3 Results

Chemical analyses of the multi-increment samples show no NG in the background samples and surface soil NG concentrations that varied between 0.31 and 2.92 mg kg^{-1}. The central lanes, 6 and 7, had the highest NG concentrations (2.92 and 2.80 mg kg^{-1}, respectively, Table 17.) consistent with the observation that these lanes are used most frequently. Variability between three multi-increment samples taken of the same decision unit was low, with relative standard deviation (RSD) between triplicates of 2, 12, and 25%. The highest %RSD was for the sample with the lowest concentrations. These low RSD indicate that the multi-increment samples accurately measured the average NG concentration present in the decision units sampled.

Table 17. Concentration of NG in multi-increment surface samples collected at the Automatic Record Fire range.

Firing point	Measured mg kg^{-1} soil	Ave ± SE (n=3)	RSD %
3	0.40	0.31 ± 0.04	25.3
	0.25		
	0.28		
4	0.85		
5	1.36	1.36 ± 0.02	2.1
	1.33		
	1.38		
6	2.92		
7	2.80		
8	0.83		
9	1.41	1.43 ± 0.1	12.3
	1.62		
	1.27		
10	0.52		
11	1.21		
12	1.16		
Average	1.34 ± 0.28		
Background	B.D.	B.D.	

SE = SD/n^2, standard error, RSD = relative standard deviation, B.D. = below detection, Control recovery 100%, blank = 0 mg L^{-1}

The top surface samples from the soil pits had NG concentrations that generally agreed with the results for the multi-increment samples (Table 18, Fig. 55). These discrete samples had higher variability (29–60% RSD) than the multi-increment samples. No NG was detected in the subsurface samples, indicating no measurable transport. We think the lack of rain is primarily responsible. The total rainfall for the month before we sampled

was about 10 mm, a quantity unlikely to cause downward transport of any dissolved NG. The maximum monthly rainfall measured, 30 mm, would also keep any dissolved NG in the surface layers of the soil. The soil characteristics may also play a role but the role is unclear. The low organic matter content suggests little attenuation of NG while the clay should adsorb and transform the NG. Both absorption and transformation of NG are positively correlated with the clay content (Brannnon and Pennington 2002), Subsurface samples collected at other ranges, e.g., Fort Richardson, Alaska, contain high NG concentrations at the surface that diminished with depth (Jenkins et al. 2008, chapter 8).

Table 18. Concentration of NG, mg kg^{-1} soil, from the 0–1 cm layer in the soil pits at the Automatic Record Fire range.

Firing point	Pit	0–1 cm soil conc.	Ave. pit ± SE (*n*=3)	%RSD	Ave. firing point ± SE (*n*=3)	%RSD
5	1	1.20	1.66±0.32	32.8	2.68±0.94	60
		1.53				
		2.27				
	2	1.71	1.83±0.19	18.3		
		1.57				
		2.21				
	3	4.82	4.55±0.16	6.0		
		4.28				
		4.55				
6	4	1.92	2.11±0.32	26.4	2.38±0.39	29
		1.68				
		2.74				
	5	2.84	3.15±0.18	9.9		
		3.14				
		3.46				
	6	1.72	1.87±0.28	25.8		
		1.48				
		2.40				

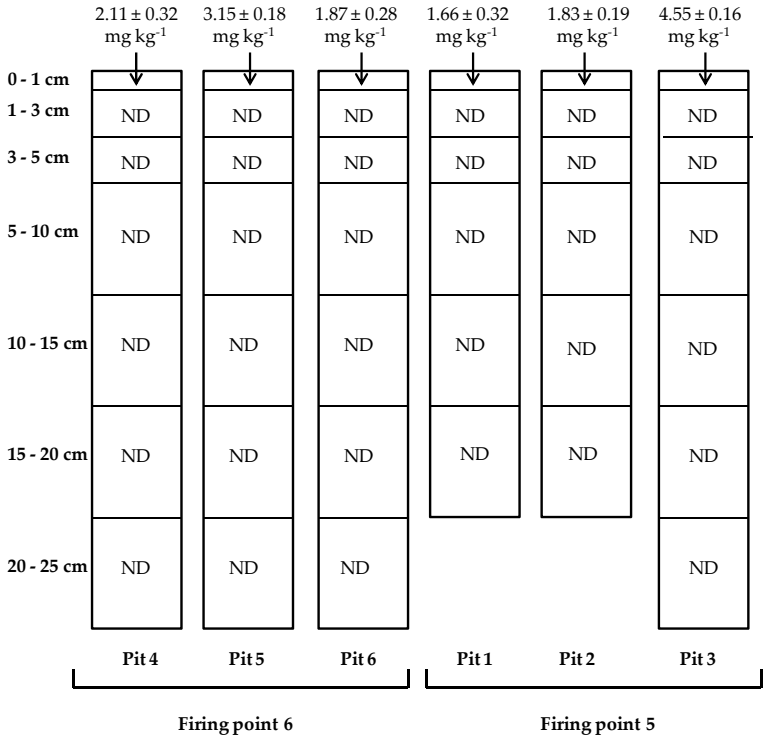

Figure 55. Depth and NG concentration of pit samples collected at the Automatic Record Fire range.

6 References

Achtnich, C., E. Fernandes, J.-M. Bollag, H.-J. Knackmuss, and H. Lenke. 1999. Covalent binding of reduced metabolites of [^{15}N3]TNT to soil organic matter during a bioremediation process analyzed by 15N NMR spectroscopy. *Environmental Science & Technology* **33**: 4448–4456.

Bangerth, W., R.Hartmann, and G. Kanschat. 2007. Deal.II—a general-purpose object oriented finite element library. *ACM Transactions on Mathematical Software* **33**(4): 24/1–24/27.

Brannon, J. M., and J. C. Pennington. 2002. *Environmental fate and transport process descriptors for explosives*. U.S. Army Engineer Research and Development Center, Environmental Laboratory, ERDC/EL TR-02-10.

Brenner, S., and L. Scott. 1994. *The Mathematical Theory of Finite Element Methods*. New York: Springer-Verlag.

Cao, A., A. Pandva, G. Serhatkulu, et al. 2007. A Robust Method for automated background subtraction of tissue fluorescence. *Journal of Raman Spectroscopy* **38** (9): 1199–1205.

Clausen, J., J. Robb, D. Curry, and N. Korte. 2004. A case study of contaminants on military ranges: Camp Edwards, Massachusetts, USA. *Environmental Pollution* **129**: 13–21.

Confocal Raman Microscopy General Overview. 2012. *Princeton Instruments*. http://content.piacton.com/Uploads/Princeton/Documents/Library/UpdatedLibrary/Confocal_raman_microscopy_note.pdf.

Crank, J. 1975. *The Mathematics of Diffusion*, 2nd Edition. Oxford: Clarendon Press.

Defense Ammunition Center, U.S.A. 2006. *Propellant Identification Manual*. McAlester, OK: Defense Ammunition Center.

Dontsova, K. M., J. C. Pennington, C. Hayes, J. Šimunek, and C. W. Williford. 2009. Dissolution and transport of 2,4-DNT and 2,6-DNT from M1 propellant in soil. *Chemosphere* **77**: 597–603.

Dontsova, K. M., J. C. Pennington, S. Yost, and C. Hayes. 2007. Transport of nitroglycerin, nitroguanidine and diphenylamine in soils. In *Characterization and Fate of Gun and Rocket Propellant Residues on Testing and Training Ranges: Interim Report 1*. . U.S. Army Engineer Research and Development Center, Environmental Laboratory, ERDC/EL TR-07-1.

Dontsova, K. M., M. Chappell, J. Šimunek, and J. C. Pennington. 2008. Dissolution and transport of nitroglycerin, nitroguanidine and ethyl centralite from M9 and M30 propellants in soils. In *Characterization and fate of gun and rocket propellant residues on testing and training ranges: Final report*. U.S. Army Engineer Research and Development Center, ERDC TR-08-1.

Dontsova, K. M., S. L. Yost, J. Šimunek, J. C. Pennington, and C. W. Williford. 2006. Dissolution and transport of TNT, RDX, and Composition B in saturated soil columns. *J. Environ. Qual.* **35**: 2043–2054.

Fielding, G. 2012. Personal communication, Arizona Army National Guard.

Haag, W. R., R. Spanggord, T. Mill, R. T. Podoll, T.-W. Chou, D. S. Tse, and J. C. Harper. 1990. Aquatic environmental fate of nitroguanidine. *Environ. Toxicol. Chem.* **9**: 1359–1367.

Haderlein, S. B., K. W. Weissmahr and R. P. Schwarzenbach. 1996. Specific adsorption of nitroaromatic explosives and pesticides to clay minerals. *Environ. Sci. Technol.* **30**: 612–622.

Hathaway, G. J., N. H. Proctor, J. P. Hughes, and M. L. Fischman. 1991. *Proctor and Hughes' Chemical Hazards of the Workplace*. 3rd Edition. New York: Van Nostrand Reinhold.

Hernández, M. D., I. Santiago, and I. Y. Padilla. 2006. Macro-sorption of 2,4-dinitrotoluene onto sandy and clay soils. In *Detection and Remediation Technologies for Mines and Minelike Targets XI* (J. T. Broach et al., Eds.), Vol. 6217. SPIE, Orlando (Kissimmee), FL, USA, pp. 6217-36

Hewitt, A., and S. Bigl. 2005. *Elution of energetic compounds from propellant and Composition B residues*. U.S. Army Engineer Research and Development Center, Cold Regions Research and Engineering Laboratory, ERDC/CRREL TR-05-13.

Hiatt, G. F., S. K. Sano, C. R. Wheeler, and D. W. Korte, Jr. 1988. *Acute oral toxicity of nitroguanidine in mice*. San Francisco, CA: Letterman Army Inst of Research, p. 55.

Howard, P. H., R. S. Boethling, W. F. Jarvis, W. M. Meylan, and E. M. Michalenko. 1991. *Handbook of Environmental Degradation Rates*. Chelsea, MI: Lewis Publishers.

Jenkins ,T. F. et al. 2008. *Characterization and fate of gun and rocket propellant residues on testing and training ranges: Final report*. U.S. Army Engineer Research and Development Center, ERDC TR-08-1.

Jenkins, T. F., C. Bartolini, and T. Ranney. 2003. *Stability of CL-20, TNAZ, HMX, RDX, NG and PETN in moist, unsaturated soil*. U.S. Army Engineer Research and Development Center, ERDC TR-03-7.

Ksiazczak, A., A. Radomski, and T. Zielenkiewicz. 2003. Nitrocellulose porosity-thermoporometry. *Journal of Thermal Analysis and Caolorimetry* **74**: 559–568.

Levy M. E. 1955. *Microscopic studies of ball propellant*. Philadelphia, PA: USA, Pitman-Dunn Laboratories, Frankford Arsenal Report.

Lever, J. H, S. Taylor, L. Perovich, K. Bjella, and B. Packer. 2005. Dissolution of Composition B residuals. *Environmental Science and Technology* **39**: 8803–8811.

Mirecki, J. E., B. Porter, and C. A. Weiss. 2006. *Environmental transport and fate process descriptors for propellant compounds*. U.S. Army Engineer Research and Development Center, Environmental Laboratory, ERDC/EL TR-06-7.

Miyares, P. H., and T. F. Jenkins. 2000. *Estimating the half-lives of key components of the chemical vapor signature of land mines*. U.S. Army Engineer Research and Development Center, Cold Regions Research and Engineering Laboratory, ERDC/CRREL TR-00-17.

Mulherin, N. D., T. F. Jenkins, and M. E. Walsh. 2005. *Stability of nitroguanidine in moist, unsaturated soils*. U.S. Army Engineer Research and Development Center, Cold Regions Research and Engineering Laboratory, ERDC/CRREL TR-05-2.

Nipper, M., R. S. Carr, and G. R. Lotufo. 2009. Aquatic toxicology of explosives. In *Ecotoxicology of Explosives* (G. I. Sunahara, G. Lotufo, R. G. Kuperman and J. Hawari, Eds.). CRC Press, pp 325.

Pennington, J. C., D. Gunnison, D. W. Harrelson, J. M. Brannon, et al. 1999. *Natural attenuation of explosives in soil and water systems at Department of Defense sites: Interim Report*. U.S. Army Waterways Experiment Station, Environmental Laboratory, TR EL-99-8.

Pennington, J. C., J. M. Brannon, T. E. Berry, Jr. , T. F. Jenkins, P. H. Miyares, M. E. Walsh, A. D. Hewitt, N. Perron, T. A. Ranney, J. Lynch, J. J. Delfino, and C. A. Hayes. 2001. *Distribution and fate of energetics on DoD test and training ranges: Interim report 1*. U.S. Army Engineer Research and Development Center, ERDC TR-01-13-1.

Pennington, J. C., K. A. Thorn, C. A. Hayes, B. E. Porter, and K. R. Kennedy. 2003. *Immobilization of 2,4- and 2,6-dinitrotoluenes in soils and compost*. U.S. Army Engineer Research and Development Center, Environmental Laboratory, ERDC/EL TR-03-2.

Pennington, J. C., T. F. Jenkins, G. Ampleman, S. Thiboutot, J. M. Brannon, J. Lynch, T. A. Ranney, J. A. Stark, M. E. Walsh, J. Lewis, C. A. Hayes, J. E. Mirecki, A. D. Hewitt, N. Perron, D. Lambert, J. Clausen, and J. J. Delfino. 2002. *Distribution and fate of energetics on DoD test and training ranges: Interim Report 2*. U.S. Army Engineer Research and Development Center, ERDC TR-02-8.

Pennington, J.C., T.F. Jenkins, G. Ampleman, and S. Thiboutot (2004) Distribution and fate of energetics on DoD test and training ranges: interim report 4. Technical report TR-04-4.

Phelan, J. M., and J. L. Barnett. 2001. Phase partitioning of TNT and DNT in soils. Albuquerque, NM: Sandia National Laboratories Report SAND2001-0310.

Pitt, J. S. 2011. *Numerical modeling of NG diffusion in propellant grains*. U.S. Army Engineer Research and Development Center, Cold Regions Research and Engineering Laboratory, ERDC/CRREL LR-12-04.

Quigley, D. R. 1994. *Handbook of Emergency Chemical Management*. Boca Raton, FL: CRC Press.

Richie, S. 2012. Personal communication. ATK.

Roach, P. J. 2002. Code verification by the method of manufactured solutions. *Journal of Fluids Engineering—Transactions of the ASME* **124**(1): 4–10.

Rosenblatt, D. H., E. P. Burrows, W. R. Mitchell, and D. L. Parmer. 1991. Organic explosives and related compounds. In *The Handbook of Environmental Chemistry* (O. Hutzinger, Ed.). Heidelberg, Germany: Springer-Verlag Berlin, pp. 195–234.

Selim, H. M., J. M. Davidson, and R. S. Mansell. 1976. Evaluation of a two-site adsorption-desorption model for describing solute transport in soils. In *Summer Computer Simulation Conference Proceedings. NSF, Washington, DC.*

Šimunek J., M. T. van Genuchten, and M. Šejna. 2005. *The HYDRUS-1D software package for simulating the one-dimensional movement of water, heat, and multiple solutes in variably-saturated media*, Version 3.0. Riverside, CA: Department of Environmental Sciences, University of California Riverside.

Šimunek, J., and J. W. Hopmans. 2002. Parameter optimization and nonlinear fitting. In *Methods of Soil Analysis. Part 1. Physical Methods* (J.H. Dane and G.C. Topp, Eds.). 3rd Edition. Madison, WI: SSSA, p. 139–157.

Skelland, A. H. P. 1974. *Diffusional Mass Transfer*. New York: Wiley & Sons.

Soil Survey Staff, Natural Resources Conservation Service, United States Department of Agriculture. *Web Soil Survey*. Available online at http://websoilsurvey.nrcs.usda.gov/. Accessed 02/15/2012.

Speitel, G. E., H. Yamamoto, R. L. Autenrieth, and T. McDonald. 2002. *Laboratory fate and transport studies of high explosives at the Massachusetts Military Reservation. Final Report*. University of Texas at Austin and Texas A&M University.

Taylor, S., J. H. Lever, B. Bostick, M.R. Walsh, M.E. Walsh, and B. Packer. 2004. Underground UXO: Are they a significant source of explosives in soil compared to low- and high-order detonations? U.S. Army Engineer Research and Development Center, Cold Regions Research and Engineering Laboratory, ERDC/CRREL TR-04-23.

Taylor, S., J. H. Lever, J. Fadden, N. Perron, and B. Packer. 2009a. Simulated rainfall-driven dissolution of TNT, Tritonal, Comp B and Octol particles. *Chemosphere* **75**: 1074–1081.

Taylor, S., J. H. Lever, J. Fadden, N. Perron, and B. Packer. 2009b. Outdoor dissolution of tnt and tritonal. *Chemosphere* **77**: 1338–1345.

Technical Manual 43-0001-27, *Data Sheets: Small Caliber Ammunition*.

Thorn, K. A. and K. R. Kennedy. 2002. 15N NMR investigation of the covalent binding of reduced TNT amines to soil humic acid, model compounds, and lignocellulose. *Environmental Science & Technology* **36**: 3787–3796.

Thorn, K. A., J. C. Pennington, K. R. Kennedy, L. G. Cox, C. A. Hayes, and B. E. Porter. 2008. N-15 NMR study of the immobilization of 2,4- and 2,6-dinitrotoluene in aerobic compost. *Environmental Science & Technology* **42**: 2542–2550.

Trewartha, S., J. Shapter, C. Gibson, et al. 2011. Determination of Deterrent Profiles in Nitrocellulose Grains Using Confocal Raman Microscopy. *Propellants, Explosives, Pyrotechnics* **36**(5): 451–458. doi: 10.1002/prep.201000081.

U.S. Environmental Protection Agency. 2006. Nitroaromatics, nitramines and nitrate esters by high performance liquid chromatography (HPLC), SW-846 Method 8330B. Washington, DC: Office of Solid Waste and Emergency Response. http://www.epa.gov/epaoswer/hazwaste/test/new-meth.htm#8330B

U.S. Environmental Protection Agency—EPA. 2012. *Region 9 human health screening levels*. www.epa.gov/Region9/superfund/prg/.

U.S. Environmental Protection Agency—EPA. 2007. Human Health ScreeningValues Source: Version 10. http://www.epa.gov/earth1r6/6pd/rcra_c/pd-n/screen.htm.

van Genuchten, M. T., and R. J. Wagenet. 1989. Two-site/two-region models for pesticide transport and degradation: Theoretical development and analytical solutions. *Soil Sci. Soc. Am. J.* **53**: 1303–1310.

Walsh, M. E. 1989. *Analytical methods for determining nitroguanidine in soil and water*. U.S. Army Cold Regions Research and Engineering Laboratory, CRREL Special Report 89-35.

Walsh, M. E., C. A. Ramsey, S. Taylor, A. D. Hewitt, K. Bjella, and C. M. Collins. 2007. Sub-sampling Variance for 2,4-DNT in Firing Point Soils. *Soil and Sediment Contamination: an International Journal* **16**: 459–472.

Walsh, M. R., M. E. Walsh, and A. Hewitt. 2009. Energetic residues from the expedient disposal of artillery propellants. U.S. Army Engineer Research and Development Center, Cold Regions Research and Engineering Laboratory, ERDC/CRREL TR-09-8.

Walsh, M. R., M. E. Walsh, S. R. Bigl, N. M. Perron, D. J. Lambert, and A. D. Hewitt. 2007. *Propellant residue deposition from small arms munitions*. U.S. Army Engineer Research and Development Center, Cold Regions Research and Engineering Laboratory, ERDC/CRREL TR-07-17.

Walsh, M. R., S. Thiboutot, M. E. Walsh, G. Ampleman, R. Martel, I. Poulin and S. Taylor. 2011. Characterization and fate of gun and rocket propellant residues on testing and training ranges. U.S. Army Engineer Research and Development Center, Cold Regions Research and Engineering Laboratory, ERDC/CRREL TR-11-13.

Wilke, C. R. 1949. *Chem. Eng. Prog.* **45**: 218.

Windholz, M. 1976, *The Merck Index,* 9th Edition. Rahway, N.J.: Merck and Co., Inc.

Winkler, D. A. 1985. Conformational analysis of nitroglycerin. *Propellants, Explosives, Pyrotechnics* **10**: 43–46.

Yamamoto, H., M .C. Morley, G. E. Speitel, and J. Clausen. 2004. Fate and transport of high explosives in a sandy soil: adsorption and desorption. *Soil and Sediment Contamination* **13**: 361–379.

Yang, H., A. Halasz, J.-S. Zhao, F. Monteil-Rivera, and J. Hawari. 2008. *Experimental evidence for in situ natural attenuation of 2,4- and 2,6-dinitrotoluene in marine sediment*. **70**: 791–799.

Yazici R., and D. M. Kalyon. 1998. *Microstructure and mixing distribution analysis in M30 triple-base propellants*.

Yinon, J. 1999. *Forensic and Environmental Detection of Explosives*. Chichester, UK: John Wiley, p. 285.

Yost, S. 2004. Effects of redox potential and pH on the fate of nitroglycerin in a surface and aquifer soil, M. S. Thesis, Louisiana State University, Baton Rouge, LA.

Appendix A: Propellant and Soil Property Data

Table A1. Nitrocellulose-based propellants used by the U.S. Army.*

Used in	Propellant	Constituent	Percent	shape
	Single-base			
mortars	M10	NC	98	flake
mortars	M10	NC	98	single perforated grain
mortars	M10	NC	98	multi-perforated grain
tank training	M14	DNT	8	multi-perforated cylinder
artillery	M1	DNT	10	single or multi-perforated cylinder
artillery	M1	DNT	10	single or multi-perforated cylinde
artillery	M1	DNT	10	single or multi-perforated cylinde
40- to 155-mm rounds	M6	DNT	10	multi-perforated cylinder
75-mm	M6+2	DNT	10	multi-perforated cylinder
	Double-base			
?	M38	NG	2	grains
120-mm mortar	M45	NG	10	grain with single perforation
120-mm mortar	M47	NG	10	grains
90-mm artillery round	M5	NG	15	single-perforated cylinder
40 mm grenades	M2	NG	19.5	single perforated grain
76- and 90-mm artillery	M2	NG	19.5	multi-perforated cylinder
?	M28	NG	23	Cast grain
106-mm round	M26	NG	25	multi-perforated cylinder
152-mm round	M26A1	NG	25	multi-perforated cylinder
76 mm	M7	NG	32	single perforated stick
5 in round	M7	NG	35.5	single perforated stick
40-, 60- and 81-mm rounds	M9	NG	40	flake
60-, 80-mmand 4.2" mortars	M8	NG	43	sheet
120-mm mortar	M44	NG	44	Single perforated stick
small arms	WC844	NG	10	ball propellant
small arms	WC846	NG	10	ball propellant
small arms	WC860	NG	10	ball propellant
small arms	WPR289	NG	10	ball propellant

Used in	Propellant	Constituent	Percent	shape
artillery	Triple-base			
155 mm	M30A2	NQ&NG	46	7-perforated cylinder
155 mm	M30A1	NQ&NG	47	7-perforated cylinder
90- 155mm	M30	NQ&NG	48	7-perforated cylinder
8”	M31A1	NQ&NG	54	7-perforated cylinder
76-,90-, 120-mm	M15	NQ&NG	55	single or multi-perforated cylinder
120, 155-mm	M31	NQ&NG	55	single or multi-perforated cylinder
155 mm	M31A1E1	NQ&NG	55	multi-perforated cylinder
Rocket motor	M7	NQ&NG	55	Single perforated stick

*Data taken from Propellants: A guide to recognizing and identifying specific types of nitrocellulose-based propellant-online resource. Contact information for manual:

mcal.dac.sjmac-avpersonnel@conus.army.mil

U.S. Army Defense Ammunition Center (DAC), McAlester, OK

Table A2. Propellant constituent adsorption coefficients (K_d) and associated soil property data.

	Soil Type	K_d ($cm^3\ g^{-1}$)	CEC $cmol^+$ (kg^{-1})	TOC (%)	Clay (%)	Reference
2,4-DNT						
Sharkey/Yokena clay	Surface	12.5	38.9	2.4	48.7	Pennington et al., 2001
Plymouth	Surface	0.28–2.01	4.4	0.49	0.8	Dontsova et al., 2009
Plymouth	Surface	3.3	9.2	1.84	NM	Yamamoto et al., 2004
Yokena/Sharkey clay	Surface	9.43	38.9	2.4	49	Pennington et al., 2003
Picatinny	Surface	2.06	9.8	0.63	5	Pennington et al., 2003
Grange Hall	Surface	0.43	16.7	0.29	10	Pennington et al., 2003
Cotto clay	Surface	1.46	25.7	0.67	NM	Hernández et al., 2006
Isabella sand	Surface	0.0172	2.21	0.07	NM	Hernández et al., 2006
Halifax marine sed.	Sediment	11.7	14.5	1.9	8.25	Yang et al., 2008
K+-kaolinite	Pure clay	690	0.3	NM	NM	Haderlein et al., 1996
K+-illite	Pure clay	3650	1.6	NM	NM	Haderlein et al., 1996
K+-montmorillonite	Pure clay	7400	12	NM	NM	Haderlein et al., 1996
2,6-DNT						
Sharkey clay	Surface	5.96	38.9	2.4	48.7	Pennington et al., 2001
Plymouth	Surface	0.84–0.97	4.4	0.49	0.8	Dontsova et al., 2009
Yokena/Sharkey clay	Surface	3.56	38.9	2.4	49	Pennington et al., 2003
Picatinny	Surface	1.61	9.8	0.63	5	Pennington et al., 2003
Grange Hall	Surface	0.07	16.7	0.29	10	Pennington et al., 2003
Halifax marine	Sediment	8.3	14.5	1.9	8.25	Yang et al., 2008
K+-kaolinite	Pure clay	10	0.3	NM	NM	Haderlein et al., 1996

	Soil Type	K_d ($cm^3\ g^{-1}$)	CEC cmol+ (kg^{-1})	TOC (%)	Clay (%)	Reference
K+-illite	Pure clay	52	1.6	NM	NM	Haderlein et al., 1996
K+-montmorillonite	Pure clay	125	12	NM	NM	Haderlein et al., 1996
NG						
Plymouth	Surface	0.17	4.4	0.49	0.8	Dontsova et al., 2007
Adler	Surface	0.08	16.6	0.29	4.2	Dontsova et al., 2007
Plymouth	Surface	0.165	4.4	0.49	0.8	Dontsova et al., 2008
Adler	Surface	0.113	16.6	0.29	4.2	Dontsova et al., 2008
Plymouth	Surface	2.8	9.2	1.84	NM	Speitel et al., 2002
Picatinny	Surface	3.8	9.8	0.634	5	Pennington et al., 2002
NQ						
Plymouth	Surface	0.14	4.4	0.49	0.8	Dontsova et al., 2007
Adler	Surface	0.03	16.6	0.29	4.2	Dontsova et al., 2007
Plymouth	Surface	0.069	4.4	0.49	0.8	Dontsova et al., 2008
Adler	Surface	0.034	16.6	0.29	4.2	Dontsova et al., 2008
soil		< 0.1				Haag et al., 1990
Grange Hall	Surface	0.15	16.7	0.3	10	Pennington et al., 2004
Yokena clay	Surface	0.43	38.9	2.4	48.75	Pennington et al., 2004

Table A3. Soil transformation rate coefficients (k) for energetic compounds under different soil conditions.

Soil	Oxid	k (hr^{-1})	Half life (h)	CEC (μmol/g)	%TOC	%Clay	Reference
2,4-DNT							
LAAP ML	An	0.017	40	3.5	0.015	5	Pennington et al., 1999
LAAP SP-SM	An	0.0017	410	3.6	0.015	5	Pennington et al., 1999
LAAP CL	An	0.0021	330	8.1	0.162	15	Pennington et al., 1999
LAAP SM	An	0.0021	320	5.5	0.02	7.5	Pennington et al., 1999
Yokena clay	An	Rapid		38.9	2.4	48.7	Pennington et al., 2001
Plymouth	Aero	0.002–0.023 8	347-29	4.4	0.49	0.8	Dontsova et al., 2009
2,6-DNT							
LAAP C	An	0.0023	301	6.6	0.08	12	Pennington et al., 2001
LAAP D	An	0.0035	198	15.5	0.2	32	Pennington et al., 2001
Yokena clay	An	0.0235	29	38.9	2.4	48.7	Pennington et al., 2001
Plymouth		0.0085	82	4.4	0.49*	0.8	Dontsova et al., 2009
2,4-and 2,6-DNT							
Groundwater	Aero	0.00011	4320–672	NM	NM	NM	Howard et al., 1991
Groundwater	An	0.01441	300–48	NM	NM	NM	Howard et al., 1991
Soil	Aero	0.2–1.51E–3	4320–672	NM	NM	NM	Howard et al., 1991
NG							

Soil	Oxid	*k* (hr^{-1})	Half life (h)	CEC (µmol/g)	%TOC	%Clay	Reference
LAAP-D/SM		0.002	335	5.5	0.02	7.5	Pennington et al., 2002
Picatinny		0.008	84	9.8	0.634	5	Pennington et al., 2002
Yokena clay		0.095	7.3	38.9	2.4	48.75	Pennington et al., 2002
Plymouth2		0.008	88.1	4.4	0.49	0.8	Dontsova et al., 2007
Adler2		NS	NS	16.6	0.29	4.2	Dontsova et al., 2007
Yakima TC		>0.029	<24	19.6	2	20.1	Jenkins et al., 2003
Camp Guernsey		>0.029	<24	30.3	1.6	25.0	Jenkins et al., 2003
Fort Greely		0.059	11.8	9.0	1.1	3	Jenkins et al., 2003
LAAP-D	Aero	0.020	38.3	15.5	0.2	32	Yost, 2004
Yokena clay	Aero	0.018	38.1	38.9	2.4	34	Yost, 2004
LAAP-D	An	0.310	3.2	15.5	0.2	32	Yost, 2004
Yokena clay	An	0.263	2.7	38.9	2.4	34	Yost, 2004
NQ							
Yakima		0.0449	15.4	23.6	1.06	15	Mulherin et al., 2005
Lebanon Landfill		0.0123	56.4	NM	0.3	50	Mulherin et al., 2005
Fort Edwards Clay		0.0128	54.2	NM	0.6	14	Mulherin et al., 2005
Plymouth		NS	NS	4.4	0.49	0.8	Dontsova et al., 2007
Adler		NS	NS	16.6	0.29	4.2	Dontsova et al., 2007
Grange Hall		NS	NS	16.7	0.3	10	Pennington et al., 2004
LAAP D (SM?)		NS	NS	5.5	0.02	7.5	Pennington et al., 2004
Yokena clay		NS	NS	38.9	2.4	48.75	Pennington et al., 2004
DPA							
Adler		0.011	62.3	4.4	0.49	0.8	Dontsova et al., 2007
Plymouth		0.014	48.1	16.6	0.29	4.2	Dontsova et al., 2007
Grange Hall		0.0027	256	16.7	0.3	10	Pennington et al., 2004
LAAP D/SM		NS	NS	5.5	0.02	7.5	Pennington et al., 2004
Yokena clay		1.098	0.63	38.9	2.4	48.75	Pennington et al., 2004
EC							
Grange Hall		NS	NS	16.7	0.3	10	Pennington et al., 2004
LAAP D/SM		NS	NS	5.5	0.02	7.5	Pennington et al., 2004
Yokena clay		NS	NS	38.9	2.4	48.75	Pennington et al., 2004

1. Estimated; 2. C-14 data; Oxid=Oxidation Status; An=anaerobic; Areo=aerobic; NS = not significantly different from zero; NM = not measured.

Appendix B: Soil Properties and Soil Column Test Data

Table B1. Properties of soils used in column studies.

Soil	Sassafras			Plymouth			Catlin		
Property	aver.		stdev	aver.		stdev	aver.		stdev
pH	4.40	±	0.01	4.23	±	0.01	6.87	±	0.01
EC, µS cm^{-1}	212	±	27	130	±	6	538	±	20
CEC, $cmol_c$ kg^{-1}	16.58	±	1.32	18.78	±	2.87	23.59	±	0.98
OC, %	1.30		0.02	1.72		0.05	3.75		0.15
Clay, %	16.37	±	0.07	14.40	±	0.74	15.73	±	0.20
Silt, %	42.27	±	0.15	22.15	±	0.31	71.53	±	0.06
Sand, %	41.37	±	0.09	63.46	±	1.05	12.75	±	0.26
Texture	loam			sandy loam			silt loam		

pH (1:1 soil:water); EC = electrical conductivity in 1:1 soil:water, (µS cm^{-1}); CEC = cation exchange capacity by sodium acetate method, $cmol_c$ kg^{-1}; OC = total organic carbon by combustion, %; % Clay (<2 µm), Silt (2 - 50 µm), and Sand (50 - 2000 µm) by laser diffraction.

Table B2. NG loss from unfired and fired WC860 propellant and unfired M31 propellant in column experiments conducted at 0.01 and 0.02 mL min^{-1} flow measured by extraction of propellants and propellant residues after experiment completion.

Soil	U/F	CF/ IF	Set	Col.	HPLC Measured conc. (µg L^{-1}C	Dilut. Factor	Total NG in extract (µg L^{-1})	ACN (mL)	Total ppb in ACN	Propellant weight (g)	Meas. NG conc. in prop. (mg g^{-1})	Original NG conc. in prop. (%)	Final meas. NG left (%)	NG lost (%)
0.01 mL min^{-1} WC860														
Sassafras	U	IF	III	c1	1465	200	292900	20	5858	0.0860	68.12	9.7	6.81	29.78
Sassafras	U	CF	III	c2	1883	200	376633	20	7533	0.1009	74.65	9.7	7.47	23.04
Plymouth	U	IF	I	c3	NE	NE	NE	NE	NE	NE	NE	NE	NE	NE
Plymouth	U	CF	I	c4	NE	NE	NE	NE	NE	NE	NE	NE	NE	NE
Sassafras	F	IF	III	c3	2018	20	40360	20	807	0.0149	54.17	7.8	5.42	30.55
Sassafras	F	CF	III	c4	2438	20	48753	20	975	0.0167	58.39	7.8	5.84	25.14
Plymouth	F	IF	I	c5	NE	NE	NE	NE	NE	NE	NE	NE	NE	NE
Plymouth	F	CF	I	c6	NE	NE	NE	NE	NE	NE	NE	NE	NE	NE
0.02 mL min^{-1} WC860														
Sassafras	U	IF	IV	c1	1928	200	385667	20	7713	0.0970	79.52	9.7	7.95	18.02
Sassafras	U	CF	IV	c2	1931	200	386100	20	7722	0.0960	80.44	9.7	8.04	17.07

Soil	U/F	CF/ IF	Set	Col.	HPLC Measured conc. (μg L⁻¹C	Dilut. Factor	Total NG in extract (μg L-1)	ACN (mL)	Total ppb in ACN	Propellant weight (g)	Meas. NG conc. in prop. (mg g⁻¹)	Original NG conc. in prop. (%)	Final meas. NG left (%)	NG lost (%)
Plymouth	U	IF	II	c1	1344	200	268700	20	5374	0.0820	65.54	9.7	6.55	32.44
Plymouth	U	CF	II	c2	1777	200	355333	20	7107	0.0895	79.40	9.7	7.94	18.14
Average														21.42
SE														3.68
Sassafras	F	CF	IV	c3	2234	20	44677	20	894	0.0145	61.62	7.8	6.16	21.00
Plymouth	F	CF	II	c3	1418	40	56720	20	1134	0.0140	81.03	7.8	8.10	-3.88
Plymouth	F	IF	II	c4	1984	20	39680	20	794	0.0160	49.60	7.8	4.96	36.41
Average														17.84
SE														10.17
0.01 mL min⁻¹ M31														
Sassafras	U	IF	III	c5	1159	200	231800	20	4636	0.0765	60.60	19	6.06	68.10
Sassafras	U	IF	III	c6	1453	200	290600	20	5812	0.0748	77.70	19	7.77	59.10
Plymouth	U	IF	III	c7	1748	200	349533	20	6991	0.0767	91.14	19	9.11	52.03
Plymouth	U	CF	III	c8	1308	200	261633	20	5233	0.0784	66.74	19	6.67	64.87
Average														61.03
SE														3.53
0.02 mL min⁻¹ M31														
Sassafras	U	CF	IV	c5	3831	100	383067	20	7661	0.0810	94.58	19	9.46	50.22
Sassafras	U	CF	IV	c6	1770	200	354000	20	7080	0.0808	87.62	19	8.76	53.88
Plymouth	U	IF	IV	c7	1176	200	235267	20	4705	0.0420	112.03	19	11.20	41.04
Plymouth	U	CF	IV	c8	1876	200	375267	20	7505	0.0796	94.29	19	9.43	50.37
Average														48.88
SE														2.75

ACN=acetonitrile; SE = Standard error; CF=continuous flow; IF=interrupted flow; PV = pore volume; NE= not extracted; *=Accounting for transformation. NG transformation rate (k) used to calculate this value was determined in batch experiments and equaled to 0.0193 h^{-1}in Sassafras soil and 0.0117 h^{-1} in Plymouth soil (Table 7).

Table B3. Soil concentrations of NG in column tests using WC860 and M31 propellants and soil concentrations of 2,4-DNT in column tests using M1 propellant. For sets IV and V, the column was divided into top, middle and bottom sections and each of these extracted separately.

Propellant	Soil	U/F	CF/ IF	Set	Col.	Position	Soil conc. mg kg^{-1}
WC860	Sassafras	U	IF	III	c1		3.47
WC860	Sassafras	U	CF	III	c2		3.53
WC860	Sassafras	F	IF	III	c3		6.14
WC860	Sassafras	F	CF	III	c4		2.86
WC860	Sassafras	U	IF	IV	c1	T,M,B	ND
WC860	Sassafras	U	CF	IV	c2	T,M,B	ND
WC860	Sassafras	F	CF	IV	c3	T,M,B	ND
WC860	Plymouth	U	IF	II	c1		ND
WC860	Plymouth	U	CF	II	c2		ND
WC860	Plymouth	F	CF	II	c3		ND
WC860	Plymouth	F	IF	II	c4		2.76
M31	Sassafras	U	IF	III	c5		ND
M31	Sassafras	U	IF	III	c6		ND
M31	Sassafras	U	CF	IV	c5	T,M,B	ND
M31	Sassafras	U	CF	IV	c6	T,M,B	ND
M31	Plymouth	U	IF	III	c7		2.15
M31	Plymouth	U	CF	III	c8		2.42
M31	Plymouth	U	IF	IV	c7	Top	1.11
						Middle	0.94
						Bottom	1.75
M31	Plymouth	U	CF	IV	c8	Top	2.29
						Middle	1.17
						Bottom	0.84
M1	Sassafras	U	IF	V	c1	Top	0.34
						M,B	ND
M1	Sassafras	U	CF	V	c2	T,M,B	ND
M1	Sassafras	F	CF	V	c3	T,M,B	ND
M1	Sassafras	F	IF	V	c4	T,M,B	ND
M1	Plymouth	U	IF	V	c5	Top	1.07
						Middle	0.61
						Bottom	0.50
M1	Plymouth	U	CF	V	c6	Top	1.59
						Middle	0.58
						Bottom	ND
M1	Plymouth	F	IF	V	c7	T,M,B	ND
M1	Plymouth	F	CF	V	c8	Top	1.21
						M,B	ND

U=Unfired, F= Fired; CF=continuous flow; IF=interrupted flow; ND=not detected

Appendix C: Breakthrough Curves for Soil Column Tests

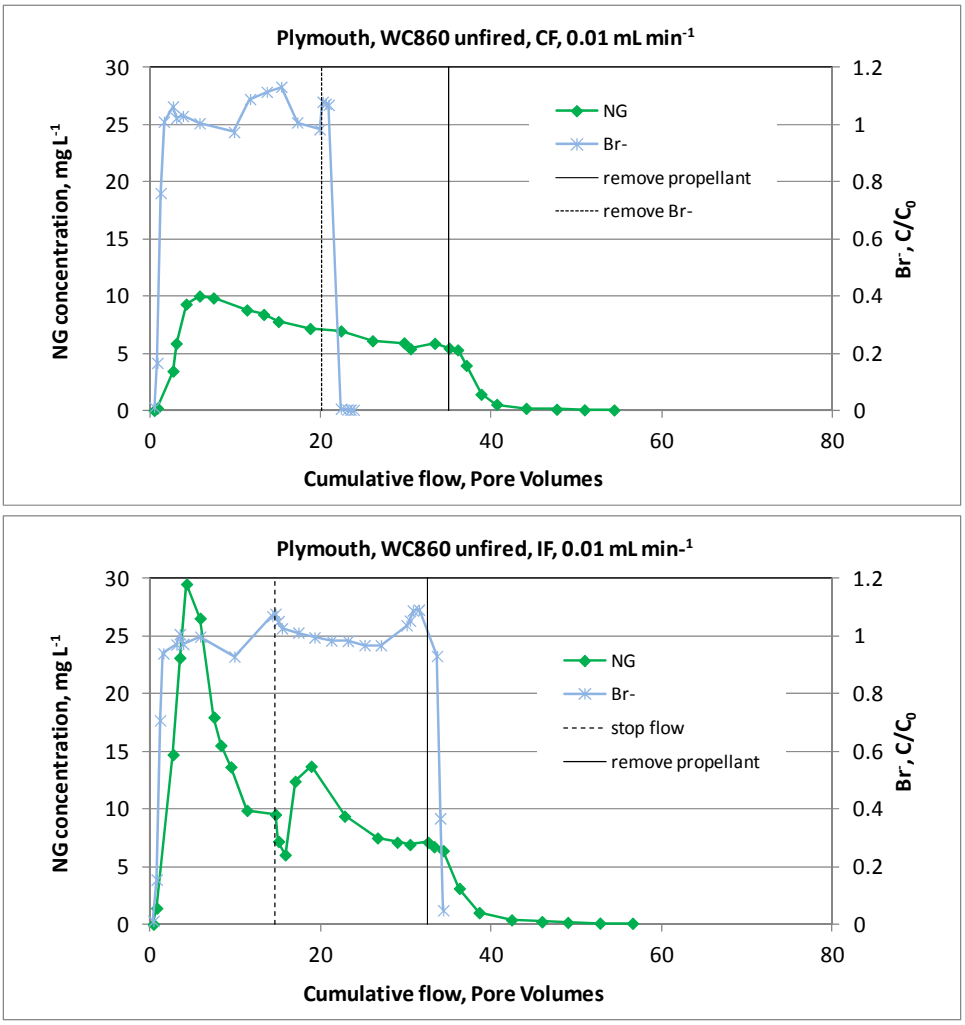

Figure C1. Breakthrough curves for continuous (CF) and interrupted (IF) water flow at 0.01 mL min^{-1} rate onto unfired 0.50-cal. propellants in Plymouth soil. The solid vertical line indicates when the propellant was removed from the soil surface.

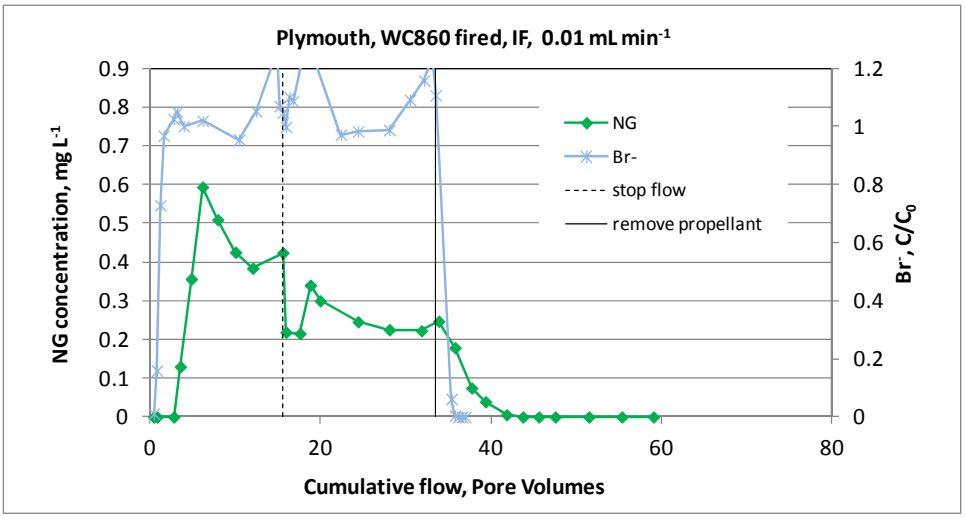

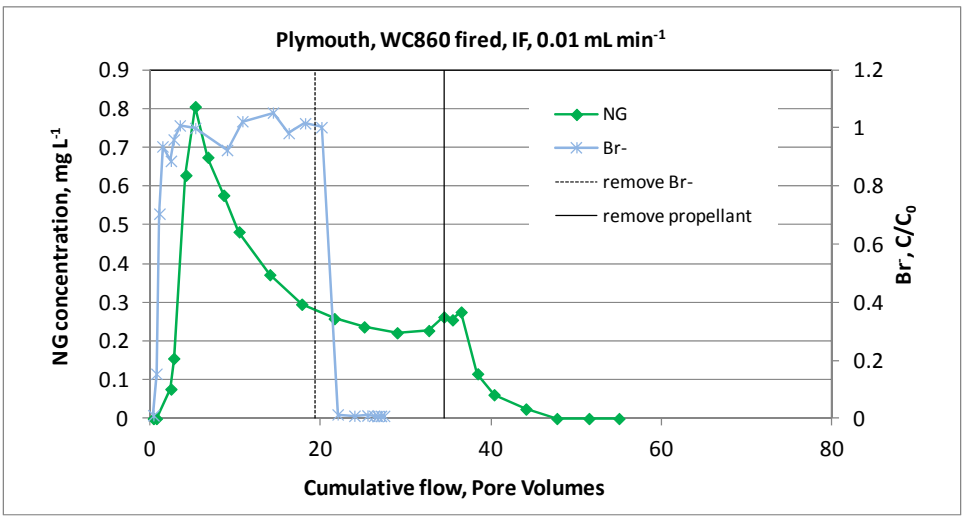

Figure C2. Breakthrough curves for continuous (CF) and interrupted (IF) water flow at 0.01 mL min^{-1} rate onto fired 0.50-cal. propellants in Plymouth soil. The solid vertical line indicates when the propellant was removed from the soil surface.

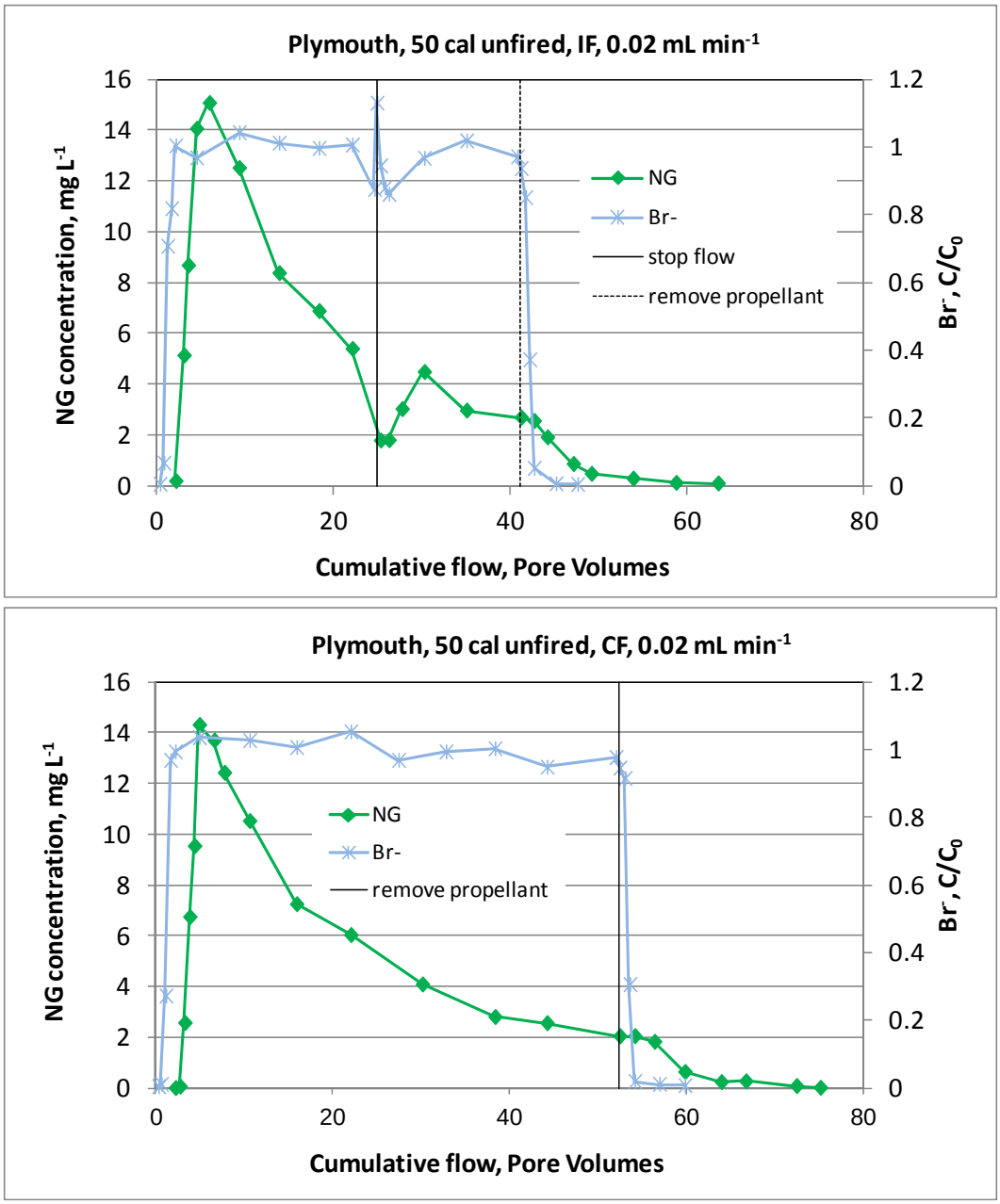

Figure C3. Breakthrough curves for continuous (CF) and interrupted (IF) water flow at 0.02 mL min^{-1} rate onto unfired and fired 0.50-cal propellants in Plymouth soil. The solid vertical line at ~30 pore volumes shows when the propellant was removed from the soil surface.

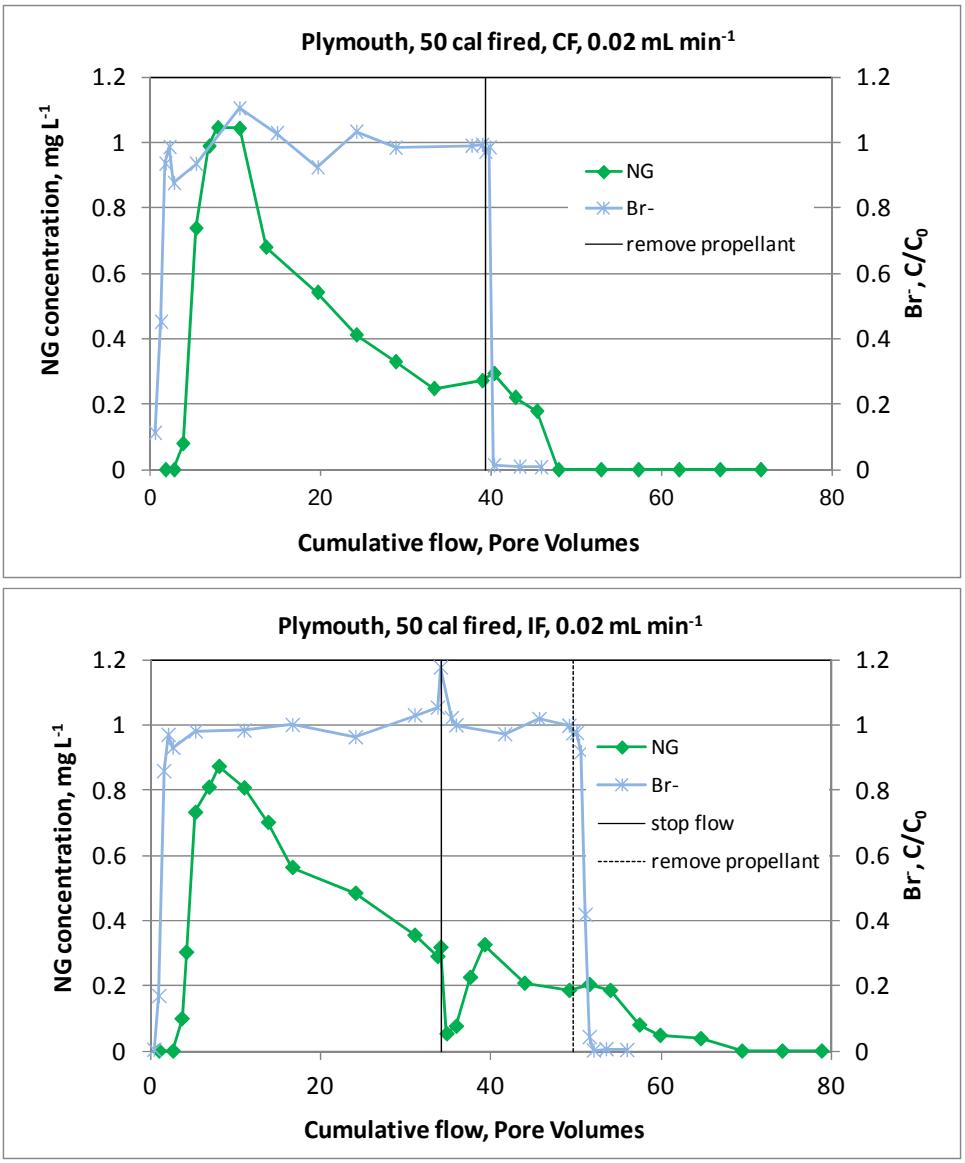

Figure C4. Breakthrough curves for continuous (CF) and interrupted (IF) water flow at 0.02 mL min^{-1} rate onto unfired and fired 0.50-cal. propellants in Plymouth soil. The solid vertical line indicates when the propellant was removed from the soil surface.

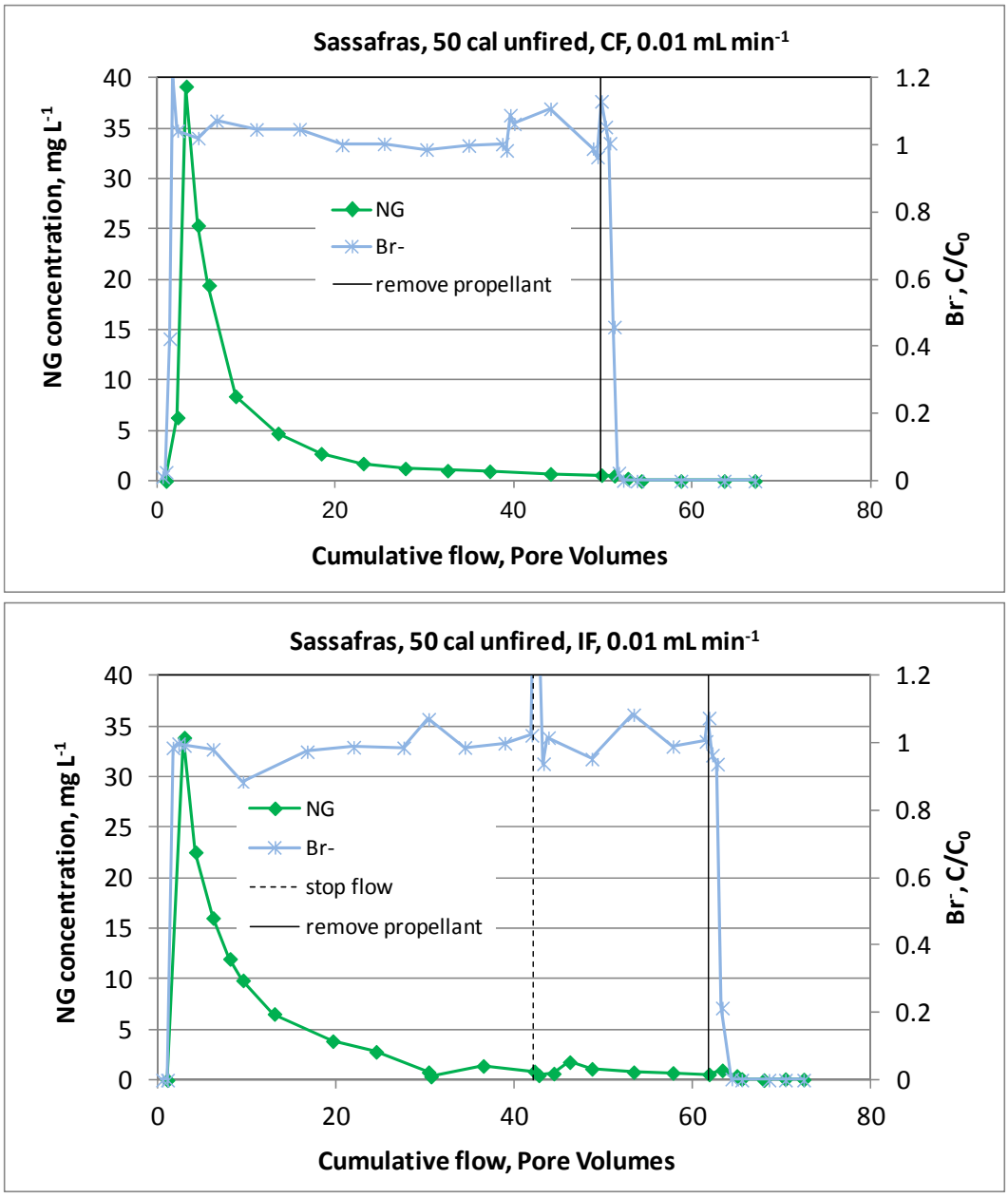

Figure C5. Breakthrough curves for continuous (CF) and interrupted (IF) water flow at 0.01 mL min^{-1} rate onto unfired and fired 0.50-cal. propellants in Sassafras soil. The solid vertical line indicates when the propellant was removed from the soil surface.

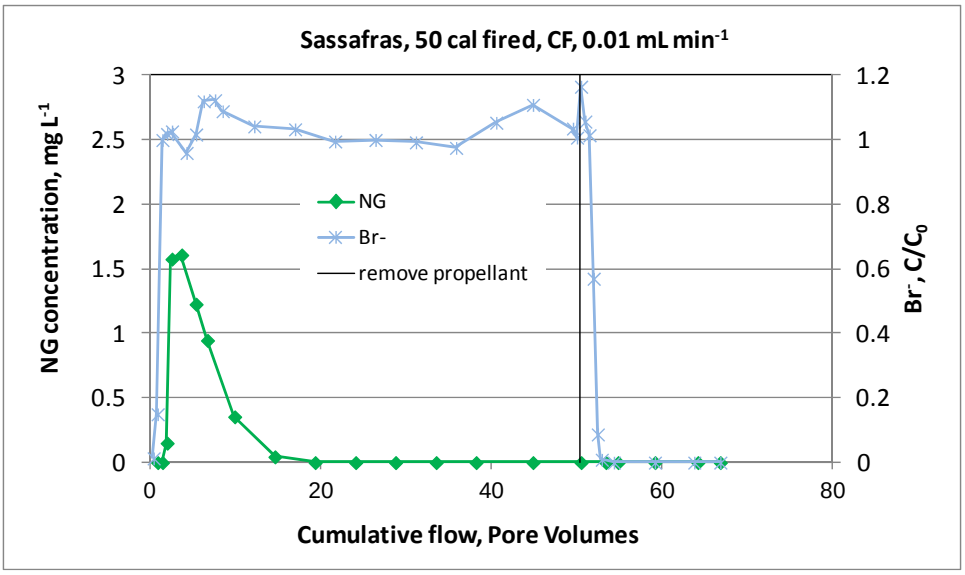

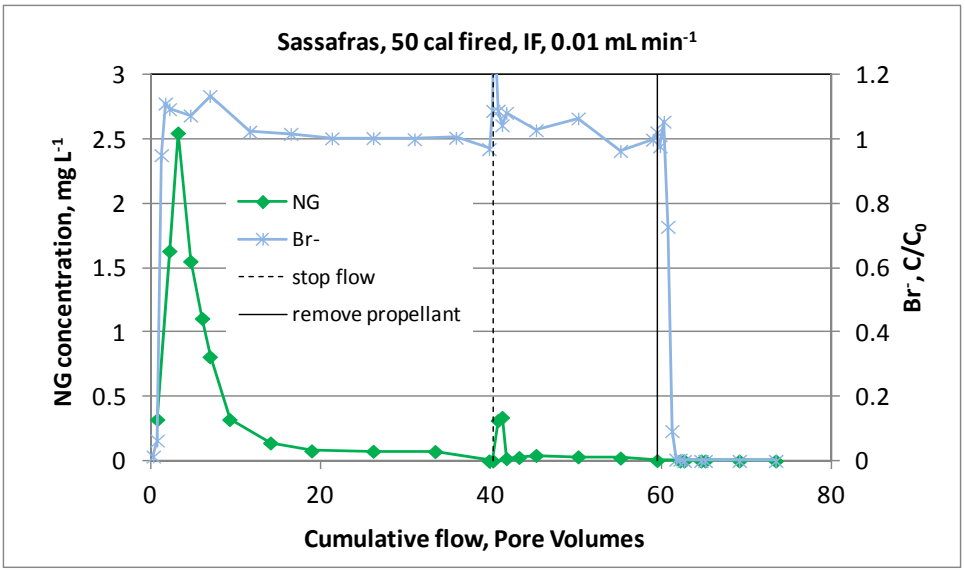

Figure C6. Breakthrough curves for continuous (CF) and interrupted (IF) water flow at 0.01 mL min^{-1} rate onto unfired and fired 0.50-cal. propellants in Sassafras soil. The solid vertical line indicates when the propellant was removed from the soil surface.

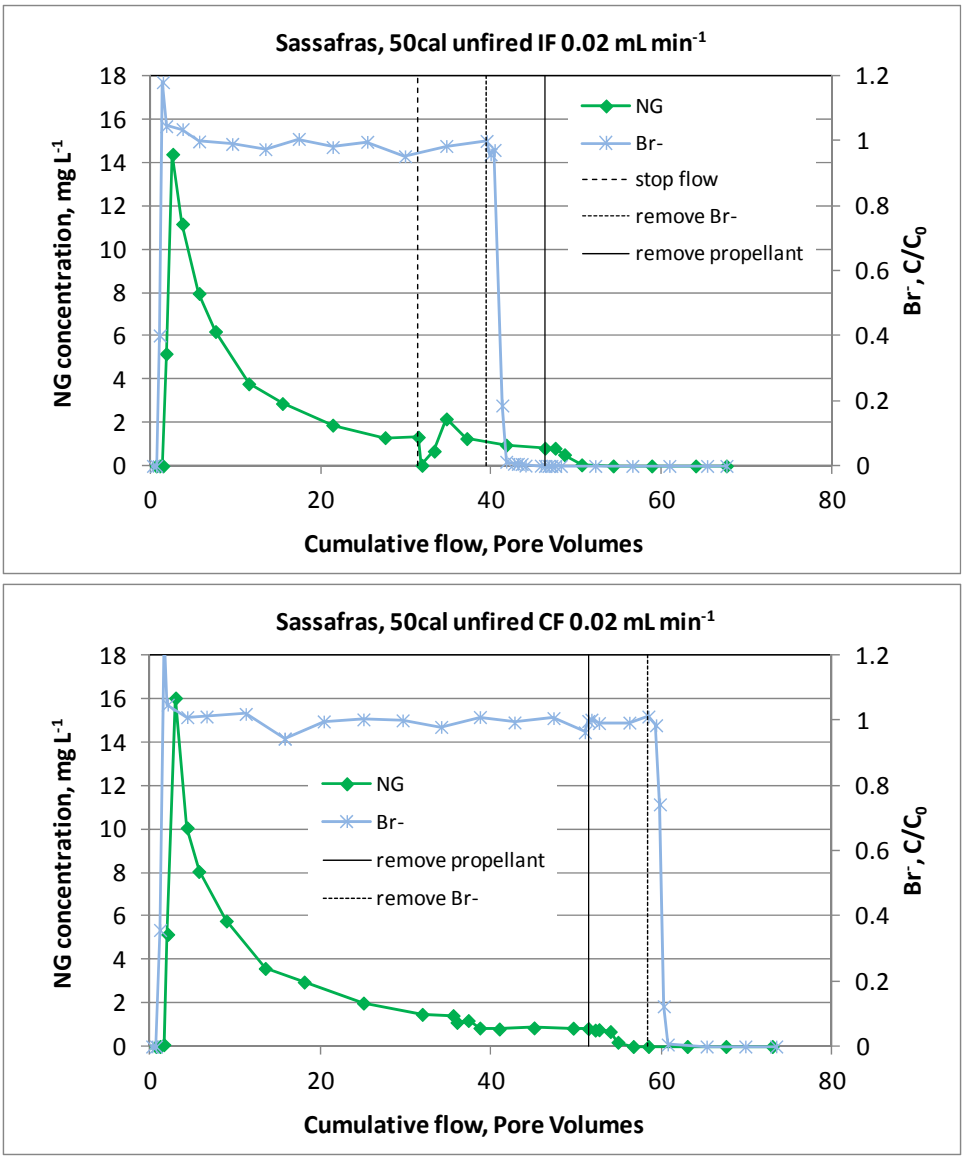

Figure C7. Breakthrough curves for continuous (CF) and interrupted (IF) water flow at 0.02 mL min^{-1} rate onto unfired and fired 0.50-cal. propellants in Sassafras soil. The solid vertical line indicates when the propellant was removed from the soil surface.

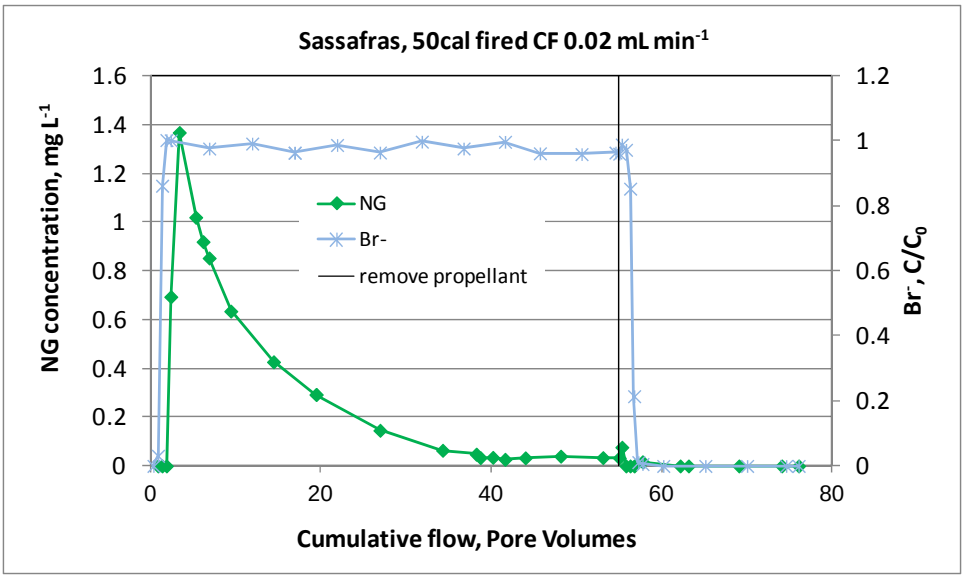

Figure C8. Breakthrough curves for continuous water flow at 0.02 mL min^{-1} rate onto fired 0.50-cal. propellants in Sassafras soil. The solid vertical line indicates when the propellant was removed from the soil surface.

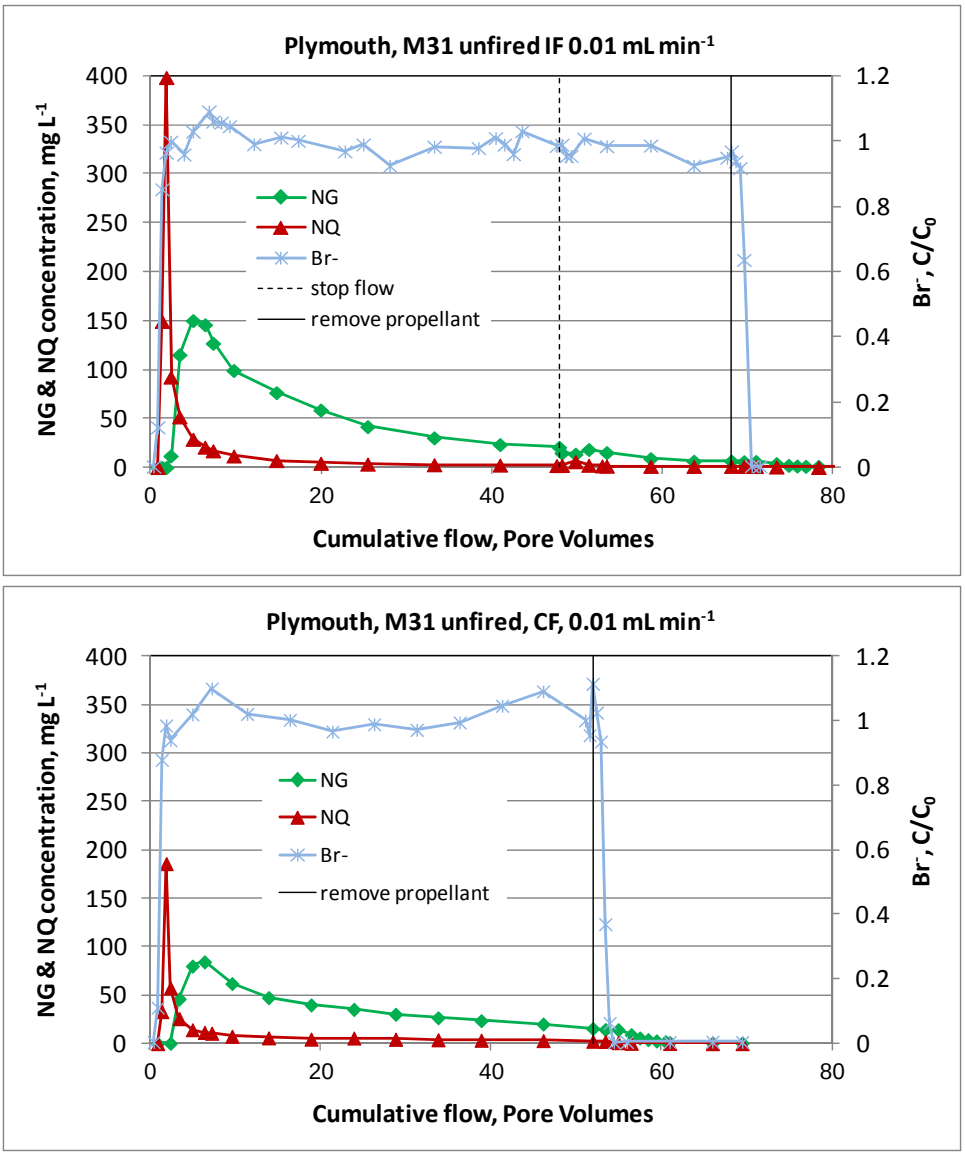

Figure C9. Breakthrough curves for continuous (CF) and interrupted (IF) water flow at 0.01 mL min^{-1} rate onto unfired M31 propellant in Plymouth soil. The solid vertical line indicates when the propellant was removed from the soil surface.

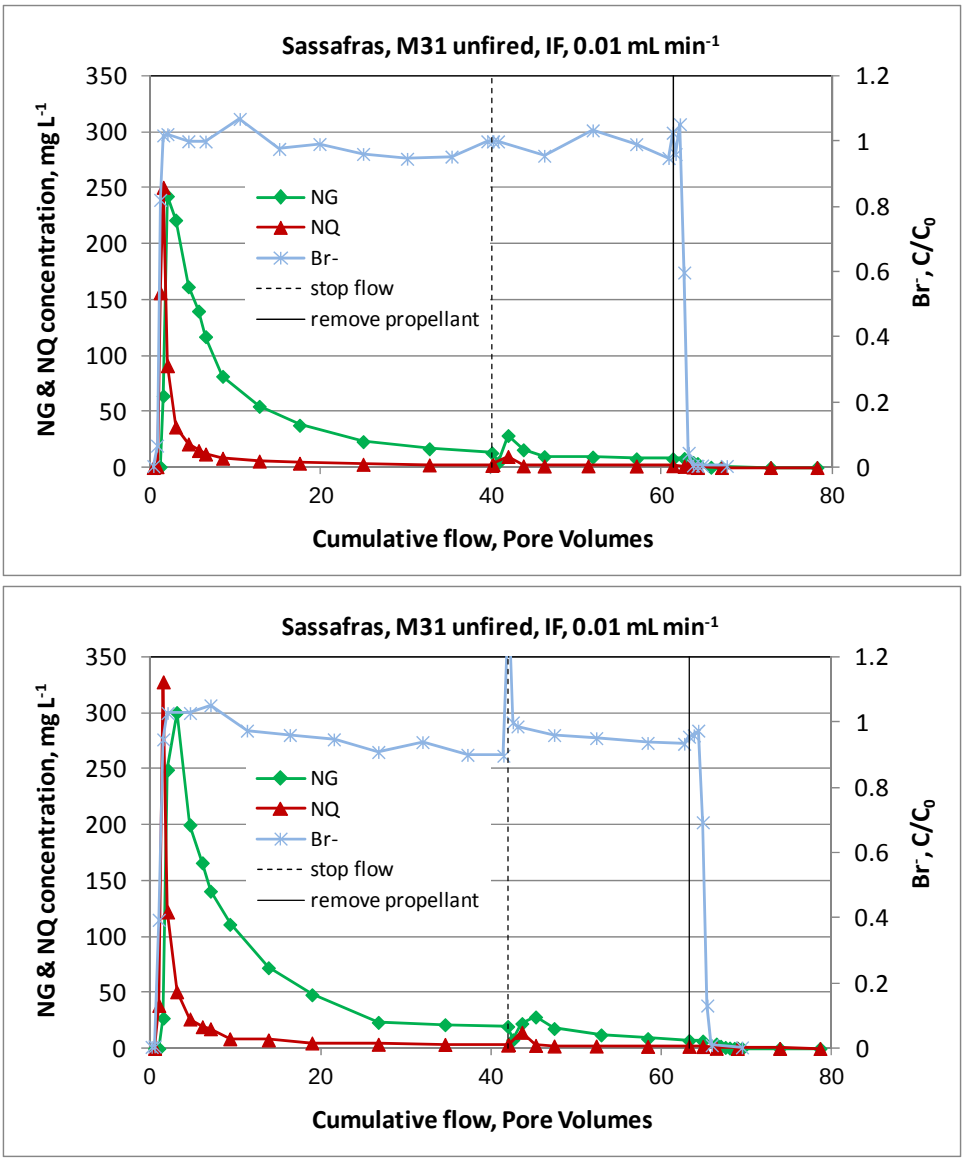

Figure C10. Breakthrough curves for continuous (CF) and interrupted (IF) water flow at 0.01 mL min^{-1} rate onto unfired M31 propellant in Sassafras soil. The solid vertical line indicates when the propellant was removed from the soil surface.

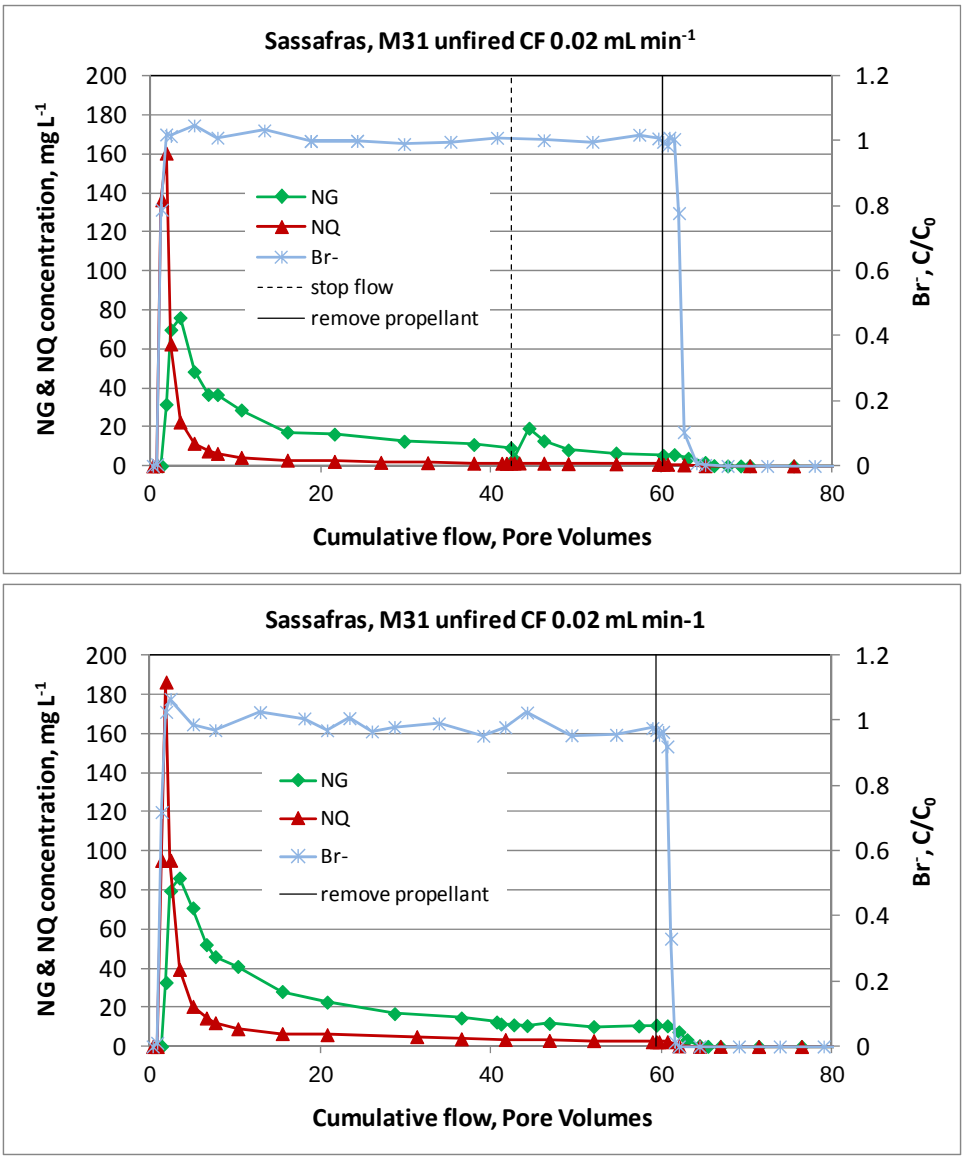

Figure C11. Breakthrough curves for continuous (CF) and interrupted (IF) water flow at 0.02 mL min^{-1} rate onto unfired M31 propellant in Sassafras soil. The solid vertical line indicates when the propellant was removed from the soil surface.

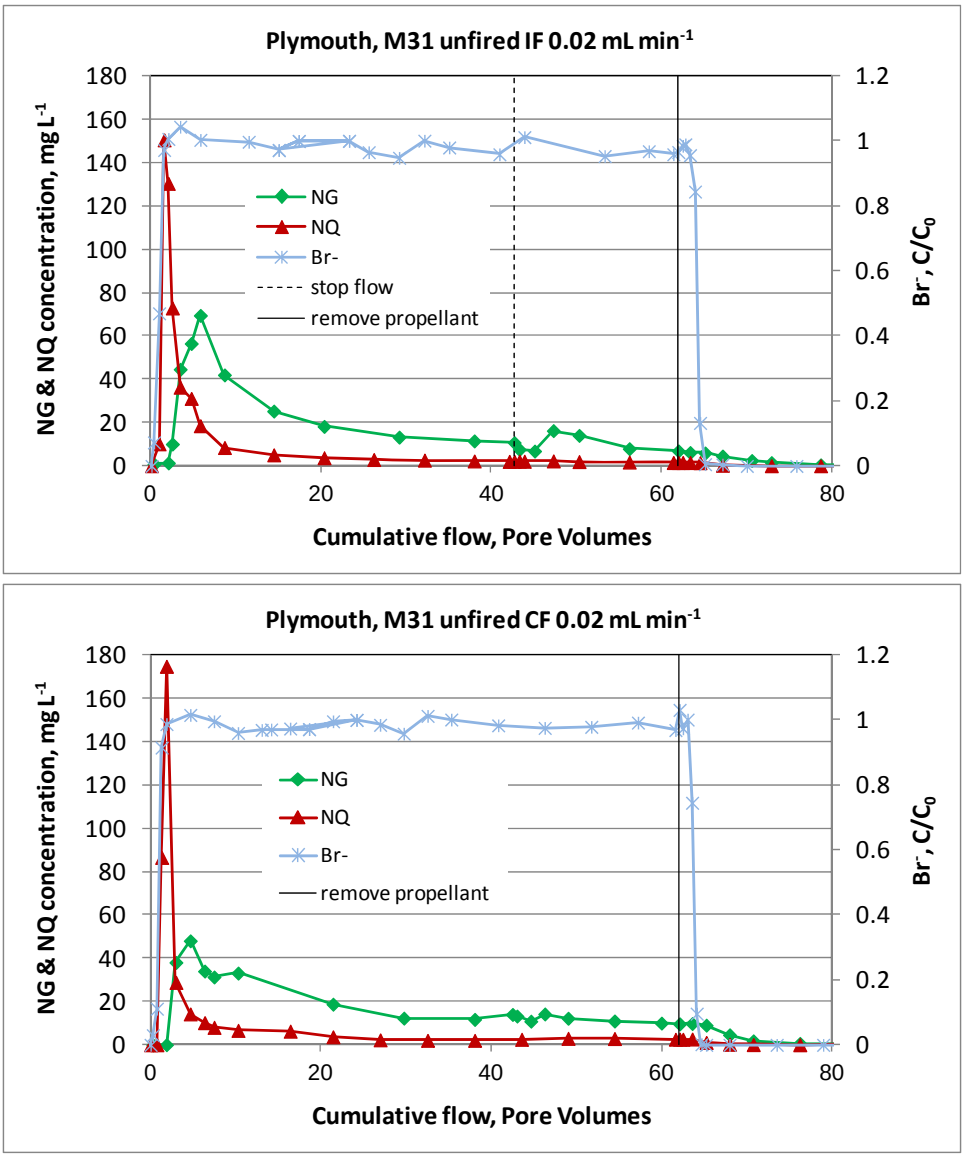

Figure C12. Breakthrough curves for continuous (CF) and interrupted (IF) water flow at 0.02 mL min^{-1} rate onto unfired M31 propellant in Plymouth soil. The solid vertical line indicates when the propellant was removed from the soil surface.

Appendix D: Raman Spectroscopy of Propellants

We tested the applicability of Raman spectroscopy and confocal Raman microscopy for distinguishing between nitroglycerin (NG), nitroguanidine (NQ) and nitrocellulose (NC) phases in double and triple-based propellants. In Raman spectroscopy a laser is shone onto a sample surface and a detector records the sample's emitted radiation at different wavelengths, generating a Raman spectrum of the point with wavelength numbers between 0 and 4000 cm^{-1}. As NG, NC and NQ all have distinct spectra (Fig. D1), wavelengths at which prominent peaks in the spectra of a compound occur, can be used to map the location of that compound (Confocal Raman Microscopy General Overview 2012; Trewartha et al. 2007). Confocal Raman microscopy merges Raman spectroscopy techniques with a confocal microscope. The confocal microscope focuses the laser beam on a very small area of the sample's surface, thereby increasing the spatial resolution of the Raman spectra.

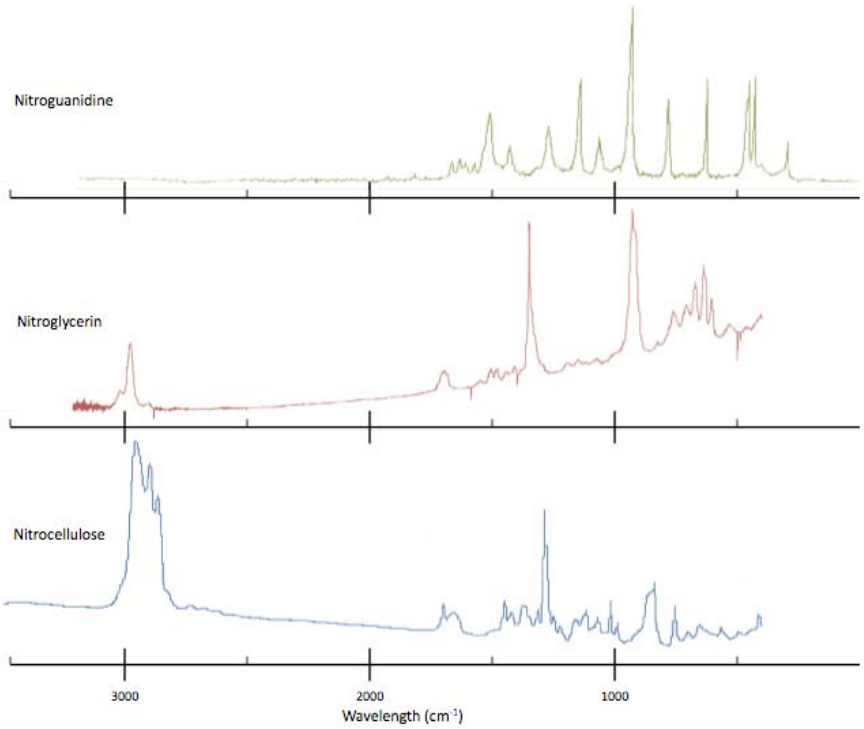

Figure D1. Raman spectra of nitroguanadine, nitroglycerine and nitrocellulose.

For the Raman analyses it helps to have flat samples. We potted a single-base (M10 with only NC), double-base (M9, 0.50-cal.) and triple-base (M31) propellant in both wax and epoxy and sectioned their surfaces to produce a flat working surface. Both of these potting materials are less than ideal; the epoxy interacts with constituents in the propellants causing changes to their compositions (Fig. D2); the wax is soft and the propellants occasionally move while being sectioned. We used the wax, potted butts to obtain point and line spectra from these samples. For the confocal microscope Raman analyses, the areas were small enough that we did not have to section the sample. Samples were observed using a 20× objective lens and excited by a laser at 532 nm. Raman spectra were obtained from a series of adjacent points on the samples, allowing us to map the different chemical phases.

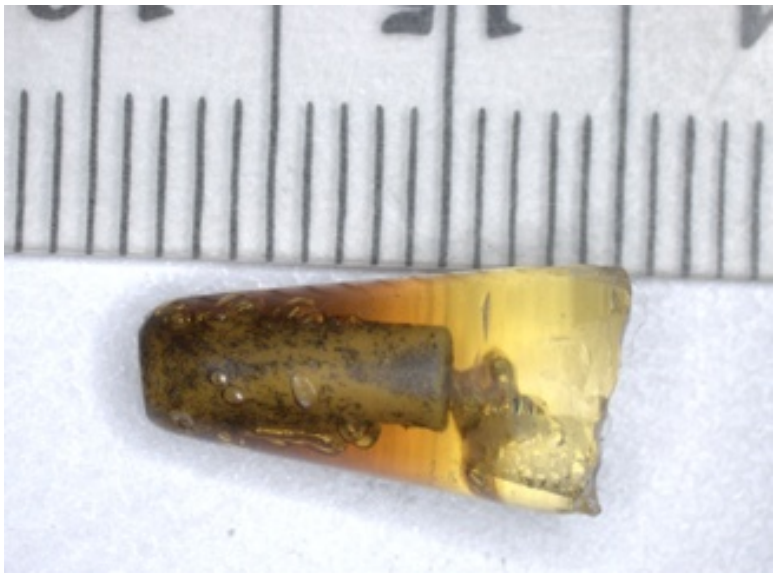

Figure D2. M31 propellant in epoxy; note bubbles formed by the interaction of the propellant with the epoxy.

Figure D3 is a line scan across a 0.50-cal. propellant. There are three peaks—a doublet centered at 1300 cm^{-1} and a broad peak at ~850 cm^{-1}. None of these peaks are clearly associated with NG, although the doublet might be a combination of NG and NC. Nitroguanadine, on the other hand, could be identified in point spectra (Fig. D4) and it could be mapped using the confocal Raman (Fig. D5). In Figure D5, NQ crystals (bright yellow) are different from the NC/NG matrix. These results show that 5-µm crystals of NQ are visible using Raman but that the more intimately mixed NC and NG cannot be separated from one another using either regular or confocal microscope Raman.

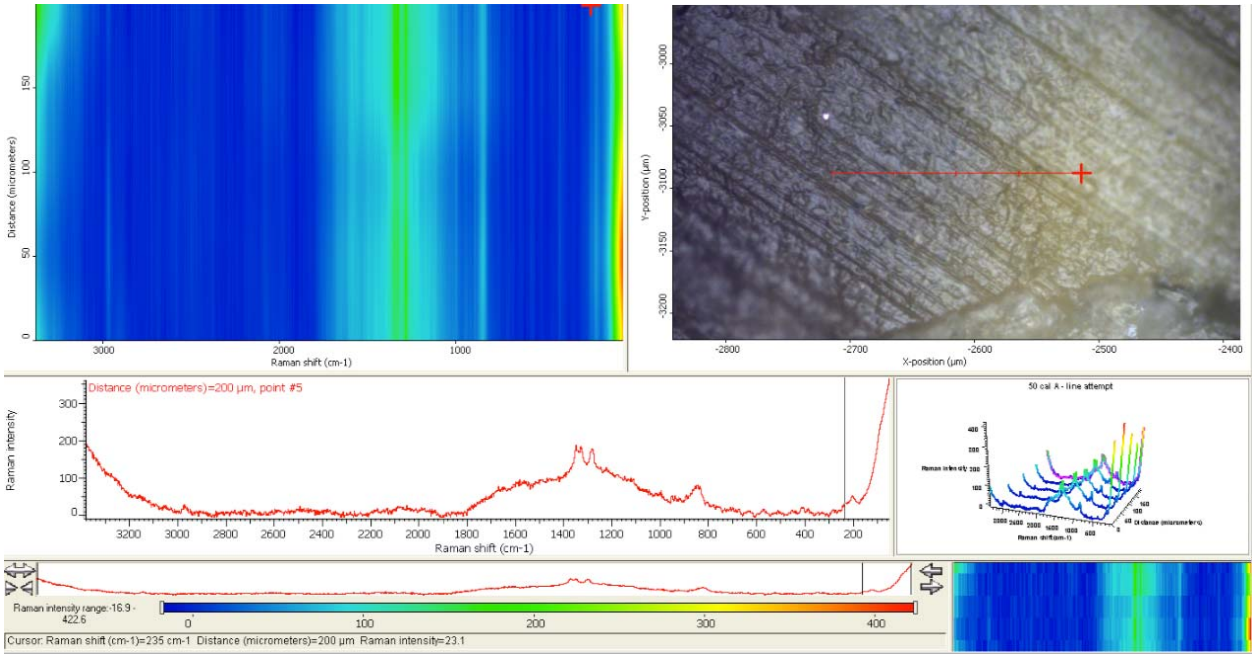

Figure D3. Line scan spectrum across a section of a 0.50-cal. double-base propellant.

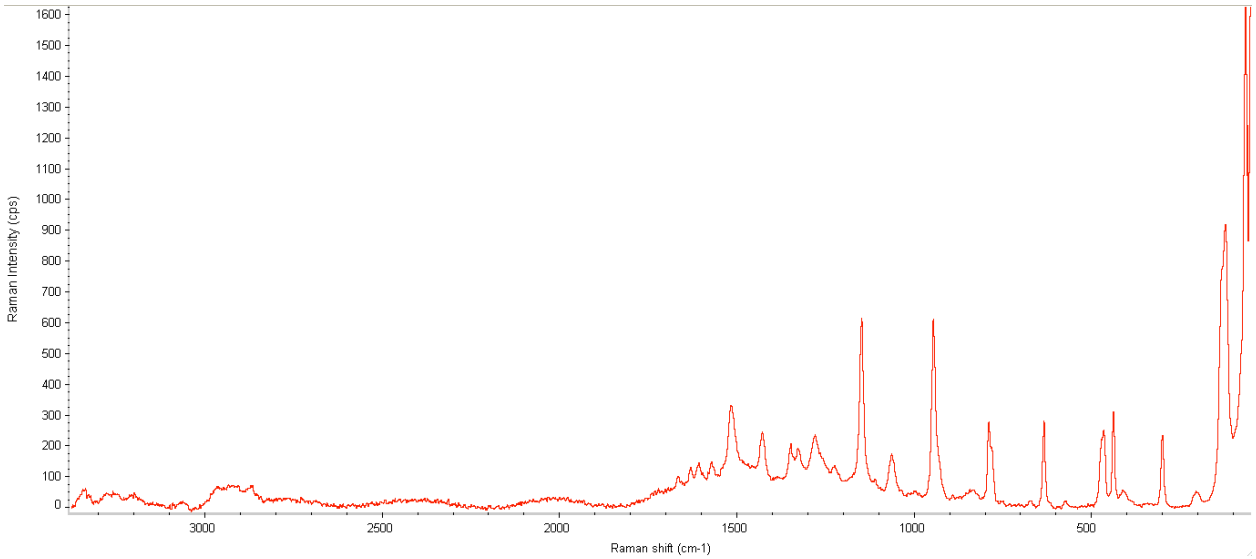

Figure D4. Raman point measurement of NQ in a triple-base propellant.

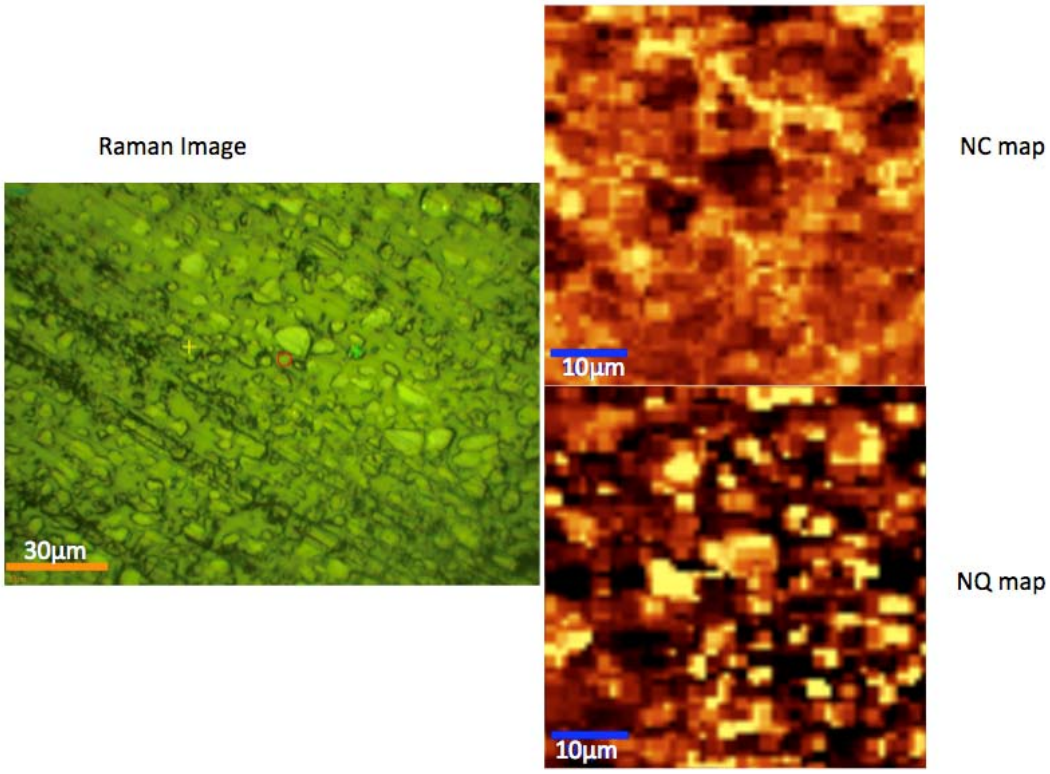

Figure D5. M31 surface map; the red circle on the optical image (left) is the center of the NC/NG and NQ maps shown on the right; the + mark the edges of the maps. Note that the NQ crystals are easily seen on the optical image.

Raman and Confocal Raman were able to distinguish NQ from the background NC and NG matrix, but were not able to distinguish between NC and NG. These techniques also have some limitations. First, spectra can only be taken from the surface of the samples, requiring sectioning of samples if analysis of an entire particle is desired. Second, although Confocal Raman can map the surface at high resolution, mapping a large area of the surface is time-consuming as only a tiny portion of the surface is in focus at each point. Finally, the propellant samples fluoresce, thereby degrading the quality of the spectra and the resulting maps. If Raman microscopy is to be used for future investigations, the fluorescence should be removed using commercially available background subtraction software (Cao et al. 2007) and more work is needed to develop better potting and sectioning methods. For this project we decided to use more established procedures for propellant analysis.

Appendix E:-List of Publication Resulting from This Work

Dontsova, K., J. Simunek, S. Taylor, and E. Hunt. In prep for submission to *Chemosphere*. Dissolution and transport of propellant constituents in soils.

Pitt, J. S. 2012. *Numerical modeling of NG diffusion in propellant grains*. U.S. Army research and Engineering Center, Cold Regions Research and Engineering Laboratory, ERDC/CRREL Letter Report, LR-12-04.

Taylor S., C. Richardson, J. H. Lever, J. Pitt, S. Bigl, N. Perron and J. P. Bradley. Accepted. Dissolution of nitroglycerin from small arms propellants and their residues. *International Journal of Energetic Materials and Chemical Propulsion*.

Taylor S., K. Dontsova, M. E. Walsh, and J. Šimůnek. In prep for submission to *Chemosphere*. Comparison of dissolution mecahnisms in single-, double- and triple-based propellants.

Taylor S., K. Dontsova, S. Bigl, C. Richardson, J. H. Lever, J. Pitt, J. P. Bradley, M. E. Walsh, and J. Šimůnek. 2012. *Dissolution of propellant energetics from nitrocellulose matrices*. U.S. Army research and Engineering Center, Cold Regions Research and Engineering Laboratory, ERDC/CRREL Technical Report, TR-12-XX.

REPORT DOCUMENTATION PAGE

Form Approved
OMB No. 0704-0188

Public reporting burden for this collection of information is estimated to average 1 hour per response, including the time for reviewing instructions, searching existing data sources, gathering and maintaining the data needed, and completing and reviewing this collection of information. Send comments regarding this burden estimate or any other aspect of this collection of information, including suggestions for reducing this burden to Department of Defense, Washington Headquarters Services, Directorate for Information Operations and Reports (0704-0188), 1215 Jefferson Davis Highway, Suite 1204, Arlington, VA 22202-4302. Respondents should be aware that notwithstanding any other provision of law, no person shall be subject to any penalty for failing to comply with a collection of information if it does not display a currently valid OMB control number. **PLEASE DO NOT RETURN YOUR FORM TO THE ABOVE ADDRESS.**

1. REPORT DATE *(DD-MM-YYYY)*
September 2012

2. REPORT TYPE
Final

3. DATES COVERED *(From - To)*

4. TITLE AND SUBTITLE
Dissolution Rate of Propellant Energetics from Nitrocellulose Matrices

5a. CONTRACT NUMBER

5b. GRANT NUMBER

5c. PROGRAM ELEMENT NUMBER

6. AUTHOR(S)
Susan Taylor, Katerina Dontsova, Susan Bigl, Colleen Richardson, James Lever, Jonathan Pitt, John P. Bradley, Marianne Walsh, and Jiří Šimůnek

5d. PROJECT NUMBER

5e. TASK NUMBER

5f. WORK UNIT NUMBER

7. PERFORMING ORGANIZATION NAME(S) AND ADDRESS(ES)
Cold regions Research and Engineering Laboratory
U.S. Army Engineer Research and Development Center
72 Lyme Road
Hanover, NH 03755

8. PERFORMING ORGANIZATION REPORT NUMBER
ERDC/CRREL TR-12-9

9. SPONSORING / MONITORING AGENCY NAME(S) AND ADDRESS(ES)
The Strategic Environmental Research and Development Program
Under SERDP ER-1691

10. SPONSOR/MONITOR'S ACRONYM(S)

11. SPONSOR/MONITOR'S REPORT NUMBER(S)

12. DISTRIBUTION / AVAILABILITY STATEMENT
Approved for public release; distribution is unlimited

13. SUPPLEMENTARY NOTES

14. ABSTRACT

During firing, propellant residues are scattered onto the soil surface where their energetic compounds can be dissolved by precipitation. The residues, like the unfired propellants, are composed of nitrocellulose imbibed with either 2,4-DNT (single-base), nitroglycerin (NG) (double-base) or NG and nitroguanidine (NQ) (triple-base). Although nitrocellulose is insoluble, 2,4-DNT, NG, and NQ are soluble; and 2,4-DNT and NG are also toxic. Consequently, data on how quickly 2,4-DNT, NG, and NQ are dissolved from propellant residues are needed to determine the flux of these compounds to soil. Once in soil solution, the partition coefficient, K_d, and degradation rate, k values are needed to predict the transport of energetics through the vadose zone and to groundwater. We measured the 2,4-DNT, NG, and NQ dissolution rates for different propellants using laboratory batch and drip tests where no soil was present and soil column studies, which used similar propellant and residues as source terms, to determine partition coefficients and degradation rates. Because the surfaces of propellants and residues may play an important role in dissolution of the energetic constituents, we studied these using both light and electron microscopy. We found that 2,4-DNT is well bound to NC and dissolves out slowly, but that both NG and NQ have fast initial dissolution followed by slower mass loss. The amount of NG dissolved is a function of the NG/NC ratio in the propellant and both our mass loss data and our microscopy results suggest that NG exists as fine liquid droplets within an NC matrix rather than as dispersed molecules.

15. SUBJECT TERMS
Diffusion
Dissolution
Nitrocellulose
Nitroglycerin
Nitroguanidine
Propellant residues
Propellants

16. SECURITY CLASSIFICATION OF:			**17. LIMITATION OF ABSTRACT**	**18. NUMBER OF PAGES**	**19a. NAME OF RESPONSIBLE PERSON**
a. REPORT	**b. ABSTRACT**	**c. THIS PAGE**			**19b. TELEPHONE NUMBER** *(include area code)*
U	U	U	None	131	

Standard Form 298 (Rev. 8-98)
Prescribed by ANSI Std. 239.18

14. ABSTRACT (cont'd)

NG droplets near the grain surface are quickly dissolved and once this layer of liquid NG is depleted, NG diffuses through the NC matrix slowly (~10^{-14} $cm^2 s^{-1}$). The NQ also dissolves rapidly initially but quickly mass loss for the NQ becomes smaller than that for NG, despite higher NQ concentrations in the studied triple-base propellants. NQ is added as a crystal during manufacturing, and was observed to remain solid in the propellant, so dissolution of the NQ crystal would have to precede its removal by water. Both 2,4-DNT and NG are added as liquids and cannot be distinguished from the NC matrix. Therefore, their distribution and movement within the nitrocellulose matrix is poorly understood, hampering our ability to derive a physically based dissolution model that can predict energetic losses from a variety of propellant types. Different interactions between 2,4-DNT, NG, NQ, and the soils were seen in both the soil batch and column studies. The 2,4-DNT interacted strongly with soils and had the highest adsorption and transformation rates measured. As a result, no 2,-4-DNT was detected in column outflow. NG experienced both adsorption and transformation in the soils, resulting in retardation of the breakthrough curve and decreased concentrations in the outflow. The short half-life of NG in most soils suggests that it should rarely reach groundwater. NQ, on the other hand, does not readily adsorb to soil, and does not degrade or transform. We would expect that NQ dissolved from propellants would reach groundwater.